The Abitibi-Opatica transition, Superior Province, Quebec, Canada: structural analysis, 40Ar/39Ar thermochronology and implications for Archean tectonics

Yannick Daoudene, Alain Tremblay, Gilles Ruffet, François Leclerc

Precambrian Research

The Abitibi-Opatica transition, Superior Province, Quebec, Canada: structural analysis, 40Ar/39Ar thermochronology and implications for Archean tectonics

--Manuscript Draft--

Manuscript Number:	PRECAM-D-22-00042R2
Article Type:	Research Paper
Keywords:	Abitibi greenstone belt; Opatica plutonic belt; structures; 40Ar/39Ar geochronology; Archean tectonism
Corresponding Author:	Yannick Daoudene, Ph.D CANADA
First Author:	Yannick Daoudene, Ph.D
Order of Authors:	Yannick Daoudene, Ph.D
	Alain Tremblay, Ph.D
	Gilles Ruffet, Ph.D
	François Leclerc, Ph.D
Abstract:	We present a structural and metamorphic study of the Abitibi greenstone belt (AGB) and Opatica Plutonic Belt (OPB) of the Archean Superior Province. The AGB-OPB contact is considered as an archetype example of Archean subduction, based on a LITHOPROBE seismic profile showing a North-dipping lithospheric-scale reflector interpreted as the vestige of subduction. Our mapping indicates that the AGB overlies the OPB, and that the AGB-OPB contact does not show evidence of significant shear deformation, as expected for a major upper plate-lower plate boundary. There is no metamorphic break at the AGB-OPB transition but rather a progressive increase of metamorphic grade toward the OPB. Therefore, we think that the OPB simply exposes the deepest part of a composite AGB-OPB sequence. 40 Ar/ 39 Ar ages suggest that the AGB and OPB rocks were exhumed from amphibolite-facies conditions at ~ 2678 Ma and ~ 2668 Ma, respectively, and then that both terranes share the same succession of thermal disturbances at c. 2650 Ma and 2600 Ma, the latter corresponding to shearing along the Nottaway River Shear Zone. We suggest that progressive cooling of both assemblages was accompanied by strain localisation along strike-slip shear zones and occurred when lateral flow of the lower crust became predominant over the convective overturn and vertical crustal material transfer. Comparison with adjacent areas suggests that regional metamorphism has been coeval over a large region, which is consistent with pervasive deformation and slow cooling as expected for vertical tectonic models and diapiric magmagenesis and ascent during the Archean.
Suggested Reviewers:	Bruno Lafrance Laurentian University BLafrance@laurentian.ca
	Lyal Harris Institut national de la recherche scientifique lyal.harris@inrs.ca
	Phil C. Thurston Laurentian University PThurston@laurentienne.ca
	Laurent Godin Queen's university, Ontario , Canada godinl@queensu.ca
	Michael Brown University of Maryland at College Park mbrown@umd.edu

Response to Reviewers:	

Dear Editors,

Please find attached a paper we wish to submit to Precambrian Research.

The paper deals with the contact between two large subprovinces of the Archean Superior Province of Canada : the Abitibi greenstone belt (AGB) and the Opatica plutonic belt (OPB).

Since the middle of the 1990s, the AGB-OPB transition zone was frequently interpreted as the trace of an Archean subduction zone, mainly based on a Grenville-Abitibi Lithoprobe seismic transect acquired in the 90's. In the paper, we emphasize the fact that the ABG-OPB contact is not marked by significant shear deformation and metamorphic break, as expected for a major upper plate-lower plate boundary. In contrast, we infer that the OPB exposes the deepest part of a composite Abitibi-Opatica crust formed prior to the main regional deformation event.

We also present new Ar-Ar ages of amphibole, biotite and muscovite grains from both the AGB and OPB, the results suggesting that the two domains share a common metamorphic history from c. 2678 Ma and the same subsequent thermal disturbances.

Our structural and métamorphic observations combined with Ar-Ar age data support a model of crustal overturned in which vertical transfers of crustal material are predominant and lead to a dome-and-basin crustal geometry. Comparison with adjacent areas also suggests that regional metamorphism, that peaked around 2680-2670 Ma, has been coeval over a large region of the SE Superior province. Such characteristics are in good agreement with pervasive deformation as expected for a diapiric/doming and basins tectonic model rather than one associated with subduction/collision processes.

The paper is original because it discusses the nature of a major contact zone between two contrasted Archean domains in the Superior province, one being famous for its ore deposits (i.e. the AGB). We think that this contribution would be of interest to a large audience, because it is dealing with Archean tectonics that is currently worldwide debated. We hope that it will appear sufficiently new, documented and of large interest enough to be considered for publication in Precambrian Research

Potential reviewers are: B. Lafrance (Laurentian University, Ontario, Canada), L. Harris (INRS, Québec, Canada), Phil C. Thurston (Laurentian University, Ontario, Canada), Laurent Godin (Queen's University, Ontario, Québec) and Michael Brown (University of Maryland, College Park, Maryland, US)

Yours sincerely,
Yannick Daoudene (corresponding author)

The Abitibi-Opatica transition, Superior Province, Quebec, Canada: structural analysis, $^{40}Ar/^{39}Ar$ thermochronology and implications for Archean tectonics

Yannick Daoudene[a,*], Alain Tremblay[b], Gilles Ruffet[c], François Leclerc[a]

[a] Ministère de l'Énergie et des Ressources naturelles, 5700, 4e Avenue Ouest, G1H 6R1, Québec, Québec, Canada.
[b] Université du Québec à Montréal, Département des Sciences de la Terre et de l'Atmosphère and GEOTOP, 201 avenue du Président Kennedy, H2X 3Y7, Montréal, Québec, Canada.
[c] CNRS (CNRS/INSU) UMR 6118, Université de Rennes 1, Géosciences Rennes, F-35042 Rennes Cedex, France
* Corresponding author.
E-mail address: Yannick.Daoudene@mern.gouv.qc.ca

ABSTRACT

We present a structural and metamorphic study of the Abitibi greenstone belt (AGB) and Opatica Plutonic Belt (OPB) of the Archean Superior Province. The AGB-OPB contact is considered as an archetype example of Archean subduction, based on a LITHOPROBE seismic profile showing a North-dipping lithospheric-scale reflector interpreted as the vestige of subduction. Our mapping indicates that the AGB overlies the OPB, and that the AGB-OPB contact does not show evidence of significant shear deformation, as expected for a major upper plate-lower plate boundary. There is no metamorphic break at the AGB-OPB transition but rather a progressive increase of metamorphic grade toward the OPB. Therefore, we think that the OPB simply exposes the deepest part of a composite AGB-OPB sequence. $^{40}Ar/^{39}Ar$ ages suggest that the AGB and OPB rocks were exhumed from amphibolite-facies conditions at ~ 2678 Ma and ~ 2668 Ma, respectively, and then that both terranes share the same succession of thermal disturbances at c. 2650 Ma and 2600 Ma, the latter corresponding to shearing along the Nottaway River Shear Zone. We suggest that progressive cooling of both assemblages was accompanied by strain localisation along strike-slip shear zones and occurred when lateral flow of the lower crust became predominant over the convective overturn and vertical crustal material transfer. Comparison with adjacent areas suggests that regional metamorphism has been coeval over a large region, which is consistent with pervasive deformation and slow cooling as expected for vertical tectonic models and diapiric magmagenesis and ascent during the Archean.

Keywords: Abitibi greenstone belt, Opatica plutonic belt, structures, $^{40}Ar/^{39}Ar$ geochronology, Archean tectonism.

1. INTRODUCTION

Orogenic sutures mark the consumption of oceanic plate lithosphere by subduction and of subsequent arc-continent and/or continent-continent collision, if any. In modern plate tectonics, subduction zones are linear and continuous areas of planetary extent where one plate moves under another and is forced to sink due to high gravitational potential energy into the mantle (e.g. Stern, 2002; Bédard, 2018; Brown et al., 2020). Typically, such areas are characterized by an upper plate-lower plate geometry with contrasting geological characteristics. In Phanerozoic belts, subduction sutures are a typical product of plate tectonics. Although their recognition can be sometimes dubious (e.g. Dewey, 1987), they are usually marked by linear belts of intense deformation, where distinct terranes with different magmatic, metamorphic, structural and geochronological histories have been juxtaposed by plate convergence. In the Archean, the nature of global tectonism remains debated, the main problem concerning similarities and differences with present-day plate tectonics (e.g. Stern, 2008; Brown et al., 2020).

Archean cratons largely consist of greenstone belts juxtaposed to deeper crustal rocks dominated by plutonic (TTG's) and orthogneissic rocks, the greenstone belts usually show steep folds and shear zones whereas plutonic belts display large-scale dome-like structures and fabric~~s~~. These rocks usually preserve MT/HT-LP/MP metamorphism that varies from greenschist- to granulite-facies, from the upper to the lower crustal domains. The most widely used arguments in favor of Archean subduction are the occurrence of calk-alkaline igneous rocks, the structural style of orogenic belts, the nature and asymmetric distribution of metamorphism, and seismic reflection data. In seismic reflection, there are few clear examples of relict slabs beneath Archean collisional belts. An example of it is found in the Lithoprobe seismic transect of the Superior Province (Calvert et al., 1995) at the contact between the Abitibi Greenstone Belt and the Opatica Plutonic Belt. In scientific literature, it has been and is still interpreted as a fossilized subduction zone and a key argument to support Archean plate tectonics (Calvert et al., 1995; Calvert and Ludden, 1999; Ludden and Hynes, 2000; Wyman et al., 2002; van der Velden and Cook, 2005; Cawood et al, 2006; Percival, 2007; van Hunen and Moyen, 2012; among others).

The Archean Superior Province (Fig. 1) consists of a series of volcano-sedimentary and plutonic domains, subprovinces and/or terranes that amalgamated during the Late Archean Kenoran orogeny (e.g. Percival, 2007). The occurrence of unconformable sedimentary rocks as old as 2.48 Ga (i.e. the Huronian Supergroup) over the volcanic and

plutonic rocks indicates that tectonic accretion occurred prior to 2.5 Ga. Although the internal geological characteristics of the domains/subprovinces/terranes are relatively well known, the nature of their boundaries remains poorly constrained and, sometimes, debated. Current views on the tectonic evolution of the Superior Province are that the orogenic collage of Mesoarchean continental fragments and Neoarchean oceanic plates occurred during a complex history of subduction-driven accretionary collision (e.g. Bleeker, 2003; Percival, 2007; Percival et al., 2006; 2012, among others). Hence, several authors have interpreted a series of high-strain deformation corridors and structural lineaments of the Superior Province as the trace of potential orogenic sutures (Ludden et al., 1986; Mueller et al., 1996; Daigneault et al., 2002, 2004). The Abitibi-Opatica contact, for instance, is considered as the surface expression of south-verging crustal-scale thrust faults rooting into an inferred North-dipping subduction zone, the existence of that subduction being attested by a lithospheric-scale seismic reflector extending from c. 40 to c. 70 km-depth.

In this contribution, we present a structural and metamorphic study of rocks lying on both sides of the Abitibi-Opatica contact in northern Quebec for a strike length of c. 300 km, between the Lac-au-Goéland area to the west and the town of Chibougamau to the east (Fig. 2). The main objectives of fieldwork have been to test (1) how the overall geometry of regional structures fits with south-verging collisional tectonism and thrusting of the OPB over the AGB, and (2) if the structural and metamorphic characteristics of both belts are consistent with an upper-lower plate geometry, as inferred by the subduction model. The determination of the age and duration of structural and metamorphic event(s) that have affected both terranes being critical for a better understanding of their respective geological evolution and mutual relationships, we have performed a series of single-grain ^{40}Ar /^{39}Ar analyses for representative samples of both belts.

2. GEOLOGICAL SETTING

The Superior Province forms the principal Archean basement of North America (Fig. 1~~a, upper left inset~~). It is made up of several tectonostratigraphic terranes or subprovinces grouped into four major tectonostratigraphic types/domains (Card, 1990; Card and Ciesielski, 1986; Hocq, 1994; Stott et al., 2010), (1) metasedimentary rocks, (2) volcanic and plutonic rocks, (3) tonalite-trondjhemite-granite (TTG)-dominated domains, and (4) high-grade metamorphic rocks. Most tectonic models suggest that these tectonostratigraphic terranes were amalgamated, regionally deformed and metamorphosed during multiple episodes of

subduction/collision (e.g. Kimura et al., 1993; Daigneault et al., 2002; Percival et al., 2006, 2012) between ca. 2.72 Ga and 2.68 Ga (Percival, 2007). The southeastern part of the Superior Province comprises, from north to south, the Opatica, Abitibi and Pontiac subprovinces, the former two being designated here as the Opatica Plutonic Belt (OPB) and the Abitibi Greenstone Belt (AGB) (Fig. 1b).

2.1 The Opatica Plutonic Belt

The OPB is located in the northern part of the southeastern Superior Province. It is separated in two structural domains of plutonic rocks, north and south of the Frotet-Evans greenstone belt that extends east-west over a strike length of approximately 250 km (Figs. 1b and 2). The detailed geology of the OPB is poorly documented, mainly due to difficult road access and a limited mineral resources interest as compared to the adjacent Abitibi subprovince. Existing regional studies indicate that the OPB is a large domain of igneous rocks essentially consisting of foliated tonalites and diorites and equivalent gneisses. The latter were designated as «grey gneisses» by Sawyer and Benn (1993). They are characterized by well-developed compositional layering and locally abundant occurrences of diatexite migmatites in their more fractionated members, mainly in the southern part of the belt (Benn et al., 1992; Sawyer and Benn, 1993; Hocq, 1994; Sawyer, 1998). The gneissic tonalites and diorites are intruded by abundant, slightly- to undeformed plutons of granodiorite and granite. The crystallization age of the OPB intrusive rocks is not precisely constrained but the available geochronological data suggest that they formed mostly between 2.83 and 2.68 Ga (Gariépy and Allègre, 1985; Davis et al., 1992; 1994, 1995; Pedreira-Perez et al., 2020). According to Sawyer (1998), partial melting and migmatization occurred at 2.68-2.67 Ga.

In the Lac-au-Goéland area (Fig. 3), the Nomans tonalite, which is surrounded by metavolcanic and metasedimentary rocks of the AGB, possesses petrological and structural characteristics that are identical to those observed in tonalitic rocks of the OPB (Daoudene et al., 2013~~4~~). It represents an antiformal window of the OPB within the AGB (Goutier, 2005; Daoudene et al., 2013~~4~~; see below). Previous mapping (i.e. Hocq, 1994), as well as our own observations, shows that the OPB contains km-scale, scattered «lenses» of greenstone-type rocks (Figs. 2 and 3) consisting of amphibolite-grade mafic volcanic rocks and mafic-ultramafic intrusive rocks (Figs. 4a and b). The texture of these mafic volcanic rocks varies from primary, with locally preserved breccia and pillow structures (Fig. 4a), to migmatitic.

The Frotet-Evans greenstone belt (Fig. 2) is a large-scale example of metavolcanic belts surrounded by plutonic rocks of the OPB. It is divided into four segments, ~~(cf. Boily, 2000)~~from west to east, the Evans-Ouagama, Storm-Evans, Assinica and Frotet-Troilus segments (cf. Boily, 2000). Figure 2 shows the two easternmost segments, the Frotet-Troilus and Assinica segments. The Frotet-Evans greenstone belt has been interpreted as the erosional remnant of an allochthonous thrust sheet by Sawyer and Benn (1993) but it rather represents an autochthonous synformal sequence within the OPB (see below). It preserves evidence for amphibolite-facies metamorphic conditions, except for its central part where greenschist-facies metasedimentary rocks are predominant (Simard, 1987; Brisson et al., 1997a and b). Volcanic and sedimentary rocks of the Frotet-Troilus segment are included into the Frotet Group; U-Pb zircon ages from felsic tuff layers and a felsic dyke yielded crystallization ages of 2780 ± 28 Ma and 2750 ± 28 Ma (Thibault, 1985), and 2782 ± 6 Ma (Pilote et al., 1997), respectively. The Assinica segment represents the western extension of the Frotet-Troilus segment (Fig. 2). It comprises a lower unit of mafic to felsic volcanic rocks, the Assinica Group, and an upper unit of sub-concordant, clastic sedimentary rocks, the Broadback Group. There are currently no isotopic data to constrain the age of the Assinica Group but correlation with the Rabbit Formation of the Evans Group in the Storm-Evans segment to the west, suggests that it is probably ca. 2758 ± 4 Ma (U-Pb on zircon; David, 2018 in Groulier et al., 2020), which indicates that the overlying clastic sequence of the Broadback Group is ca. 2755 Ma or younger. ~~segment.~~

2.2 The Abitibi Greenstone Belt

The AGB is made up of ultramafic, mafic, felsic volcanic rocks and syn-volcanic intrusions of Late Archean age. It consists of several, east-west-trending assemblages of volcanic, volcanoclastic and sedimentary rocks (Fig. 1b) that have been deformed and metamorphosed at greenschist- to amphibolite-facies conditions (e.g. Daigneault et al., 2002). The volcanic domains are separated by narrow and linear belts of clastic sedimentary rocks that are frequently associated with major fault zones (Ludden et al., 1986; Percival, 2007). The youngest sequence of these clastic sedimentary rocks, the Temiskaming Group, was deposited above angular unconformities between ca. 2679 and ca. 2670 Ma (e.g. Robert et al., 2005). Based on the age of the various volcanic sequences, the AGB is subdivided into the Northern and Southern Volcanic zones originally separated by the Destor-Porcupine fault zone (Ludden et al., 1986; Chown et al., 1992; Daigneault et al., 2004) but relocated

approximately 50 km northward by Thurston et al. (2008; see their Figure 2). In the Southern Volcanic zone, corresponding to the Tisdale (2710-2704 Ma) and Blake River (2704-2695 Ma) assemblages of Thurston et al. (2008; Fig. 1b), peak of regional metamorphism has been bracketed at 2680-2660 Ma by Powell et al. (1995), and at 2665-2660 Ma by Robert et al. (2005) and Tremblay et al. (2020~~). The AGB consists of several, east-west-trending assemblages of volcanic, volcanoclastic and sedimentary rocks (Fig. 1) that have been deformed and metamorphosed at greenschist- to amphibolite-facies conditions (e.g. Daigneault et al., 2002). In the southern part of the belt, peak of regional metamorphism has been bracketed at 2680-2660 Ma by Powell et al. (1995), and at 2665-2660 Ma by Robert et al. (2005) and Tremblay et al. (2020).~~ The volcanic and sedimentary rocks, which together represent about 50-60% of the AGB, bound large plutonic domains dominated by TTG-type plutons (Fig. 1b), and both the volcano-sedimentary assemblages and plutonic domains are intruded by syn- and post-tectonic granite, granodiorite and syenite plutons that span ages as young as ca. 2650 Ma ~~syn-volcanic to syn- and post-tectonic intrusions~~ (Feng et al., 1992; Daigneault et al., 2002; Robert et al., 2005). In the Val d'Or area (Fig. 1b), the Preissac-Lacorne batholith is a typical example of these syn- to late-orogenic intrusions. It is made up of a composite series of intrusions in which two distinct types and ages of granitic rocks are present: an early, subalkaline to alkaline, monzodiorite-monzonite-granodiorite-syenite series emplaced between 2690 and 2670 Ma; and a younger, S-type garnet-muscovite granite series dated between 2660 and 2642 Ma, and probably derived from a major metasedimentary source (Feng et al., 1992; Ducharme et al., 1997; Daigneault et al, 2002).~~Based on the age of the various volcanic sequences, the AGB is subdivided into the Northern and Southern Volcanic zones separated by the Destor-Porcupine fault zone (Ludden et al., 1986; Chown et al., 1992; Daigneault et al., 2004), the Southern Volcanic zone corresponding to the Tisdale (2710-2704 Ma) and Blake River (2704-2695 Ma) assemblages of Thurston et al. (2008; Fig. 1)~~.

In the study area (Fig. ~~3~~2), the volcanic rocks of the AGB belong to the Northern Volcanic zone. It mainly consists of two volcanic cycles formed between ca. 2.8 and 2.7 Ga (e.g. Leclerc et al., 2011), and belongs to 27~~11-27~~50-2711 Ma volcanic rocks of the Kidd-Monro, Stoughton-Roquemaure, Deloro and Pacaud assemblages with local >2750 Ma occurrences (Fig. ~~2~~1b; Thurston et al., 2008). In ~~the~~ Chibougamau ~~area~~ (Fig. 2), the base of the volcanic sequence belongs to the Chrissie Formation, which is currently one of the oldest volcanic units of the AGB at 2791.4 +3.7/-2.8 Ma (U-Pb zircon age; David et al., 2011). It

consists of mafic to felsic volcaniclastic rocks, calk-alkaline rhyolites, and tholeiitic-to-andesitic basalts. The Roy Group overlies the Chrissie Formation. It includes two volcanic and sedimentary cycles and is estimated to be up to 13 km-thick (Allard et al., 1985; Dimroth et al., 1984; Daigneault et al., 1990). The lower cycle consists of tholeiitic basalts, the Obatogamau Formation, overlain by tholeiitic rhyolites and calk-alkaline volcaniclastic.rocks of the ca. 2732 Ma to ca. 2726 Ma Waconichi Formation (Daigneault and Allard, 1990; Legault, 2003; Leclerc et al., 2011; David et al., 2012). The upper cycle of the Roy Group comprises, from base to top, the Bruneau, Blondeau, Scorpion and Bordeleau formations, which consist of basalt and andesitic basalt at the base overlain by a well-bedded sequence of volcaniclastic and sedimentary rocks (Leclerc et al., 2011). In the Chibougamau area, a lapilli tuff of the Scorpion Formation yielded U-Pb crystallization age on zircon of 2716,4 ±1,0 Ma (David et al., 2012). In the Lac-au-Goéland area (Fig. 3), rocks correlatives to the Bordeleau Formation belong to the Bell River and Dussieux formations and yielded zircon U-Pb ages of ~~a~~ 2725-2717 Ma (Goutier et al., 2004; David, 2005; David et al., 2006).

The Opémisca Group (Fig. 2) is a sequence of clastic sedimentary and volcanic rocks overlying the Roy Group (Charbonneau et al., 1991; Leclerc et al., 2008; Leclerc and Houle, 2013). From base to top, it consists of the La Trêve, Daubrée, Stella and Haüy formations (Charbonneau et al., 1991). In the Chibougamau area, the Stella Formation has been interpreted as a lateral equivalent to the La Trêve and Daubrée formations (Charbonneau et al., 1991). The La Trêve Formation consists mainly of polygenic conglomerates with heterogeneous clasts, including TTG granitoids and mafic-to-felsic volcanics, whereas the Daubrée Formation is ~~basically~~ made up of turbidites ~~(Fig. 4c)~~. The Haüy Formation corresponds to a volcanic sequence mainly composed of K-rich porphyric andesites with lenses of conglomerate. The Haüy lava flows and associated volcaniclastic sediments have been interpreted as the result of evolved arc volcanism and backarc basin sedimentation (Mueller, 1991). In the Stella and Haüy formations, detrital zircons provided maximum ages of deposition of 2704 ± 2 Ma (Leclerc et al., 2012) and 2691.7 ± 2.9 Ma (David et al., 2007), respectively. In the Lac-au-Goéland area (Fig. 3), the Daubrée Formation is intruded by the Inconnue River Diorite, which yielded a U-Pb zircon age of 2693.6 ± 2.9 Ma (McNicoll and Goutier, 2008).

3. REGIONAL STRUCTURES

According to Sawyer and Benn (1993), the OPB records three generations of structures. The oldest is related to D_1 and a penetrative, moderately dipping foliation (S_1) hosting broadly distributed, WSW-ENE-trending mineral and stretching lineations (Fig. 4b). S_1 corresponds to the regional gneissic foliation (Fig. 4c) and defines a metamorphic layering ~~(Fig. 4c)~~ that is axial-planar to intrafolial F_1 folds. D_1 has been attributed to a top-to-the SW verging deformation. Sawyer and Benn (1993) argued that S_1 was folded during a D_2 deformational event, marked by East-West trending, steeply North- or South-dipping compressive shear zones. S_2 is a steeply dipping biotite foliation recording amphibolite-greenschist facies metamorphic conditions, although it may locally attain the amphibolite facies. It frequently forms a composite $S_{1\text{-}2}$ fabric with D_1 structures. D_1 and D_2 has been attributed to the progressive development of an overall SSE-verging fold-and-thrust belt (and inferred backthrusting) along the AGB-OPB boundary and southward (Benn et al., 1992; Sawyer and Benn, 1993; Lacroix and Sawyer, 1995). Sawyer and Benn (1993) also recognized a D_3 event, related to NE-SW and NW-SE-trending strike-slip shear zones cutting across both the Frotet-Evans and the Abitibi greenstone belts (see Fig. 2).

In the AGB of the study area, existing structural studies of regional extent have documented four deformational phases (e.g. Dimroth et al., 1986, Daigneault et al., 1990; Leclerc et al., 2012; Mathieu et al., 2020), the youngest one (D_4) being related to the Mesoproterozoic Grenvillian orogenic cycle (Daigneault et al., 1990). D_1 has been attributed to an early-formed series of drape folds devoid of axial-planar schistosity (Daigneault et al., 1990). D_2 is related to syn-metamorphic folding and the development of the regional EW-trending schistosity (S_2), it corresponds to F_{2a} and F_{2b} folds as described by Leclerc et al. (2012). D_1 and D_2 of the AGB correlate with the Benn's et al. (1993) $D_{1\text{-}2}$ phase of the OPB. According to Mathieu et al. (2020), the D_3 phase corresponds to the waning stage of the main deformation event that reactivated E- W- striking D_2 reverse faults as transcurrent strike- slip faults. In contrast, Leclerc et al. (2012) described D_3 structures as NE-striking shear zones cutting across earlier E-W trending D_2 shears/faults (Fig. 2).

Our comprehension and interpretation of structures in the study area are similar to those described above. We think that $D_{1\text{-}2}$ and D_3 belong to progressive and long-lasting deformational events. In the following sections, we describe fabric~~s~~ and structures related to those $D_{1\text{-}2}$ to D_3 events in both the AGB and the OPB. These descriptions are based on our own field observations and from previous studies.

3.1 $D_{1\text{-}2}$ phase of deformation

D_2 deformation structures are regionally-developed and associated with folding of the volcanic and sedimentary rocks of the AGB (Figs. 2 and 3) whereas the D_1 metamorphic layering is restricted to the lowermost stratigraphic part of that belt. Regional folds (F_2) have variable wavelength and their axial traces strike East-West, although they are locally reoriented due to younger D_3 strike-slip shears, such as the Nottaway shear zone (Fig. 2). In the Lac-au-Goéland area (Fig. 3), for instance, to the southwest of the Nottaway shear zone, S_2 trajectories within the AGB are NW-SE trending and define a F_3 syncline, the Maicasagi syncline (Fig. 3; Goutier, 2005). Overall, the regional pattern of folding of the AGB is characterized by a north-south succession of F_2 synclines and anticlines. The core of synclines is usually occupied by the Opémisca Group, whereas the anticline crests expose the underlying volcanic rocks of the Roy Group which are, locally, crosscut by large pre- to syn-tectonic intrusions such as the Opémisca and Chibougamau plutons (Fig. 2).

The volcanic and sedimentary rocks of the AGB are characterized by a weakly to moderately developed regional schistosity (S_2), although some rock exposures seem to be~~are~~ devoid of structural fabric~~s~~ development (Fig. 4d). When present, S_2 is pervasive, strikes East-West and dips steeply either to the north or the south (Figs 5 and 6a). Towards the contact with the OPB, the volcanic rocks of the Roy Group are more intensely foliated, the dominant foliation (S_1) is there tightly folded by F_2 (Fig. 4e), although that, most of the time, it forms a composite $S_{1\text{-}2}$ fabric and consists of a metamorphic layering marked by metamorphic minerals such as biotite and hornblende (~~Fig. 4b,~~ see section 4), that corresponds northward to the flat-lying S_1 gneissic fabric of the OPB gneisses. Our interpretation is that the OPB gneissic foliation is verticalized and transposed into S_2, it forms there ~~then~~ a $S_{1\text{-}2}$ metamorphic layering that is subparallel to the contact between the OPB and the AGB (Fig. ~~6~~5) and is absent farther south in the up-stratigraphy, lower-grade rocks of the AGB. The ~~B~~bedding plane, when visible, is usually parallel to the regional S_2 that is marked by the alignment of amphibole and biotite in amphibolite-grade rocks (as for S_1) and by chlorite, epidote and albite in greenschist and sub-greenschist facies rocks of the AGB.

East-West-trending shear zones cut the volcanic and sedimentary sequences of the AGB. These sub-vertical shear zones are poorly exposed. Previous studies (e.g. Dimroth et al., 1986; Daigneault et al., 1990; Leclerc et al., 2012) indicate they are mainly located on the limbs of regional-scale F_2 folds (Fig. 2), some of the latter being synformal troughs occupied by lower grade sedimentary rocks of the Opémisca Group (Fig. 4~~c~~d). As for F_2 folds, these

shear zones are deflected in the vicinity of younger NE- and NW-trending strike-slip shear zones (Figs. 2 and 3). S_2 increases in intensity toward and within these D_2 shear zones and hosts steeply plunging stretching and/or mineral lineation, suggesting significant subvertical elongation (Dimroth et al., 1986; Daigneault et al., 1990). Shear-sense indicators are rare but when present, they suggest that the shear zones correspond to north or south side-up reverse faults.

In the OPB, dominant deformation fabric~~s~~ are attributed to D_1 and expressed by a weakly- to well-developed metamorphic foliation (S_1) showing variable orientations (Fig. 5). S_1 trajectories in the OPB define an East-West trending, elongated dome-and-basin geometry, consistent with the overall trend of D_2 regional folds and structures in the adjacent AGB (Fig. 5). Mineral lineations, defined by the alignment of quartz-feldspar aggregates, are more discrete and of variable orientation as compared to the AGB (Fig. 6b). These lineations plunge at low angle within the regional foliation. In the area located between the Frotet-Evans and Abitibi greenstone belts (Fig. 2), there are abundant decametre-scale of foliated, amphibolite-grade lenses of basaltic metavolcanic rocks within the OPB gneisses. The foliation in these metavolcanic rocks trends parallel to the S_1 metamorphic layering in the surrounding gneisses.

The AGB-OPB contact is not clearly exposed in the area of Figure 2. Rock exposures are sparse along that contact which is locally mask~~ed~~ by syn- and post-orogenic intrusions, such as the Barlow pluton in the Chibougamau area (Fig. 2) and the Canet and Maicasagi plutons (Sawyer and Benn, 1993; Goutier, 2005; Daoudene et al., 201~~3~~4) in the Lac-aux-Goéland area (Fig. 3). In the latter area, the Nomans tonalite, located to the south of the inferred AGB-OPB contact, shows the same structural style as the gneissic rocks of the OPB. S_1 trajectories within the tonalite (Fig. 5) indicate that it is a D_2-related structural dome that is attached to the OPB at depth (Goutier, 2005; Daoudene et al., 201~~3~~4). The occurrence of foliation-parallel, amphibolite lenses along the AGB-OPB contact has been considered as evidence for the structural imbrication of both terranes and the allochthonous nature of the AGB (Sawyer and Benn, 1993). We do not think that this boundary corresponds to a major displacement zone (see section 4 below), although S_1 appears there to be more intensely developed in both the metavolcanic rocks of the AGB and the OPB tonalites. S_1 trajectories are parallel to the AGB-OPB contact (Fig. 5), suggesting that it formed, or was transposed, during D_1. There are relatively few lineation measurements in the study area (Fig. 6). Sawyer and Benn (1993) reported SE-plunging mineral lineations in the hanging wall of the Lac

Matagami shear zone, a late (D_3) sinistral fault located west of the Lac-au-Goéland area, as well as down-dip lineations along the Barlow fault in the Chibougamau area. In this latter area, stretching lineations plunge moderately to the south, but locally show significant variations of orientation due to the proximity of syn- and post-tectonic intrusions (Bedeaux et al. 2021).

The Abitibi and Frotet-Evans greenstone belts share a similar internal geometry and relationships with the underlying plutonic rocks of the OPB. However, the Frotet-Evans greenstone belt is of higher metamorphic grade and structurally more complex than the AGB (see Gosselin, 1996). It occupies the core of a large-scale series of east-west-trending F_2 synclines (Figs. 2 and 5) within the OPB gneisses, some of them being marked, as for the AGB, by steeply dipping reverse faults on their limbs (Simard, 1987; Gosselin, 1996; Brisson et al., 1997a and 1997b).

In the study area, we did not observe unambiguous shear-sense criteria within the AGB-OPB contact zone. Along the AGB-OPB contact, there are numerous tonalitic to granitic dykes crosscutting basaltic amphibolites of the AGB (Fig. 4f). Most of these dykes are in irregular and diffuse contacts with the host rocks and are slightly to moderately foliated, suggesting ~~high-temperature~~high temperature syntectonic emplacement.

3.2 D_3 structures

The D_3 phase of regional deformation is more localized as compared to D_{1-2}. It is essentially associated with strike-slip displacement along NE- and NW-trending shear zones. The Nottaway River shear zone (Figs 2 and 3) is the largest of the NW-SE-trending D_3 shear zones in the study area. It cuts across the D_{1-2} structures of both the AGB and OPB. It delimits the western boundary of the Frotet-Evans greenstone belt, which is also cut by another major NW-trending shear in its middle part, the Lucky Strike River shear zone (Fig. 2). A mylonitic S_3 schistosity is pervasively developed along these shear zones (Fig. 7a). F_3 dextral folds, with S_3 as an axial-planar foliation, can be observed in the vicinity of D_3 shear zones (Fig. 7b). S_3 hosts a well-developed, sub-horizontal stretching lineation (Fig. 7c), indicating that D_3 is dominated by strike-slip motions. Abundant macroscopic and microscopic shear-sense indicators, such as shear bands, S-C fabric~~s~~ (Fig. 7a and 7d), mica fish (Fig. 7e), drag folds and asymmetrical boudinage (Fig. 7f) are widely present and attest for dextral displacement along the NW-SE-trending shear zones. NE-trending shears, such as the Lac Lamark shear zone (Fig. 2), are characterized by the same type of ductile fabric~~s~~ but are sinistral, as

indicated by regional mapping and the offset of marker horizons in the Chibougamau area (e.g. Chown et al., 1992; Daigneault et al., 2002). The two sets of strike-slip shear zones, NW- and NE-trending, form a conjugate system.

4. METAMORPHISM

In this section, we describe the metamorphic characteristics of rocks in the study area, from top to base of the AGB stratigraphy, and from the lower-grade rocks of the AGB towards the high-grade metamorphic units of the OPB.

The sedimentary rocks of the Opémisca Group, which occupy the core of regional F_2 synclines, do not show macroscopic evidence of metamorphic recrystallization. Primary sedimentary structures, such as bedding (Fig. 4~~c~~d), and pillow structures in volcanic rocks of the underlying Roy Group are frequently well-preserved (Fig. 8a). Low-grade metamorphic minerals, such as chlorite, sericite, epidote, and actinolite-tremolite progressively appear down into the stratigraphic pile and can be relatively abundant at the margins of synclines, indicating that the lowermost part of the Opémisca Group attained greenschist-facies. The metamorphic grade of these sedimentary rocks even reaches the amphibolite facies towards the AGB-OPB contact, specifically along the northern boundary of the Waconichi Lake syncline (Figs 2 ~~and 3~~) where the Opémisca metapelites contain biotite, garnet, and staurolite (Fig. 8b). Staurolite occurs as mcm-long, oblong-shaped and corroded crystals defining the S_2 foliation. Lithologies of the Opémisca Group also locally contain late- to post-kinematic metamorphic minerals such as, for instance, randomly oriented chloritoïds (Fig. 8c) suggesting late-stage growth.

The mafic rocks of the Roy Group were dominantly metamorphosed to the greenschist-facies (Allard et al., 1985). These rocks are pervasively chloritized and contain typical low-grade metamorphic minerals such as albite, epidote and actinolite-tremolite defining the S_2 schistosity. In the vicinity to the contact with the OPB, they contain, however, metamorphic minerals of higher temperature characteristic of the amphibolite facies. Actinolite-tremolite is there replaced by hornblende and biotite. Garnet is present and usually forms irregular patches that are preferentially distributed along the pillow margins of mafic volcanic flows (Fig. 8d). Garnet is frequently retrogressed into a mixture of epidote, amphibole and chlorite. Some basaltic amphibolites contain epidote porphyroblasts overprinting the composite S_{1-2} foliation as well as randomly oriented crystals of actinolite, suggesting retrogressive conditions after peak metamorphism.

Metamorphic conditions recorded by the OPB are more difficult to evaluate precisely, mainly because these rocks essentially consist of intermediate and felsic plutonic rocks. However, most of the mafic rocks of the Opatica contain hornblende+andesine assemblages, which, with the occurrence of rare garnet- or clinopyroxene, imply amphibolite-facies conditions (Sawyer, 1998). The intermediate and felsic gneissic rocks are commonly plastically deformed and show coarse-grain recrystallization textures. Feldspar and quartz crystals display evidence for syn-kinematic growth and recrystallization. Grain boundaries are cuspate and undulated (Fig. 8e), which is indicative of extensive high-temperature grain boundary migration during deformation (Gower and Simpson, 1992). Myrmekitic textures preserved in some coarse-grained K-feldspars also indicate metamorphic temperatures in excess of 500-550°C (Simpson, 1985; Simpson and Wintsch, 1989). All these observations indicate that the regional D_1 deformation structures in the OPB gneisses were acquired at amphibolite-facies conditions of metamorphism, or higher. Some felsic rocks display quartz grains with a chessboard texture, which is typical of intra-crystalline slip textures developed at subsolidus temperatures (i.e. above 600°C; Blumenfeld et al., 1986; Gapais and Barbarin, 1986; Mainprice et al., 1986; Schmid and Casey, 1986). Evidence for anatectic melting is abundant in the deepest crustal domains of the OPB and marked by the occurrence of migmatites (Fig. 8f). Anatectic melt occurs in D_2 shear~~s~~ zones located near to the center of the OPB (Sawyer and Benn, 1993). However, according to Sawyer (1998), melting is late- to post-D_1, as suggested by S_1 disappearing within neosome patches and paleosome material showing remnants of the S_1 foliation.

There are very few pressure-temperature (P-T) studies for metamorphic rocks of the AGB. At the scale of the belt, regional metamorphism ranges in grade from subgreenschist-facies to the greenschist-amphibolite facies transition. In the Blake River and Tisdale assemblages (Fig. 1b), low-pressure regional metamorphism is indicated both by the occurrence of the actinolite-oligoclase zone, and the persistence of pre-regional metamorphism andalusite. According to Powell et al. (1995), pressure of regional metamorphism and of late to post-orogenic contact metamorphism were similar (360-400 MPa), indicating that low-pressure conditions persisted throughout the tectonic evolution of the AGB. Regionally, isograds dip shallowly to the north and trend subparallel to lithological and structural trends (Powell et al., 1995; Faure, 2015). In the Chibougamau area (Fig. 2), Bedeaux et al. (2020) suggested P-T conditions of 550±50ºC and 6±1.2 kbar for basaltic amphibolites of the AGB cropping out in the vicinity of the contact with the OPB. In the

OPB, Sawyer (1998) determined a peak metamorphism temperature of 760ºC for the migmatite facies rocks, and pressures of 5.2-6.2 and 6.3-7.1 kbar for diatexite migmatites and adjacent amphibolites, respectively. Pressure measured in the Canet pluton of the Lac-au-Goéland area (Fig. 3) were significantly lower, at 1.7-2.6 kbar (Sawyer, 1998), suggesting that the emplacement of this pluton occurred during exhumation of the OPB gneisses.

Figure 9 presents a series of north-south trending, interpretative structural profiles between the Lac-au-Goéland (profile A-A') and the Chibougamau areas (profile D-D'). These profiles show that the OPB exposes deeper crustal rocks and higher-grade metamorphic rocks as compared to the adjacent and overlying volcanic rocks of both the Frotet-Evans and Abitibi greenstone belts, and that both the OPB and AGB originally constituted an almost continuous middle-lower (the OPB) to upper crust sequence (the AGB). This contrasts with Sawyer and Benn's (1993) interpretation showing the Frotet-Evans greenstone belt as a far-travelled, south-directed allochthonous nappe thrusted over the OPB gneisses, and both units forming a basement-cored nappe thrusted southward over the AGB (see their ~~F~~figures 6 and 8). We think that their structural interpretation is unlikely for the following reasons, (i) in typical crustal-scale thrust systems (Boyer and Elliott, 2002; Butler and Bond, 2020), older rock units and/or higher grade (deeper) metamorphic rocks are transported over younger and/or lower grade (shallower) metamorphic rocks, which is obviously not the case here, and (ii) it would imply that the Frotet-Evans greenstone belt represents a klippen that roots 50 km, or more to the north, in the Colomb-Chabouillé Group of the Nemiscau subprovince along its southern ~~the~~ boundary with the OPB (see Fig. 2); there are, however, no metamorphic break and major suture between the Nemiscau and Opatica subprovinces, and regional mapping and structural analyses rather suggest the relative exhumation of the OPB as compared to the Nemiscau (Pedreira-Perez et al., 2020), which do~~es~~ not fit the Sawyer and Benn's (1993) thrusting model.

5. $^{40}Ar/^{39}Ar$ GEOCHRONOLOGY

In the following section, we present thirty-one $^{40}Ar/^{39}Ar$ laser probe experiments on single grains of amphibole, biotite and muscovite from eighteen rock samples from both the AGB and OPB.

5.1 Analytical method and procedures

Single grains of amphibole, biotite and muscovite were handpicked under a binocular microscope from 250μm to 1000μm mineral fractions. Separated minerals were irradiated with Cd-shielding, in the 5C high neutron flux facility of the McMaster Nuclear Reactor (Hamilton, Ontario, Canada). This process lasted 298 h with a global efficiency (J/h) of 5.83×10^{-5} h^{-1}. The irradiation standard was amphibole Hb3gr (Turner et al. 1971; Roddick 1983, Jourdan et al. 2006; Jourdan and Renne 2007); 1081.0 ± 1.2 Ma according to Renne et al. (2010, 2011).

Single grains of amphibole, biotite and/or white mica were analyzed by the $^{40}Ar/^{39}Ar$ method in step-heating using a CO_2 laser probe coupled with a MAP 215 mass spectrometer. The analytical procedure is described by Ruffet et al. (1991, 1995, 1997). The five argon isotopes and the background baselines were measured in eleven cycles, in peak-jumping mode. Blanks were performed routinely each first or third/fourth run and subtracted from the subsequent sample gas fractions. All isotopic measurements account for K and Ca isotopic interferences, mass discrimination and atmospheric argon contamination. Apparent age errors are plotted at the 1σ level and do not include the errors on the $^{40}Ar^*/^{39}Ar_K$ ratio, age of the monitor and decay constant.

A plateau is obtained when calculated $^{40}Ar^*/^{39}Ar_K$ ratios of at least three consecutive steps, containing a minimum of 70% of the ^{39}Ar released, agree with the weighted mean calculated $^{40}Ar^*/^{39}Ar_K$ ratio of the plateau segment. This 70% threshold is a requirement criterion that we use in all our geochronological studies, and it is much more restrictive than the 50% threshold set subjectively (in their own words) used by Fleck et al. (1977) and still adopted by most users of the $^{40}Ar/^{39}Ar$ method (e.g. Schaen et al., 2021). Since the amount of $^{39}Ar_K$ released is not a disqualifying criterion, we use the concept of pseudo-plateau (Cheilletz et al., 1999), which meets the same statistical criteria except for the cut-off threshold (<70% of $^{39}Ar_K$), and which is much more efficient for the analysis of complex mineral phases. In our detailed analysis of spectra, we also use a plateau-like descriptive terminology which refers to a weighted average age calculated over segments of apparent ages, not necessarily joined (e.g. edges of a saddle-shaped segment), but which are considered to be geologically significant. The errors on the $^{40}Ar^*/^{39}Ar_K$ ratio and age of the monitor and decay constant are included in the final calculation of the error margins on the pseudo- and plateau ages or for apparent ages individually cited. $^{40}Ar/^{39}Ar$ ages are provided with 1σ errors. Analytical data, parameters used for calculations (isotopic ratios measured on K and Ca pure salts; mass

discrimination; atmospheric argon ratios; J parameter; decay constants, etc.) and reference sources are available in the complementary data repository.

5.2 Isotopic closure temperatures

A radiochronological system is the combination of the crystal lattice of a mineral phase and an isotopic pair consisting of a radiogenic element and its radioactive precursor, e.g. $^{40}Ar^*$ and ^{40}K, the latter (K) being or not a constituent of the lattice. The analysis of isotopic systems, particularly those involving noble gases, has long focused on the behaviour of the radiogenic element, in this case $^{40}Ar^*$, the host minerals being themselves considered inert and the fate of the isotopic system being exclusively governed by the diffusion of the gas under temperature control, as described by Fick's laws. This led to the notion of isotopic blocking temperature initially introduced by Jäger et al. (1967), formalized as the isotopic closure temperature (T_c) by Dodson (1973) and then nuanced with the notion of isotopic closure window by Dunlap (1997). Therefore, during cooling and for a given isotopic system (mineral and isotopic pair), the isotopic chronometer initializes when diffusion becomes negligible because the temperature has dropped below its isotopic closure temperature.

T_c for amphibole is difficult to estimate. In addition to the effect of cooling rate and size of diffusion domains, amphibole diffusivity is influenced by ionic porosity (Fortier and Giletti, 1989; Dahl, 1996). On the basis of natural hornblende compositions, Dahl (1996) suggested a T_c range of 480-550°C, which has been re-evaluated at 550-560°C by Villa (1998) on the basis of Kamber's et al. (1995) experiments suggesting that, depending on the crystal lattice characteristics, hornblende may form a closed system to Ar diffusion at temperature as high as 580°C and a cooling rate of 0.7°K/Ma (Villa et al., 1996). In this study, we will therefore consider a median T_c range value of 550-600°C for amphiboles.

T_c for biotite ranges from 250°C to 400°C (Harrison et al., 1985; Montigny, 1985; McDougall et Harrison, 1988; Spear, 1993). In the absence of deformation and fluid-related recrystallization, it may be at least as high as ~450°C (e.g. Villa and Puxeddu, 1994). With diffusion domains in the range 100-1000 μm and a cooling rate lower than 100°C/Ma, T_c for biotite is ca. 400°C (e.g. Grove and Harrison, 1996). We will here consider a T_c-biotite range value of 350-450°C.

Purdy and Jäger (1976) originally estimated T_c of white micas at 350°C, by calibration of isotopic ages versus metamorphic grade. This estimate was erroneous and underestimated (Villa, 1998). Subsequent studies have shown that in the absence of deformation and fluid-

enhanced recrystallisation, T_c for muscovite may reach 500°C (Villa, 1998; Bosse et al., 2005), and even temperatures higher than 550°C for phengite under blueschist facies metamorphic conditions (Lister and Baldwin, 1996). Using experimental muscovite diffusion coefficients yielded by Harrison et al. (2009), Pitra et al. (2010) calculated a 390-590°C isotopic closure temperature range for white micas, using various effective diffusion radii (100 to 1000 μm) and cooling rates (1 to 1000°C/Ma). Considering diffusion domain sizes of 100-1000 μm and cooling rates between 1°C and 10°C/Ma, a more reasonable and realistic assessment for the cooling of Archean rocks (e.g. Chardon et al., 2009), isotopic closure of white micas would occur in the temperature range 400-500°C.

The use of above T_c range estimates should only concern crystals unaffected by deformation and/or recrystallization processes, (e.g.Villa, 1998). In contexts where these phenomena occur, the other component of the radiochronological system, the crystal lattice of the mineral carrying the istopic system, must also be considered because it may no longer remain inert. Deformation can damage crystal lattices, enhances Ar diffusion, and promotes the formation of intra-crystalline domains with lower diffusion length-scales and lower T_c. In the presence of fluids, minerals (or intracrystalline sub-domains) may recrystallize and neo-grains may possibly grow, two configurations which, if they occur at $T \leq T_c$ and after initial isotopic closure, will induce the recording of younger ages. Consequently, distinct intra-crystalline domains with different chemical and isotopic compositions, and thus distinct ages, may coexist within the same mineral/grain.

Cheilletz et al. (1999), Alexandrov et al. (2002) or Tartese et al. (2011) identified and detailed a process of sequential fluid-assisted resets of K-Ar isotopic chronometer of white mica from leucogranites. Tremblay et al. (2020) showed that K-Ar isotopic system of white micas from auriferous quartz veins and hosting shear zones of the Bourlamaque pluton (Val d'Or mining district, Abitibi) was driven by sequential dynamic recrystallization (dissolution/recrystallization/neocrystallization/aggregation) linked to successive periods of fluid circulation and deformation which occurred below T_c. Dunlap (1997) suggested that, during ductile deformation, K-Ar isotopic system of white micas from mylonites could also be partly driven by neocrystallization processes below T_c, at 250-350°C. $^{40}Ar/^{39}Ar$ amphibole analyses (e.g. Tremblay et al., 2020) suggest that they also behave in the same way.

5.3 Data processing

Metamorphic minerals such as amphiboles and micas extracted from rocks deformed or disturbed by fluids are usually texturally complex (recrystallized, composite grains, etc). The $^{40}Ar/^{39}Ar$ analysis of such crystals is very useful, as information it provides integrates the effects of the disturbing processes and therefore the timing of their occurrence, even if this occurs below Tc (e.g. Cheilletz et al. 1999; Hames et al., 2008; Castonguay et al., 2007; Tremblay et al. 2020). Hence, due to the complexity of $^{40}Ar/^{39}Ar$ results that arise from the analysis of such materials, which are common in old rock series such as the Archean, their processing must go beyond the simple visual examination of age spectra.

De Putter et al. (2015), De Putter and Ruffet (2020) and Tremblay et al. (2020) presented and developed tools for the visualization and processing of complex $^{40}Ar/^{39}Ar$ systems. Three of these tools are classical: the plateau (Fleck et al., 1977) and pseudoplateau age (PPA) (Cheilletz et al., 1999) concepts, and the probability density diagrams, which have been first used for ^{39}Ar-^{40}Ar data by Deino & Potts (1992). Other tools are more atypical; (i) the degassing and the weighted age spectra, which were designed to visualize Ar degassing kinetics of $^{40}Ar/^{39}Ar$ experiments, and (ii) the resizing of age spectra which was developed to ensure their statistical representativeness.

Amphibole $^{37}Ar_{Ca}/^{39}Ar_K$ spectra transcribe the evolution of the Ca/K ratio ($^{37}Ar_{Ca}$ # Ca and $^{39}Ar_K$ # K with $^{37}Ar_{Ca}/^{39}Ar_K = CaO/K_2O$ / 2.179; Deckart et al., 1997) during step-heating (degassing) experiments. Hence, a flat $^{37}Ar_{Ca}/^{39}Ar_K$ segment (homogeneous Ca/K ratio) expresses the degassing of an amphibole component devoid of compositional zoning and/or inclusion of another mineral species.

5.4 Sampling strategy

To document and compare the tectonothermal history of the AGB and OPB on both sides of the contact zone, we performed a series of step-heating $^{40}Ar/^{39}Ar$ analyses of micas and amphiboles collected in metamorphic and plutonic units of both terranes. Sixteen samples are from the Lac-au-Goéland area, and two from the AGB-OPB contact in the Chapais-Chibougamau area. Sample locations are shown in figures 3 and 4 whereas their geographic coordinates are in Table 1.

Four amphibolite samples (YD0009A, YD0048A, YD0039A, and YD0100A) and a garnet-staurolite micaschist sample (JF4065A) are from the AGB. These rocks show a well-developed S_2 foliation marked by the preferred orientation of amphibole and/or biotite. In thin sections, hornblendes from sample YD0009A and tremolites/actinolites from sample

YD0039A are homogeneous and unaltered ~~(Fig. 8e)~~, whereas dark green hornblendes YD0048A and YD0100A show light-green rims or patches suggesting intracrystalline zonation during crystal growth or recristallization. Biotites from samples YD0009A and YD0100A are green-colored euhedral crystals whereas those from sample JF4065A (a metasedimentary rock) are dark-brown-colored euhedral ~~(Fig. 8c)~~. There is no optically discernible occurrence of secondary chlorite in these samples. Sample YD0037, from which were extracted amphibole and biotite grains, is a slightly deformed diorite that shows petrographic characteristics similar to the Rivière Inconnue Diorite (Fig. 3), which yielded a U-Pb zircon age of 2693.6 ± 0.6 Ma (McNicolls and Goutier, 2008).

YD0018B, YD0020A, YD0063A, YD0035A, JG1245A, and YD0101A are tonalite samples from the OPB. These tonalites are mainly composed of quartz and plagioclase and contain various amounts of amphibole and/or biotite, which mark the regional foliation (S_1). Amphiboles YD0018B, YD0020A, YD0063A and YD0101A are sub-automorphous. All samples contain green- to brown-colored biotites that are commonly euhedral and only rarely chloritized.

Four samples of quartz-feldspar porphyry dykes were selected in both the AGB (YD0023A, YD0048B, and YD0009B) and the OPB (YD0023A). These dykes contain randomly oriented, coarse-grained muscovite crystals lacking microscopic evidence of recrystallization and/or deformation. A biotite grain from sample YD0009B was also analysed.

Two mylonite rock samples, YD0055A and YD0059A, from the Nottaway River shear zone were analysed. Sample YD0055A is a felsic rock belonging to the AGB. It shows a well-developed mylonitic foliation and contains abundant asymmetric muscovite crystals showing mica fish structures indicative of dextral shearing. These muscovite crystals also show secondary rims of neoformed micas typical of recrystallization. Sample YD0059A is a foliated tonalite from the OPB, it contains coarse-grained biotites that appear slightly altered and corroded. Most of these biotite grains also show fine rims of recrystallization.

Finally, we analyzed one sample of syenite of the Montviel alkaline intrusion (Goutier, 2005), which is associated to a carbonatite facies that has been dated at 1894 ± 4 Ma (U-Pb on zircons; David et al., 2006).

5.5 Results.

The step-heating $^{40}Ar/^{39}Ar$ results are presented on Figures 10 to 14. The distinct age spectra provided by duplicate analyses of amphibole and mica presented in the following sections confirm, as already stressed by Tremblay et al. (2020), that the interpretation of Archean material using the $^{40}Ar/^{39}Ar$ method is challenging and requires a detailed analysis of results.

5.5.1 The Abitibi Greenstone Belt.

The $^{40}Ar/^{39}Ar$ results for the AGB amphiboles and biotites are show in Figure 10. Analysis of amphibole 1 from sample YD0037A provides a rather flat age spectrum, with nevertheless a deflection of apparent ages in the intermediate temperature steps (Fig. 10a). The apparent ages, which are concordant on both sides of that deflection, allow the calculation of a plateau-like age at 2680.1 ± 3.6 Ma (56.3% of the total $^{39}Ar_K$ released), whereas the base of the deflection yields 2637.2 ± 9.0 Ma. The deflection of apparent ages is interpreted as the expression of partial recrystallization due to a disturbing event younger than c. 2637 Ma of an amphibole grain whose isotopic system initially closed at c. 2680 Ma during cooling of the diorite below Tc. Degassing peaks expressed during this experiment confirm the coexistence of these 2 radiogenic components. The higher degassing rate of the oldest component, at c. 2680 Ma, in the first part of the spectrum and the homogeneous isotopic composition on that segment indicate that it is perfectly individualised, which is, however, apparently not the case for the younger component associated with recrystallization in the intermediate temperature domain of the spectrum where the two radiogenic components overlap. The concomitant decrease of apparent ages (from c. 2749 Ma to c. 2681 Ma), combined with calculated $^{37}Ar_{Ca}/^{39}Ar_K$ (#Ca/K) ratios (from c. 9.7 to 7.2) in the low to intermediate temperature steps of age, the $^{37}Ar_{Ca}/^{39}Ar_K$ spectra of amphibole 2 of sample YD0037A and the overall saddle shape of the age spectrum suggest the incorporation of excess argon. Calcic domains constitute reservoirs for excess argon as shown by Ruffet et al. (1990) for rimmed and patchy-zoned hornblendes. However, the convergence between the pseudo-plateau age calculated for the bottom of the saddle, at 2683.7 ± 4.9 Ma (15.4% of the total $^{39}Ar_K$ released), and the plateau-like age calculated for amphibole 1 supports the above estimated age (c. 2680 Ma) of an initial isotopic closure of amphiboles from YD0037A. The concordant plateau age at 2678.5 ± 2.9 Ma (85.6% of the total $^{39}Ar_K$ released), calculated from age spectrum of a biotite from sample YD0037A (Fig. 10a), is consistent with that interpretation and suggests a fast cooling path for that poorly-deformed diorite.

The two amphiboles of sample YD0039A, although appearing homogeneous and unaltered, also yielded distinct age spectra (Fig. 10b). Amphibole 1 yields a plateau age at 2673.1 ± 4.0 Ma (86.6% of the total $^{39}Ar_K$ released), slightly younger than the inferred age of initial closure for amphibole YD0037A, whereas amphibole 2 yielded a disturbed age spectrum showing an overall increase of apparent ages from c. 2548 Ma to c. 2620 Ma. These discrepancies are reflected in the respective $^{37}Ar_{Ca}/^{39}Ar_K$ spectra of the two experiments, which differ in terms of ratio values and overall trend for low to intermediate temperature steps. Microscopic observations reveal that some amphibole grains of YD0039A contain biotite lamellae along cleavage planes, which is attested by the presence of a small degassing peak in the first heating steps of the staircase-shaped age spectrum (amphibole 2 of Fig. 10b). If these biotite lamellae are as young as the biotite of amphibolite YD0009A (c. 2564 Ma, see below), as suggested by a low temperature pseudo plateau at 2548.3 ± 5.6 Ma, their degassing, partly concomitant with that of amphibole, may account for the staircase shape of the age spectrum. Since amphiboles from sample YD0039A are tremolite/actinolite rather than hornblende, their calculated $^{37}Ar_{Ca}/^{39}Ar_K$ ratios are significantly higher (>20) than those of the other amphiboles (hornblende), which are usually <10 (Figs. 10a, 10c, 10d and 10e).

Except for a weak deflection of apparent ages in the intermediate to high temperature steps, the age spectrum of amphibole YD0009A (Fig. 10c) yields a plateau-like age of 2677.3 ± 3.6 Ma (77.8% of the total $^{39}Ar_K$ released), which is concordant with the c. 2675-2680 Ma amphibole cooling age calculated for samples YD0037A and YD0039A. A green biotite grain from YD0009A yields a plateau age approximately 110 m.y. younger at 2564.3 ± 3.4 Ma (97.7% of the total $^{39}Ar_K$ released; Fig. 10c). However, the increase of apparent ages of its high temperature steps, up to c. 2571 Ma (Fig. 10c), possibly testifies to a nearly complete reset of its isotopic system at or after c. 2560 Ma and subsequent to its initial closure. The above-mentioned subtle deflection of amphibole age spectrum probably correlates with the younger apparent ages (from c. 2612 to c. 2630 Ma) of the low temperature steps, which are characterized by $^{37}Ar_{Ca}/^{39}Ar_K$ (#Ca/K) ratios lower than those of the main phase at c. 2678 Ma (c. 5 vs. c. 6.5). These low-temperature steps define a specific degassing peak that probably express, as for amphibole YD0039A (see above), the degassing of scarce biotite lamellae plated in amphibole cleavage planes (e.g. Castonguay et al., 2001).

The age spectrum of amphibole YD0048A (Fig. 10d) is consistent with thin section examination which shows light-green rimmed and/or patchy zoned minerals indicative of patchy recrystallisation of amphiboles. The isotopic record of cooling at c. 2675-2680 Ma

691 shown by samples YD0037A, 39A and 0009A was erased, at least locally on a grain scale,
692 during a recrystallisation event at 2643.9 ± 3.5 Ma. The analysis of the degassing rate of
693 amphibole YD0048A supports this interpretation because, unlike amphibole YD0037A, the
694 main radiogenic component (i.e. expressed by the highest degassing rate; Fig. 10d) is the
695 radiogenic component associated with recrystallisation.
696 The light-green rimmed and/or patchy zoned amphibole from sample YD0100A,
697 texturally similar to those of YD0048A, provides a roughly flat but bumpy age spectrum (Fig.
698 10e) that yields a plateau-like age at 2598.3 ± 3.0 Ma (67.3% of the total 39ArK released),
699 younger than amphibole cooling and/or disturbance ages of previous samples. It may
700 represent the best estimate of the age of the post-initial cooling disturbance recorded by
701 amphibole 1 from diorite YD0037A. A green euhhedral biotite grain from sample YD0100A
702 provides a hump-shaped age spectrum with maximum apparent ages at c. 2494 Ma. This age
703 spectrum shape indicates that the biotite grain is chloritized (Ruffet et al., 1991), which casts
704 doubt on the reliability of this age.
705 A brown biotite grain from sample YD4065A yields a staircase-shaped age spectrum
706 whose flat segment defined by high temperature steps provide a pseudo-plateau age at 2644.3
707 ± 3.6 Ma (Fig. 10f). Such a staircase-shaped age spectrum is typical of ^{40}Ar* loss by volume
708 diffusion induced by a thermal event subsequent to initial crystallization and/or cooling (e.g.
709 Turner, 1968). The apparent age at 2571.8 ± 9.4 Ma of the low-temperature step provides a
710 maximum estimate for the age of that ^{40}Ar* loss event. Its concordance with the plateau age
711 yielded by biotite from sample YD0009A suggests that ^{40}Ar* loss most likely occurred
712 around c. 2560 Ma. In this scenario of ^{40}Ar* loss, the age at c. 2644 Ma calculated from the
713 high-temperature steps should only be a minimum estimate of the age of isotopic closure
714 during initial cooling. Nevertheless, its perfect agreement with the recrystallization age of
715 amphibole YD0048A, also at c. 2644 Ma, argues for its validity.
716
717 ***5.5.2 The Opatica Plutonic Belt.***
718 Amphibole and biotite age spectra from the OPB are show in Figure 11. All samples
719 were collected in tonalites.
720 Amphibole age spectra of samples YD0018B, YD0020A, YD0063A, and YD0101A
721 are more disturbed than those of the AGB. The effects of thermal disturbances following
722 initial isotopic closure appear to be quite significant, especially those related to an event
723 equivalent to the c. 2644 Ma disturbance recorded by the AGB amphiboles. The analysis of

degassing patterns of amphiboles YD0020A and YD0063A (Figs. 11a and b) indicates that the radiogenic component associated with partial recrystallization induced by this disturbing event constitutes the main radiogenic component of these amphiboles. Related segments of age spectra allow the calculation of concordant plateau ages at 2644.5 ± 3.8 Ma (72.6 % of the total $^{39}Ar_K$ released) and 2648.4 ± 3.0 Ma (69.6 % of the total $^{39}Ar_K$ released), respectively.

Several elements of the $^{40}Ar/^{39}Ar$ experiments suggest that this latter event affected amphiboles with initial ages of 2670-2665 Ma, which correspond to the apparent age bracket yielded by high-temperature steps of amphiboles YD0020A and YD0063A (Figs. 11a and b), at 2668.8 ± 8.9 Ma and 2672.3 ± 8.9 Ma, respectively. The validity of these high temperature apparent ages is supported by consistencies with pseudo-plateau ages at 2665.6 ± 4.4 Ma and 2668.9 ± 5.3 Ma calculated from the disturbed age spectra of amphiboles YD0018B and YD0101A (Figs. 11c and d). The degassing patterns of the latter amphiboles, especially YD0101A (Fig. 11d), indicate that the related radiogenic component is a major component of their respective isotopic system. However, some aspects of the age spectrum shapes of YD0018B and YD0101A remain enigmatic; for instance, the breakdown of the high-temperature apparent ages of amphibole YD0018B (down to 2588.8 ± 9.2 Ma, Fig. 11c) coinciding with an abrupt and unusual drop of the $^{37}Ar_{Ca}/^{39}Ar_K$ ratio (down to c. 2.69), which may be due to the degassing of a non-amphibolitic component. In addition, the concomitant increase of the high temperature $^{37}Ar_{Ca}/^{39}Ar_K$ (#Ca/K) ratios of amphibole YD0101A and decrease of apparent ages (Fig.11d) are unexpected. Such unusual behaviours may be due to a younger disturbing event, as suggested by biotite plateau ages at 2600.3 ± 3.0 Ma (94.8 % of the total $^{39}Ar_K$ released), 2583.4 ± 4.5 Ma (70.7 % of the total $^{39}Ar_K$ released) and 2588.2 ± 3.5 Ma (96.3 % of the total $^{39}Ar_K$ released) yielded by samples YD0020A, YD0063A and YD0035A, respectively (Figs. 11a, b and e). The existence of even younger disturbing events is suggested by biotites YD1245A (pseudo-plateau age at 2544.3 ± 3.5 Ma) and YD0101A (plateau age at 2525.4 ± 3.1 Ma) (Figs. 11d and f). However, the chlorite alteration of some biotite grains (hump-shaped age spectrum YD1245A) and/or the apparent occurrence of $^{40}Ar^*$ loss (staircase-shaped age spectrum YD0101A) makes these latter age estimates hazardous.

5.5.3 Granitic dykes.

Three muscovite single grains from quartz-feldspars granitic dykes collected in the Lac-au-Goéland area, YD0009B, YD0023A and YD0048B, provided rather disparate results

(Fig. 12). The saddle-shaped age spectrum of muscovite YD0009B (Fig. 12a) suggests the presence of two radiogenic components whose coexistence probably relates to a fluid-induced partial recrystallization, (e.g. Cheilletz et al., 1999; Alexandrov et al., 2002; Castonguay et al., 2007; Tartèse et al., 2011; Tremblay et al., 2011; 2020). In such type of spectra, the plateau-like age at 2602.1 ± 4.5 Ma (85.6 % of the total $^{39}Ar_K$ released; Fig. 12a) yields a minimum age estimate of the former muscovite, which was partially recrystallized at or after 2567.2 ± 6.2 Ma, i.e. the apparent age yielded by the base of the saddle. The degassing pattern and the weighting of this age spectrum indicate that the older component is overwhelmingly the main radiogenic component to which it is reasonable to attribute an age of c. 2603 Ma. (Fig. 12a).

Muscovite YD0048B provides a plateau age at 2517.2 ± 2.4 Ma (93% of the total $^{39}Ar_K$ released; Fig. 12b) but a detailed examination of that age spectrum reveals a complex thermal history for this mineral. Apparent ages increase steadily from low to high temperature steps, suggesting the occurrence, around 2500 Ma, of a disturbing event which induced $^{40}Ar^*$ loss by volume diffusion (Turner, 1968) on a muscovite grain older than c. 2524 Ma (Fig. 12b).

The first 30% of the $^{39}Ar_K$ degassing of muscovite YD0023A is highly disturbed (Fig. 12c) with erratic apparent ages which could result from the occurrence of interfoliar chlorite. Overall, this age spectrum shows a saddle shape, as for muscovite YD0009B, which allows the calculation of pseudo-plateau ages at 2603.2 ± 4.3 Ma (21.6% of the total $^{39}Ar_K$ released) for the base of the saddle and at 2627.1 ± 3.7 Ma (47.4% of the total $^{39}Ar_K$ released) for the high temperature steps (Fig. 12c). Our preferred interpretation is that muscovite YD0023A crystallized at the latest at c. 2627 Ma and has been affected by a fluid-induced partial recrystallization event at c. 2603 Ma, which has been coeval with initial crystallization of muscovite YD0009B (Fig. 12a).

5.5.4 The Nottaway River shear zone.

The analyzed muscovite of sample YD0055A belongs to a population of mica-fish muscovite grains (Fig. 7e) extracted from a felsic mylonite of the Nottaway River shear zone. As for muscovite YD0023A, the first 20% of the degassing spectra of YD0055A is highly disturbed (Fig. 13a), which can also reflect the occurrence of interfoliar chlorite. The remaining 80% of the degassing produces a multi-stepped age spectrum with a global staircase shape interspersed with three flat segments. Similar muscovite age spectra have been described by Tremblay et al. (2020) for Archean rocks of the southern Abitibi suprovince;

790 they were interpreted as the result of the aggregation, via dissolution/recrystallization/
791 neocrystallization of increasingly younger white mica sub-grains as deformation increments
792 and coeval fluid inflows progress. Pseudo-plateau ages calculated from the flat segments
793 suggest periods of aggregation/remobilisation of muscovite YD0055A at 2565.2 ± 3.7 Ma and
794 2504.0 ± 5.0 Ma, at the expense of a muscovite grain that would have initially crystallized at
795 2595.6 ± 5.4 Ma (Fig. 13a). These aggregation/remobilisation processes, which partially
796 preserve the previous or initial states of white micas, occur below their isotopic closure
797 temperature, at temperatures as low as 250-350°C.
798 Despite a possible plateau age at 2527.8 ± 2.9 Ma (76.2% of the total $^{39}Ar_K$ released),
799 the age spectrum of biotite YD0059A, with recrystallized rims (Fig. 13b), shows a regular
800 increase of apparent ages from low to high temperature steps, suggesting the occurrence of a
801 disturbing event at c. 2505.5 ± 8.5 Ma of an initial grain that would be older than c. 2531 Ma.
802 The highly disturbed age spectrum of an amphibole from that sample is useless (Fig. 13b).
803
804 ***5.5.5 The Montviel Syenite.***
805 Two amphiboles and a biotite from sample YD5143A from the Montviel Syenite (see
806 Fig. 3 for location) provide highly contrasted but significant results (Fig. 14). The age
807 spectrum of amphibole 1, a hornblende according to its $^{37}Ar_{Ca}/^{39}Ar_K$ ratio values of 4.0-4.2,
808 allows the calculation of a plateau age at 2653.9 ± 2.7 Ma (83.6% of the total $^{39}Ar_K$ released;
809 Fig. 14). The age and $^{37}Ar_{Ca}/^{39}Ar_K$ spectra of amphibole 2 are clearly different in the sense
810 that, from low to high temperature steps, both the apparent ages and $^{37}Ar_{Ca}/^{39}Ar_K$ ratios
811 increase in unusual proportions, from c. 1934.4 ± 7.3 to 2911.4 ± 10.8 Ma and 2.1 to 101.6,
812 respectively, which is not complying with what can be expected for hornblendes. The
813 unrealistic age of the fusion step (at c. 2911 Ma) and its $^{37}Ar_{Ca}/^{39}Ar_K$ ratio higher than 100
814 suggest the incorporation of excess argon, most likely by a calcic component resulting from
815 the alteration of the amphibole during a disturbing event which would have occurred at c.
816 1934 Ma or after (Fig. 14).
817 The age spectrum of biotite YD5143A is also strongly discordant with that of
818 amphibole 1. However, apparent ages of the base of its saddle shape, in the range c.1967-
819 1940 Ma (Fig. 14), are consistent with the timing of the disturbance that presumably
820 destabilized amphibole 2. The destabilisation process possibly results from the emplacement
821 of the nearby Montviel Carbonatite, whose age is constrained by a U–Pb zircon age of 1894 ±
822 4 Ma (David et al., 2006).

5.6 Interpretation and significance of $^{40}Ar/^{39}Ar$ ages

A synthetic compilation of all $^{40}Ar/^{39}Ar$ ages measured during this study is show in Figure 15.

The probability density diagram established from resized age spectra for amphiboles and biotites of the AGB (Fig. 15a) allows a synthetized interpretation of analytical results. On Figure1~~6~~5a, the principal age peak is at 2678.1 ± 1.7 Ma, as defined by amphiboles YD0009A and YD0039A, as well as amphibole and biotite of sample YD0037A. The concordance of biotite and amphibole ages suggests that they are cooling ages, and that this cooling has been relatively fast between 600°C and 400°C. The asymmetrical and stepped base of that peak toward younger ages reflects the impact of subsequent disturbing events on amphiboles after initial cooling. The first of these events occurs around c. 2644 Ma. It induced a partial recrystallization of amphibole YD0048A and probably the total reset of biotite YD4065A (Fig. 10f). The second disturbing event occurred around c. 2598 Ma (Fig. 15a) and induced the complete recrystallization of amphibole YD0100A (Fig. 10e). It would have been followed by a third event (with a frequency peak at c. 2564 Ma~~; Fig. 15a~~) that would have caused an almost complete age resetting of biotite YD0009A and a partial reset for micaschist biotite YD4065A (Figs. 10c, f and 15a).

Figure 15b suggests that OPB amphiboles initially cooled down to Tc at c. 2668 Ma, before a partial recrystallization event that occurred at c. 2647 Ma. Hence, there seems to be a ca. 10 m.y. time lag between the AGB and the OPB for initial cooling below Tc for amphiboles, at approximately 2678 Ma and 2668 Ma, respectively (Figs. 15a and b). The OPB tonalites also record a younger disturbing event around c. 2593 Ma (Fig. 15b). These two latter post-cooling events correlate within errors to those recorded by the AGB amphiboles at c. 2644 Ma and c. 2598 Ma (compare Fig. 15a and b).

The three analyzed muscovite grains from granitic porphyry dykes (Fig. 15c) are indicative of a complex and polyphased thermal history that can not be precisely understood here due to the small number of analyses. This thermal evolution may have started earlier than c. 2627 Ma and ended around c. 2495-2500 Ma (Fig. 15c). The effective occurrence of a disturbing event at c. 2602.7 ± 3.1 Ma, as reported on the probability density diagram of Figure 15c, remains however proven.

The initial crystallisation of muscovite YD0055A, around 2600 Ma (Figs. 13a and 15d), can be confidently attributed to shear deformation along the Nottaway River Shear

Zone. $^{40}Ar/^{39}Ar$ age data suggest that the shear zone was discontinuously active for, at least, ca. 100 m.y., from 2595.6 ± 5.4 Ma, the minimum age estimate for white mica initial crystallisation (or the complete resetting of the Ar «clock» of pre-existing muscovites) to final shear increments around c. 2500 Ma. However, this does not exclude the possible initiation of the Nottaway River Shear Zone before 2600 Ma.

$^{40}Ar/^{39}Ar$ analyses suggest that the Montviel Syenite (Figs. 14 and 15e) and the nearby carbonatite represent two different magmatic pulses, an older one related to syenite emplacement at c. 2654 Ma and a younger one corresponding to the carbonatite intrusion at c. 1894 Ma. This is, however, in contradiction with a model proposed by Nadeau et al. (2014) in which both the syenite and the carbonatite are attributed to a single phase of magmatism at 1894 Ma.

6. DISCUSSION

The tectonic evolution of Archean terranes involves extensive rifting/plume/arc magmatism and multiple, or progressive phases of deformation and metamorphism (e.g. Cawood et al., 2009; Bédard, 2018; Brown et al., 2020; Palin et al., 2020). Understanding the nature of the related geodynamic regime(s), and identifying the various alternative model(s) to the classical plate tectonics interpretation, if any, has important implications for a better comprehension of the early Earth dynamics, the processes that led to continental crust formation and structural evolution, including the mineral deposit potential of Archean orogenic belts (e.g. Thébaud and Rey, 2013).

6.1 The AGB-OPB contact – not a subduction suture.

Subduction is a geological process by which the lithosphere is recycled into the Earth's mantle at convergent plate margins, creating an upper plate-lower plate (UP-LP) boundary. Among the different mountain belts generated by plate convergence and collision during the Phanerozoic, a significant number took place in an environment of continuing subduction and accretion along sites of oceanic lithosphere consumption. These belts are known as accretionary orogens, zones of type-B subduction, or Cordilleran-, Pacific- and Andean-type collisions (see Cawood et al., 2009 for a review). A similar type of plate setting has been suggested for the AGB-OPB boundary, with the AGB acting as the down-going plate. Phanerozoic accretionary orogens are variably deformed and metamorphosed, and characteristically occur as paired and parallel high-temperature (HT) and high-pressure (HP)

belts with metamorphic grade up to granulite and blueschist-to-eclogite facies, respectively (e.g. Brown, 1993; 2010; Ernst et al., 1994). Such orogens typically include wedge-shaped accretionary prisms (or subduction mélanges) that formed at the UP-LP interface. These accretionary prisms are organized in thrust sheets and attributed to the offscraping and underplating of material from the descending oceanic plate and of subduction-related volcanic-magmatic arc system in the upper plate (e.g. Ernst et al., 1994; Cawood et al., 2009; Wakabayashi and Dilek, 2011; Kusky et al., 2020; Palin et al., 2020; among many others). A fore-arc basin generally occurs in between. Accretionary prisms are usually elongated and depending on the plate velocity, the dip of the subduction zone, the backstop geometry of the wedge and the volume ~~amount~~ of sediments on the down-going plate, they can be relatively voluminous. The Franciscan subduction complex, for instance, is at least 50 km-wide along a strike-length of c. 900 km (e.g. Ernst et al., 1994; Wakabayashi, 2017). Accretionary prisms are essentially made up of tectonic slices of island-arcs, backarcs, forearcs, dismembered ophiolites, granulite-facies and/or ultrahigh-pressure (UHP)-HP metamorphic rocks, and pre- to syn-accretion clastic sedimentary sequences. Thrusting and reverse faulting usually led to the imbrication of the upper plate rocks with those of the lower plate, leading to complex field relationships.

The subduction model proposed for the AGB-OPB boundary is mainly based on the Lithoprobe seismic profile (e.g. Calvert and Ludden, 1999) and field structures attributed to a south-verging fold-and-thrust belt in the AGB (Sawyer and Benn, 1993; Lacroix and Sawyer, 1995). However, the AGB-OPB transition does not show any of the characteristic features of UP-LP boundary as expected for a subduction suture. There are no accretionary prism and no metamorphic break along the AGB-OPB contact. Metamorphism varies progressively from low- to high-grade from the uppermost units of the AGB toward the plutonic rocks of the OPB (Fig. 9). There are, obviously, local fault contacts between greenschist- and amphibolite-grade rocks of the AGB, such as the Barlow fault in the Chibougamau area (Bedeaux et al., 2020), but these are late reverse faults related to regional folding. Our field observations and structural analysis indicate that the volcanic and sedimentary sequences of the AGB overly the TTG-type orthogneisses of the OPB (Fig. 9), suggesting that both domains likely formed a single structural unit prior to regional deformation (e.g. Benn, 2006; Benn and Moyen, 2008). Hence, we do not think that the AGB-OPB transition represents a subduction-related, upper plate-lower plate boundary.

~~It may be argued, however, that the subduction suture is rather located south of the~~

~~AGB-OPB boundary, at the contact between the Northern and Southern volcanic zones of the AGB, for instance, that it is marked by the Destor-Porcupine-Manneville (DPM) fault zone (e.g. Daigneault et al., 2002). Although the DPM fault zone represents a major deformation corridor, it does not bear the characteristic lithologies and metamorphic features of a fossilized, crustal-scale subduction suture. Moreover, a fossil subduction model for the DMP fault zone implies that the Northern Volcanic zone (the inferred upper plate) would be significantly older than the Southern Volcanic zone (the inferred lower plate), i.e. 2730–2710 Ma for the former and 2710–2695 Ma for the latter (Daigneault et al., 2002; see also Thurston et al., 2008). It is difficult, if not impossible, to imagine how the subduction of a «young» volcanic sequence can generate an older one in the overlying plate.~~

6.2 The formation of composite OPB-AGB – speculative models.

The structural relations and metamorphic characteristics of the AGB and OPB are reminiscent of various tectonic settings such as (i) metamorphic core complexes (MCC, Lister and Davies, 1989; Whitney et al., 2013), (ii) suprastructure-infrastructure transition (e.g. Culshaw et al., 2006; Stern, 2017), two models in which the upper crust is tectonically juxtaposed to the deep crust and/or upper mantle, and (iii) the convective overturn of crustal material (Collins et al, 1998; van Kranendonk, 2011; Bédard, 2018; Wiemer et al., 2018; Vanderhaeghe et al., 2019).

6.2.1 The OPB as a metamorphic core complex.

As compared to MCC's, the OPB shares similar features: (1) synkinematic granitoids, pegmatites and migmatites restricted to domal core domains; (2) sheet-like granitoids and discontinuous high-strain migmatites towards the contact with the overlying upper crust; (3) a décollement horizon (i.e. potentially, the OPB-AGB contact) between lower crustal gneisses and the upper crust; and (4) a normal metamorphic zonation. However, MCC's are generally less than 10 km in diameter, asymmetrical (e.g. the detachment being folded due to the bowing upward of the lower crust) and usually related to major continental extension (see Lister and Davies, 1989). In contrast to detachments of typical MCC's, the OPB-AGB contact has been involved in progressive reorientation and repeated late-intrusion. Moreover, the ductility and metamorphic contrasts across the OPB-AGB interface are not extreme as in typical MCC's in which the detachment separates rocks of highly contrasting structural and metamorphic character, with deformation in the cover rocks being typically brittle. Finally,

the abundant syn-tectonic granitoids of the OPB-AGB are not confined to the proximity of the detachment, as for MCC's, but extend into the interior of both the OPB and the AGB.

6.2.2 Superstructure-infrastructure transition.

In superstructure-infrastructure (S-I) transition zones, superstructure represents a low-grade upper crust level with early, typically upright structures, whereas infrastructure constitutes a high-grade migmatitic lower crust level with late, gently inclined structures overprinting the early structures of the overlying upper crust (Culshaw et al., 2006). In typical examples, a crustal-scale detachment shear zone is observed between the upper and lower tectonic levels (Tikoff et al., 2002; Culshaw et al., 2006; Stern, 2017). The infrastructure gneissic rocks generally yield radiometric ages younger than superstructure rocks, indicating that the infrastructure was hot, partially molten and weak during the deformation of the superstructure above it (e.g. Culshaw et al., 2006; Stern, 2017). The OPB presents evidence for anatectic melting and syn-kinematic migmatites formation at ca. 2.68-2.67 Ma (Sawyer, 1998), a melting event that, according to our $^{40}Ar/^{39}Ar$ data (Figs. 15a and b), has been almost coeval with or slightly followed the ca. 2680 Ma metamorphism in the AGB. This suggests a maximum time lapse of 10 m.y. for metamorphic conditions between upper (AGB) and lower (OPB) crustal levels, which could fit with the S-I model data presented by Culshaw et al. (2006) for the Western Superior Province. In such interpretation, the amphibolite-facies rocks occurring towards the base of the AGB would define a low-angle detachment fault at the contact with deeper and hotter rocks of the OPB, a detachment that would has been subsequently folded and verticalized. In the study area, these amphibolites are several km-thick (Bedeaux et al., 2020), and may thus reasonably represent a mid-crustal decoupling zone between a ca. 15 km-thick superstructure (the AGB) and a plutonic, TTG-rich infrastructure (the OPB). However, the occurrence of F_2 folds affecting the low-angle metamorphic S_1 layering in the OPB gneisses invalidates a typical S-I transition model. The metamorphic age variations can be simply related to the differential uplift and exhumation of both belts (the ABG first and then the underlying OPB). A S-I transition model is also inconsistent with age constraints from the Attic Complex (located in the southern part of the AGB; see Fig. 1b) where U-Pb zircon dating suggests a 20 m.y gap between the formation of migmatites in tonalitic gneisses (TTG's) of the lower crust (at ca. 2716.1 ± 2.9 Ma) and those in adjacent mafic volcanic rocks (at ca. 2695 ± 1 Ma) (Revelli, 2020). This has been attributed to the diapiric ascent and crustal melting of lower crustal intrusive material and the related burial

(and prograde metamorphism) of cold and dense greenstones of the upper crust (Revelli, 2020), which agrees with a convective crustal overturn as described below.

6.2.3 Convective crustal overturn.

The third tectonic setting involves the partial convective overturn of the crust (Fig. 16). It was originally proposed by Collins et al. (1998) for Archean rocks of the Pilbara craton (Australia). In such a setting, the OPB gneissic domes represent the diapiric response of density inversion created by the accumulation of a thick (ca. 15 km) greenstone cover (the AGB) erupted over a previously stable and more-or-less continuous sialic crustal basement ≥ 2.80 Ga, both domains being intruded by syn-volcanic and syn-tectonic TTG plutons ranging from c. 2.76 to c. 2.65 Ga (Davis et al. 1995; Sawyer, 1998; Daoudene et al., 201~~5~~6, Pedreira-Perez et al., 2020) (Figs. 16a and b). Diapirism is considered here as part of a larger process involving the partial convective overturn of the crust (Collins et al., 1998; Wiemer et al., 2018). We suggest that deformation initiated by sinking and subsidence of the thick cover of greenstones within a hot and weak (ductile), laterally flowing sialic lower crust that generated the S_1 metamorphic layering both in the OPB and the lowermost part of the AGB (Fig. 16a). This produced strong horizontal temperature gradients and related changes of metamorphic facies as, for instance, in thermal models of Thébaud and Rey (2013). Due to density contrasts, both the gneissic lower crust and crosscutting TTG's ultimately migrated upward passively as accommodation structures. Material flow into the AGB synclines would has been compensated by lateral and vertical migration of the less dense sialic substrate into the domal crests of the OPB (Fig. 16b), generating a pattern of partial convective overturns in the crust (Collins et al., 1998; Weinberg, 1997). The downflow of greenstones would has been almost entirely compensated by TTG uprises (Fig. 16c). Shallow interdome depressions developed and progressively filled with clastic sediments, ~~and progressively filled with clastic sediments; s~~ such clastic sequences occupying the core of greenstone synclines and being represented by sedimentary rocks of the Opémisca and Broadback groups within the Abitibi and Frotet-Evans belts, respectively. Some of these clastic sequences possibly formed as early as ca. 2750 Ma, as suggested by stratigraphic relationships between the Broadback Group and the underlying Frotet-Evans volcanics (Brisson et al., 1998; see section 2.1). In the Opémisca Group, ~~M~~maximum sedimentation age of the Haüy Formation ~~in the Opémisca Group~~ (≤ 2691.7 ± 2.9 Ma; David et al., 2007) is coeval, at least in part, with regional metamorphism in the AGB (see section 5.5). Part of the Opémisca Group therefore deposited during regional

deformation, as proposed for most sedimentary sequences of the Superior Province (e.g. Leclair et al., 1993; Parmenter et al., 2006; Lin et al., 2013). As the greenstones and overlying sedimentary rocks progressively flow deeper into the synclines, strain intensity increased and was accommodated by horizontal shortening, the S_2 foliation became more pervasive and faults and shear zones with down-dip lineations developed (Fig. 16b). The Barlow fault (Bedeaux et al., 2021) is one of these; in the Chibougamau area, it is located along the northern flank of the Waconichi F_2 syncline (Waconichi basin on Fig. 2) and marked by upper crustal, south-dipping seismic reflectors (Mathieu et al., 2020). The Barlow fault is interpreted as a reactivated structure (Bedeaux et al., 2021), and it possibly belongs to a series of basin-bounding faults that accommodated the exhumation of the OPB gneisses and inverted during the following contraction (e.g. Mathieu et al., 2020), which is consistent with the interpretation shown on Figure 16. With time, the early generation of TTG's were progressively deformed and rotated into subconcordance with the steepening domal boundaries (Fig. 16c). Other TTG's were syn-kinematic and formed sheeted intrusions. Some of these did not move far from their source, remained heterogeneous, and can be better described as `intrusive diatexites' (Sawyer, 1998), whereas later intrusions tend to be larger, more discordant, less strongly foliated bodies and are more obvious near the AGB-OPB boundary, where they cut the OPB-AGB interface. Such an interpretation fits well with (1) the relative downflow of the AGB volcanic rocks as compared to the OPB gneisses (Fig. 9), (2) the distribution of S_1 foliations and lineations in the OPB domes (Fig. 2 and Fig. 6b), (3) the up-stratigraphy increasing proportion of plutonic clasts in polygenic conglomerates of both the Broadback and Opémisca groups (Brisson et al., 1997a; 1998; Charbonneau et al., 1991), which reflects the progressive erosion of volcanic cover rocks and underlying plutonic rocks in the source area, and (4) slightly higher pressure and temperature preserved in the OPB migmatites and amphibolites (6.3-7.1 kb and 750^{o}C, Sawyer, 1998) as compared to the amphibolite facies rocks of the AGB (c. 6 kb and c. 550^{o}C, Bedeaux et al., 2021).

$^{40}Ar/^{39}Ar$ age measurements performed during our study are in good agreement with that model. Amphibole ages suggest that the lowermost part of the AGB exhumed around 2678.1 ± 1.7 Ma (Fig. 15a). Ages from the OPB, at 2667.8 ± 3.0 Ma (Fig. 15b), suggest that it was more-or-less coeval with, or quickly followed the exhumation of the AGB, an event that we suggest has been coeval with decompression melting (Weinberg, 1997; Whitney et al., 2004) and the genesis of syn- to late-D_1 migmatites in the cores of OPB gneiss domes at 2.67-2.68 Ga (Sawyer, 1998; Fig. 16c). Then, both terranes share the same succession of thermal

disturbances at c. 2650-2645 Ma and 2600-2590 Ma, including the inferred onset of shearing along the Nottaway River Shear Zone at ca. 2600 Ma, as recorded by related mylonites (Fig. 15d) and quartz-feldspar porphyry dykes (Fig. 15c). Such a series of events is also documented in the Val d'Or mining district of the Abitibi subprovince (Tremblay et al., 2020). Besides, at the scale of the Superior Province, there is accumulating geochronological evidence for major crustal deformation event(s) and related metamorphism spreading over a timeframe much larger than suggested in literature (e.g. Percival, 2007). Easton (2000), for instance, argued that the distribution of metamorphic grade and age of metamorphism in the western Superior reflect a series of tectonic events between 2710 and 2640 Ma, which is in agreement with U-Pb zircon age constraints for metamorphism, syn-orogenic magmatism and deformation in the southern Abitibi subprovince (see Tremblay et al., 2020 for a review). North of the OPB, in the Opinaca subprovince, granulite-facies metamorphism spreads over ages varying from c. 2666 Ma to 2636 Ma (Morfin et al., 2013) whereas it even lasted down to ca. 2620–2600 Ma in supracrustal rocks of the La Grande subprovince (Fontaine et al., 2017, 2018). Combined with geochronological data from our study, this is a strong indication that peak and duration of regional metamorphism have been more-or-less coeval and long-lasting over a large region of the Superior Province, if not all over the Pontiac, Abitibi and Opatica subprovinces and beyond.

6.3 Significance of the Lithoprobe seismic reflector.

Seismic profiles showing shallow sub-horizontal to slightly dipping reflectors beneath Archean and/or Paleoproterozoic greenstone belts are relatively common. Some of these reflectors may be due, obviously, to tectonic events that are younger than, and not directly related to, the formation of the greenstone belts and, until the age of such reflectors can be determined, their bearing on the greenstone belt evolution remains speculative. However, assuming that the Lithoprobe seismic reflector of the Superior Province ~~shown in Figure 1~~ is an Archean artefact (e.g. Cawood et al., 2006) and that our interpretation of the AGB-OPB relations is correct, what can be the origin and significance of that reflector then? We envision two possibilities that we briefly discuss below, (i) mantle lithosphere imbrication (Fig. 17), and (ii) bending of a flat subduction rooted southward at the Pontiac-Abitibi interface (Fig. 18).

Gray and Pysklywec (2010) performed a series of forward numerical modeling of the thermo- mechanical evolution of continental lithosphere undergoing collision and orogenesis

under Neoarchean- like conditions for stratified mafic-to-felsic crustal domains overlying the mantle lithosphere. They have identified three dominant modes of mantle lithosphere deformation, (1) pure- shear thickening; (2) mantle imbrication; (3) and underplating. Their result for the mantle imbrication mode is reproduced on Figure 18. For that mode, numerical modeling shows that, due to a «hot» and weak lower crust, there is a decoupling between the mantle and the crust at a depth of approximately 40 km. The model shows that the lithospheric mantle becomes imbricated along major shear zones along which slices of crustal eclogites may occur, whereas the crustal domain itself essentially absorbs deformation by pure-shear thickening and folding. Gray and Pysklywec (2010) inserted a weak zone in the initial configuration of their numerical experiments ~~in order~~ to favor the onset and localization of deformation, and to mimic an original plate boundary (see their Figure 1) as well. Although that such a weak zone may has influenced the location of some shear zones within the mantle lithosphere, it did not lead to the formation of any shear zones (that could have been interpreted as a nascent subduction plane) in the upper crust. The modeled imbrication shown on Figure 17 is obviously unrelated to subduction since the crustal part of the lithosphere is not recycled into the mantle as in typical subduction settings. We think that mantle imbrications as shown by these results likely formed during the Archean and can account for deep seismic reflectors such as the Abitibi-Opatica Lithoprobe transect.

An alternative hypothesis that cannot be ignored is that the Lithoprobe seismic reflector may not represent the original location of an Abitibi-Opatica subduction zone, but the trace of a Pontiac-Abitibi subduction zone interface that flattened for several hundreds of km at depth and steepen at or close to the Abitibi-Opatica contact. Such shallow subduction flattening has been already invoked as a predominant tectonic regime during the Archean due to thicker and more buoyant oceanic lithosphere (e.g. Cawood et al., 2006). Flat subduction is documented on modern Earth. A typical example of it is the Mexican subduction zone where the young Cocos plate is shallowly subducting beneath central Mexico (Fig. 18a; Kim et al., 2012). This is well illustrated by the teleseismic imaging of a 500 km long transect between the Middle America trench to the south, and the Trans-Mexican volcanic belt (TMVB, the continental volcanic arc) to the north (Fig. 18b). This shows that subduction of the Cocos oceanic plate dips c. 15^{o} north for about 80 km along the coast, and then horizontally underplates the continental crust at c. 50 km-depth for c. 250 km northward. The slab then abruptly changes to a steeply dipping geometry at approximately 75^{o} as it bends right below the TMVB. The similarity of the geometry of the Cocos plate subduction zone and the

reinterpreted Abitibi segment of the Grenville-Abitibi seismic transect is striking (Fig. 18c), both in terms of depth and lateral extent of seismic reflectors. Hence, it is possible that the steeply north-dipping seismic reflector of the Abitibi Lithoprobe transect roots into the Pontiac-Abitibi interface rather than the AGB-OPB. The Pontiac-Abitibi contact would be then interpreted as a surface of former subduction and recycling of the oceanic crust that originally existed between the Pontiac and Opatica «basements», causing the underthrusting and burial of the Pontiac block below the Abitibi subprovince and accounting for ensuing tectono-metamorphism and magmatism (e.g. Dimroth et al., 1983; Card, 1990; Camiré and Burg, 1993; Davies, 2002; Frieman et al., 2017, among many others). This may possibly explain the contrasting pre-2700 Ma plume-driven constructive stage of the AGB as compared to its post-2700 Ma geodynamic evolution as depicted by Thurston et al. (2008) and Mole et al. (2021); the latter stage being mainly characterized, according to these authors, by subduction-related compressional lithospheric deformation, flysch sedimentation and more-or-less coeval emplacement of alkalic granodiorite, granite and syenite plutons (such as in the Preissac-Lacorne batholith). However, such an ~~this~~ uniformitarian interpretation for the Pontiac-Abitibi relations has been ~~recently~~ disputed by Piette-Lauzière et al. (2019) that argue for a multi-stage tectono-metamorphic evolution involving extensional tectonism and crustal delamination followed by re-accretion and subcretion of ribbon~~s~~ continents as suggested by Bédard (2018) for the Northern Superior.

CONCLUSION

Our structural and metamorphic analysis of the transition between the Abitibi and Opatica subprovinces does not confirm the former existence of north-dipping subduction between these two lithological assemblages, despite the occurrence of a major seismic reflector at depth. We think that both terranes originally formed a single and composite crustal sequence, the Abitibi and Frotet-Evans greenstone belts and associated sedimentary rocks representing the upper crust and the Opatica Plutonic Belt being the remnant of middle-lower crust plutonic domains. This implies that the Frotet-Evans belt originally formed an upper crust sequence that was continuous with the AGB. Although there is a lack of precise geochronological constraints for the Frotet-Evans belt, such an interpretation is consistent with available U-Pb age data from both greenstone belts. However, it does not mean that the Frotet-Evans belt has ever been as thick as the AGB (c. 10-15 km), since there are erosional unconformities on top of each volcanic sequences that may has removed more volcanic

material from the former belt (due to the progressive exhumation of the OPB; see Fig. 16) as compared to the AGB. Our interpretation also means that OPB-like orthogneissic massifs are likely to be exposed south of the OPB-AGB transition. We are not saying here that OPB gneisses are systematically present at depth below the AGB but that discontinuous masses of orthogneissic TTGs, more-or-less attached to each other and to the Opatica, are likely to occur and to be expose along the crest of antiformal/domal culminations within the Abitibi belt. Examples of such metamorphic domes may be represented by the Marest and Bernetz gneissic plutons in central Abitibi (Faure, 2015), which are currently interpreted as the crustal roots of volcanic arc(s) (Chown et al., 2002), and by the Attic Complex in the Lebel-sur-Quévillon area (Fig. 1b) that has been recently interpreted as the result of diapiric and sagduction-related processes (Revelli, 2020).

As for most Archean cratons, the structural evolution of the Opatica and Abitibi belts is the result of several episodes of regional deformation and metamorphism that spans several tens, if not hundred's, of million years. The main events, D_1 and D_2, are predominantly developed in the OPB and the AGB, respectively. S_1 is a penetrative amphibolite-grade foliation in the OPB gneisses and in metavolcanic rocks lying at the base of both the Frotet-Evans and Abitibi greenstone belts whereas S_2 is a medium- to low-grade regional schistosity of variable intensity in both the AGB and OPB. S_1 is subparallel to the OPB-AGB contact although it is frequently transposed into a composite $S_{1\text{-}2}$ fabric within the AGB. S_1 trajectories in the OPB define a dome-and-basin geometry that is the result of vertical transfert of middle- to lower-crustal material. The counterpart progressive burial of the AGB into synformal troughs generated the abrupt EW-trending S_2 schistosity and related down-dip mineral and stretching lineations. Amphiboles and micas $^{40}Ar/^{39}Ar$ ages measured in both the OPB and AGB suggest that exhumation of the latter started at $\geq$ 2678 Ma and was almost coeval with, or slightly followed, by the uplift and related migmatization of OPB gneisses at c. 2668 Ma or earlier. This is consistent with a diapiric convective overturn of the crust as illustrated on Figure 16. Both the OPB and AGB then shared the same magmatic and structural evolution, including the onset of dextral and sinistral transcurrent shearing and faulting at ca. 2600 Ma that may have lasted for c. 100 m.y. Comparison with adjacent areas suggests that magmatism and metamorphism have been coeval over a large region (Easton, 2000), which is consistent with pervasive deformation and slow cooling as expected for vertical tectonic models and diapiric magmagenesis and ascent during the evolution of the Archean Superior Province (e.g. Bédard and Harris, 2014; Bédard, 2018).

Declaration of Competing Interest.

The authors declare that they have no known competing financial interests or personal relationships that could have appeared to influence the work reported in this paper.

ACKNOWLEDGEMENTS

Y.D. benefited of a financial support from Mitacs-Acceleration and the *Ministère de l'Énergie et des Ressources* (MERN) du Québec for a postdoctoral fellowship at UQAM in 2014-16. The Natural Science and Engineering Council of Canada (NSERC) has provided research grants to A.T. (NSERC-PG105669). Thanks to A. Chabot-Bergeron, A.-S. Corriveau, P. Lamontagne-Hallé, A. Moïse, A. Nolet-Regaudie, T. Plasmodon-Tremblay, and C. Vézina for help and support during field work. Thanks are also due to Michèle Laithier for drawing some of the figures. We thank Dr Phil Thurston and three ~~an~~ anonymous reviewers for thoughtful comments that significantly improved the manuscript.

REFERENCES

Alexandrov, P., Ruffet, G., Cheilletz, A., 2002. Muscovite recrystallization and saddle-shaped $^{40}Ar/^{39}Ar$ age spectra: Example from the Blond granite (Massif Central, France). Geochim. Cosmochim. Acta 66, 1793-1807.

Allard, G.O., Caty, J.-L., and Gobeil, A. 1985. The Archean supracrustal rocks of the Chibougamau area. *In* Evolution of Archean Supracrustal Sequences. Ayres, L.D., Thurston, P.D., Card, K.D. and Weber, W. (eds). Geological Association of Canada; Special Paper 28, p. 55–63.

Bédard, J.H. 2018. Stagnant lids and mantle overturns: implications for Archean tectonics, magmagenesis, crustal growth, mantle evolution, and the start of plate tectonics. Geoscience Frontiers 9: 19-40.

Bédard, J.H. and Harris, L. 2014. Neoarchean disaggregation and reassembly of the Superior Craton. Geology 42: 951-954.

Bedeaux, P., Brochu, A, Mathieu, L., Gaboury, D. and Daigneault, R. 2020. Structural analysis and metamorphism of the Barlow Fault Zone, Chibougamau area, Neoarchean Abitibi Subprovince: implications for gold mineralization. Can. J. Earth Sci. 58.

Benn, K., 2006. Tectonic delamination of the lower crust during late Archean collision of the Abitibi-Opatica and Pontiac terranes, Superior Province, Canada. In: Benn K et al.

(Eds) Archean geodynamics and environments: American Geophysical Union, Geophysical Monograph 164, 267-282.

Benn, K., Moyen, J.F., 2008. The late Archean Abitibi-Opatica terrane, Superior Province: a modified oceanic plateau. In: Condie KC, Pease V (Eds). When didi palte tectonics begin on Planet Earth? Geological Society of America Special Paper 440, 173-197.

Benn, K., Sawyer, E.D., Bouchez, J.L., 1992. Orogen parallel and transverse shearing in the Opatica belt, Quebec: implications for the structure of the Abitibi Subprovince. Canadian Journal of Earth Sciences 29, 2429-2444.

Bleeker, W. 2003, The late Archean record: A puzzle in ca. 35 pieces. Lithos, 71, 99 – 134.

Blumenfeld, P., Mainprice, D., Bouchez, J.L., 1986. C-slip in quartz from subsolidu deformed granite. Tectonophysics 127, 97-115.

Boily, M., 2000. Géochimie des volcanites des ceintures volcano-sédimentaires de Frotet-Evans (CVFE) et de la Moyenne-Eastmain. Ministère des Ressources naturelles, MB 2000-12.

Bosse, V., Féraud, G., Ballèvre, M., Peucat, J.-J., Corsini, M., 2005. Rb-Sr and $^{40}Ar/^{39}Ar$ ages in blueschists from the Île de Groix (Armorican Massif, France): implications for closure mechanisms in isotopic systems. Chem. Geol. 220, 21-45.

Bosse, V., Féraud, G., Ruffet, G., Ballèvre, M., Peucat, J.J., de Jong, K., 2000. Late Devonian subduction and early-orogenic exhumation of eclogite-facies rocks from the Champtoceaux Complex (Variscan belt, France). Geol. J. 35, 297-325.

Boyer S.E.& Elliott D., 1982. Thrust systems. Bulletin of the American Association of Petroleum Geologists 66 (9), 1196-1230.

Brisson, H., Gosselin, C., Fallara, F, Gaulin, R., Dion, D.-J., 1998. Géologie de la région du Lac Evans. Ministère des Ressources naturelles, RG 98-06, 23 p.

Brisson, H., Gosselin, C., Baumier, M., Dion, D.J., Gaulin, R., Lefebvre, D.L., 1997a. Géologie de la région du lac Assinica (SNRC 32J/11). Ministère des Ressources naturelles, RG 96-11, 28 p.

Brisson, H., Gosselin, C., Baumier, M., Dion, D.J., Gaulin, R., Lefebvre, D.L., 1997b. Géologie de la région du ruisseau Lucky Strike (SNRC 32J/12). Ministère des naturelles, RG 96-10, 21 p.

Brown, M. 2010. Paired metamorphic belts. Gondwana Research 18: 46-59.

Brown, M. 1993. P-T-t evolution of orogenic belts and the cause of regional metamorphism. Journal of the Geological Society, London 150: 227-241.

1252 Brown, M., Johnson, T., and Gardiner, N.J. 2020. Plate tectonics and the Archean Earth. Ann.
1253 Rev. Earth Planet. Sc. 48: 291-320.
1254 Butler, R. and Bond, C. 2020. Thrust systems and contractional tectonics, *in* N. Scarselli, J.
1255 Adam and D. Chiarella, *eds,* Regional Geology and Tectonics: Principles of Geologic
1256 Analysis - Volume 1: Principles of Geologic Analysis, Elsevier, Netherlands, pp. 149-
1257 167.
1258 Calvert, A.J., Ludden, J.N., 1999. Archean continental assembly in the southeastern Superior
1259 Province of Canada. Tectonics 18 (3), 412-429.
1260 Calvert, A.J., Sawyer, E.W., Davis, W.J., Ludden, J.N., 1995. Archean subduction inferred
1261 from seismic images of a mantle suture in the Superior Province. Nature 375, 670-674.
1262 Camiré, G.E., and Burg, J.P., 1993. Late Archaean thrusting in the northwestern Pontiac
1263 Subprovince, Canadian Shield: Precambrian Research, v. 61, no. 1–2, p. 51–66, doi:
1264 10.1016/0301-9268(93)90057-9.
1265 Card, K.D., 1990. A review of the Superior Province of the Canadian Shield, a product of
1266 Archean accretion. Precambrian Research 48, 99-156.
1267 Card, K.D., Ciesielski, A., 1986. DNAG N°1 Subdivisions of the Superior Province of the
1268 Canadian Shield. Geoscience Canada 13, pp 5-13.
1269 Castonguay, S., Ruffet, G., Tremblay, A., 2007. Dating polyphase deformation across low-
1270 grade metamorphic belts: An exemple based on $^{40}Ar/^{39}Ar$ muscovite age constraints
1271 from the southern Quebec Appalachians, Canada. Geol. Soc. Am. Bull. 119, 978-992.
1272 Cawood, P.A., Kroner, A., Collins, W.J., Kusky, T.M., Mooney, W.D. and Windley, B.F.
1273 2009. Accretionary orogens through Earth history, *in* Cawood, P.A. and Kroner, A.
1274 (eds) *Earth accretionary systems in space and time.* The Geological Society, London,
1275 Special Publications, 318, p. 1-36.
1276 Cawood, P.A., Kröner, A., Pisarevsky, S., 2006. Precambrian plate tectonics: Criteria and
1277 evidence. GSA Today 16(7), 1-11.
1278 Charbonneau, J.-M., Picard, C., Dupuis-Hébert, L., 1991. Synthèse géologique de la région de
1279 Chapais-Branssat, Abitibi. Ministère des Ressources naturelles, MM 88-01, 189 p.
1280 Chardon, D., Gapais, D., Cagnard, F., 2009. Flow of ultra-hot orogens: A view from the
1281 Precambrian, clues for the Phanerozoic. Tectonophysics 477, 105-118.
1282 Cheilletz, A., Ruffet, G., Marignac, C., Kolli, O., Gasquet, D., Féraud, G., 1999. $^{40}Ar/^{39}Ar$
1283 dating of shear zones in the Variscan basement of Greater Kabyllia (Algeria). Evidence
1284 of an Eo-Alpine event at 128 Ma (hauterivian-Barremian boundary): Geodynamic

consequences. Tectonophysics 306, 97-116.

Chown, E.H., Daigneault, R., Mueller, W., Mortensen, J.K., 1992. Tectonic evolution of the Northern Volcanic Zone, Abitibi belt, Quebec. Can. J. Earth Sci. 29, 2211-2225.

Collins, W.J., Van Kranendonk, J., and Teyssier, C. 1998. Partial convective overturn of Archean crust in the east Pilbara Craton, Western Australia: driving mechanism and tectonic implications. J. Struc. Geol. 20:

Culshaw, N.G., Beaumont, C. and Jamieson, R.A. 2006. The orogenic superstructure-infrastructure concept: revisited, quantified and revived. Geology 34: 733-736.

Dahl, P.S., 1996. The effects of composition on retentivity of argon and oxygen in hornblende and related amphiboles: a field-tested empirical model. Geochim. Cosmochim. Acta 60, 3687-3700.

Daigneault, R., Allard, G.O., 1990. Le Complexe du lac Doré et son environnement géologique (region de Chibougamau - Sous-province de l'Abitibi). Ministère de l'Énergie, des Mines et des Ressources, Québec, MM 89-03, 275 p.

Daigneault, R.A., Mueller, W.U, and Chown, E.H. 2004. Abitibi greenstone belt platte tectonics: the diachronous history of arc development, accretion and collision, *in* Erikkson, P., Altermann, W., Nelson, D., Mueller, W., Catumeanu,O. and Strand, K., eds. Developments in Precambrian geology/tempos of events in Precambrian time: Amsterdam, Elsevier, p. 85-103.

Daigneault, R., Mueller, W.U., Chown, E.H., 2002. Oblique Archean subduction: accretion and exhumation of an oveanic arc during dextral transpression, Southern Volcanic Zone, Abitibi Subprovince Canada. Precambrian Research 115, 261-290.

Daigneault, R., St Julien, P., Allard, G.O., 1990. Tectonic evolution of the northeast portion of the Archean Abitibi greenstone belt, Chibougamau area, Quebec. Can. J. Earth Sci. 27, 1714-1736.

Daoudene, Y., Tremblay, A., ~~Goutier, J.,~~ Ruffet, G., Leclerc, F., 2014. Étude structurale et métamorphique de la bordure nord-est de la ceinture de roches vertes de l'Abitibi, Québec, Canada : apport de la thermochronologie $^{40}Ar/^{39}Ar$ et implications tectoniques~~Relations tectoniques entre les sous-provinces de l'Abitibi et d'Opatica, et apports de la géochronologie $^{40}Ar/^{39}Ar$ dans le sud de l'Abitibi, Province du Supérieur (nord du Québec)~~. Ministère des Ressources naturelles, Québec, MB 2014-04, 55 pages.

Daoudene, Y., ~~Tremblay, A., and~~ Leclerc, F., Tremblay, A., 201~~5~~6. Une histoire tectono-

métamorphique commune et de longue durée pour les sous-provinces d'Abitibi et d'Opatica, Province du Supérieur, Québec, Canada.~~Déformation et métamorphisme du domaine sud-est de la Province archéenne du Supérieur : une histoire longue, continue et étendue.~~ Ministère des Ressources naturelles, Québec, MB 2016-01, 41 pages.

David, J., Davis, D.W., Dion, C., Goutier, J., Legault, M., Roy, P., 2007. U-Pb age dating in the Abitibi Subprovince in 2005-2006. Ministère des Ressources naturelles et de la Faune, RP 2007-01(A), 17 pages.

David, J., Dion, C., Goutier, J., Roy, P., Bandyayera, D., Legault, M., Rhéaume, P., 2006. Datations U-Pb effectuées dans la Sous-province de l'Abitibi à la suite des travaux de 2004-2005. Ministère des Ressources naturelles et de la Faune, RP 2006-04, 22 pages.

David, J. 2005. Rapport préliminaire sur des travaux de géochronologie U-Pb, année 2004-2005. Ministère des Ressources naturelles et de la Faune, Québec, GM :62069, 31 pages.

David, J. 2012. Datations isotopiques effectuées dans le nord-est de la Province du Supérieur, Travaux de 2001, 2002 et 2003. Ministère des Ressources naturelles et de la Faune, Québec, DV 2012-05, 82 pages.

David, J., 2018. Datations U-Pb dans la Province du Supérieur effectuées au GEOTOP en 2015-2016. Ministère de l'Énergie et des Ressources naturelles du Québec. MB 2018-16, 24 pages.

David, J., McNicoll, V., Simard, M., Bandyayera, D., Hammouche, H., Goutier, J., Pilote, P., Rhéaume, P., Leclerc, F. et Dion, C. (2011). Datations U-Pb effectuées dans les provinces du Supérieur et de Churchill en 2009-2010. Ministère des Ressources naturelles et de la Faune, Québec. RP 2011-02, 37 pages.

Davis, D.W., 2002. U–Pb geochronology of Archean metasedimentary rocks in the Pontiac and Abitibi subprovinces, Quebec, constraints on timing, provenance and regional tectonics: Precambrian Research, v. 115, no. 1–4, p. 97–117, doi: 10.1016/S0301-9268(02)00007-4.

Davis, D.W., Simard, M., Hammouche, H,, Bandyayera, Goutier, J., Pilote, P. 2014. Datations U-Pb effectuées dans les Provinces du Supérieur et de Churchill en 2011-12. MERN report RP 2014-05 : Ministère de l'Énergie et des Ressources naturelles, Québec, RP 2014-05, 61 pages.

Davis, D.W. and Dion, C. 2012. Datations ID-TIMS d'échantillons recueillis en 2011-2012 par Géologie Québec. Ministère de l'Énergie et des Ressources naturelles, Québec, GM

66443, 26 pages.
Davis, W.J., Sawyer, E., Machado, N., Gariépy, C., Benn, K., 1992. U-Pb Geochronology of plutonism and metamorphism in the Opatica Belt : initial Results. Lithoprobe Report 33, 147-149.
Davis, W.J., Machado, N., Gariépy, C., Sawyer, E.W., Benn, K., 1995. U-Pb geochronology of the Opatica tonalite-gneiss belt and its Relationship to the Abitibi greenstone belt, Superior Province, Quebec. Canadian Journal of Earth Sciences 32, 113-127.
Davis, W.J., Gariépy, C., Sawyer, E.W., 1994. Pre-2.8 Ga crust in the Opatica gneiss belt : A potential source of detrital zircons in the Abitibi and Pontiac subpriovince, canada. Geology 22, 1111-1114.
Deino, A., and Potts, R. 1992. Age-probability spectra for examination of single-crystal 40Ar/39Ar dating results: examples from Olorge sailie, southern Kenya Rift. Quat Int 13/14:47–53
De Putter, T. and Ruffet, G., 2020. Supergene manganese ore records 75 Myr-long Campanian to Pleistocene geodynamic evolution and weathering history of the Central African Great Lakes region - Te–tonic drives, climate assists. Gondwana Research 83: 96-117.
De Putter, T., Ruffet, G., Yans, J., and Mees, F. 2015. The age of supergene manganese deposits in Katanga and its implications for the Neogen evolution of African Great Lakes Region. Ore Geology Reviews 71: 350-362.
Dewey J.F., 1987. Suture. In: Structural Geology and Tectonics. Encyclopedia of Earth Science. Springer, Berlin, Heidelberg. https://doi.org/10.1007/3-540-31080-0_115.
Dimroth, E., Mueller, W., Daigneault, R., Brisson, H., Poitras, A., Rocheleau, M., 1986. Diapirism during regional compression: the structural pattern in the Chibougamau region of the Archean Abitibi belt, Québec. Geologische Rundschau 75(3), 715-736.
Dimroth, E., Rocheleau, M., Mueller, W., 1984. Paleogeography. Isostasy and crustal evolution of the Archean Abitibi belt: a comparison between the Rouyn-Noranda and Chibougamau-Chapais areas. In: Guha, J., and Chown. E.H. (Eds) Chibougamau.
Dimroth, E., Imreh, L., Goulet, N., and Rocheleau, M., 1983. Evolution of the south-central segment of the Archean Abitibi Belt, Quebec. Part II: Tectonic evolution and geomechanical model. Canadian Journal of Earth Sciences, v. 20, no. 9, p. 1374–1388.
Dodson, M.H., 1973. Closure temperatures in cooling geochronological and petrological systems. Contribution to Mineral Petrology 40, 259-274.

Ducharme, Y., Stevenson, R.K., Machado, N., 1997. Sm-Nd geochemistry and U-Pb geochronology of the Preissac and La Motte leucogranites, Abitibi Subprovince. Canadian Journal of Earth Sciences 34, 1059–1071.

Ernst, G.W., Liou, J.G. and Hacker, B.R. 1994. Petrotectonic significance of high and ultrahigh-pressure metamorphic belts: inferences from subduction-zone histories. International Geology Review 36: 213-237.

Faure, S., 2015. Relations entre les minéralisations aurifères et les isogrades métamorphiques en Abitibi. Rapport, Projet CONSOREM 2013-03, 52 p.

Feng, R., Kerrich, R., McBride, S. and Farrar, E. 1992. 40Ar/39Ar age constraints on the thermal history of the Archean Abitibi greenstone belt and the Pontiac subprovince: implications for terrane collision, differential uplift, and overprinting of gold deposits. Candian Journal of Earth Sciences 29: 1389-1411.

Fleck, R.J., Sutter, J.F., and Elliot, D.H., 1977. Interpretation of discordant 40Ar/39Ar age spectra of Mesozoic tholeiites from Antarctica. Geochimica Cosmochimica Acta 41: 15-32.

Fortier, S.M., Giletti, B.J., 1989. An empirical model for predicting diffusion coefficients in silicate minerals. Science 245, 1481-1484.

Frieman, B.M., Kuiper, Y.D., Kelly, N.M., Monecke, T., and Kylander-Clark, A., 2017. Constraints on the geodynamic evolution of the southern Superior Province: U-Pb LA-ICP-MS analysis of detrital zircon in successor basins of the Archean Abitibi and Pontiac subprovinces of Ontario and Quebec, Canada: Precambrian Research, v. 292, p. 398–416, doi: 10.1016/j.precamres.2017.01.027.

Gapais, D., Barbarin, B., 1986. Quartz fabric transition in cooling syntectonic granite (Hermitage massif, France). Tectonophysics 124, 357-370.

Gariépy, C., Allègre, C.J., 1985. The lead isotope geochemistry and geochronology of late kinematic intrusives from the Abitibi greenstone belt, and the implications for late Archean crustal evolution. Geochim. Cosmochim. Acta 49, 2371-2383.

Gosselin, C., 1996. Synthèse géologique de la région de Frotet-Troilus. Ministère des Resssources Naturelles du Québec, ET-96-02, 21 p.

Goutier, J., 2005. Géologie de la région du lac au Goéland (32F/15). Ministère des Ressources naturelles et de la Faune, Québec. RG 2005-05, 39 pages.

Goutier, J., Rhéaume, P., Davis, D.W., 2004. Géologie de la région du lac Olga (32F14). Géologie Québec, RG 2003-09, 42 p.

1417 Gower, R.J.W, Simpson, C., 1992. Phase boundary mobility in naturally deformed, high-
1418 grade quartzofeldspathic rocks: evidence for diffusional creep. J. Struct. Geol 14 (3),
1419 301-313.
1420 Gray, R. and Pysklywec, R.N., 2010. Geodynamic models of Archean continental
1421 collision and the formation of mantle lithosphere keels. Geophysical Research Letters
1422 37: 1-5.
1423 Groulier, P.A., De Souza, S., Daoudene, Y. et Massei, F., 2020. Synthèse gîtologique de la
1424 ceinture de roches vertes de Frotet-Evans, segments Evans-Ouagama et Storm-Evans.
1425 Ministère de l'Énergie et des Ressources naturelles, Québec. MB 2020-14, 128 pages.
1426 Grove, M., Harrison, T.M., 1996. ^{40}Ar diffusion in Fe-rich biotite. Am. Min. 81, 940-951.
1427 Hames, W. E., Cheney, J. T., Tracy, R. J., 2008. Single-crystal ^{40}Ar/^{39}Ar age variation in
1428 muscovite of the Gassetts Schist and associated gneiss, Vermont Appalachians. Am.
1429 Mineral. 93, 384-395.
1430 Harrison, T.M, Celerier, J., Aikman, A.B, Hemaqnn, J., Heizler, M.T., 2009. Diffusion of 40Ar
1431 in muscovite. Geochim. Cosmochim. Acta. 73, 1039-1051.
1432 Harrison, T.M., Duncan, I., McDougall, I., 1985. Diffusion of 40Ar in biotite: temperature,
1433 pressure and compositional effects. Geochim. Cosmochim, Acta 55, 1435-1448.
1434 Hocq, M., 1994. La Province du Supérieur. In: Géologie du Québec. Ministère des
1435 Ressources naturelles, Québec, MM94-01, 7-20.
1436 Jäger, E., 1967. Die Bedeutung des Biotit-Aterswerte. In: Jäger, E., Niggli, E., Wenk, E.
1437 (Eds), Rb-Sr Alersbestimmugen an Glimmern der Zentralalpen. Beitr. Geol. Karte
1438 Scweiz, NF 134, 28-31.
1439 Kamber, B.S., Blenkinsop, T.G., Villa, I.M., Dahl, P.S., 1995. Proterozoic transpressive
1440 deformation in the Northern Marginal Zone, Limpopo Belt, Zimbabwe. J. Geol. 103,
1441 493-508.
1442 Kim, Y.H., Miller, M.S., Pearce, F. and Clayton, R.W. 2012. Seismic imaging of the Cocos
1443 plate subduction zone system in central Mexico. Geochem. Geophys. Geosyst. 13, doi:
1444 10.1029/2012GC004033.
1445 Kimura, G., Ludden, J.N., Desrochers, J.P., Hori, R., 1993. A model of ocean-crust accretion
1446 for the Superior province, Canada. Lithos 30, 337-355.
1447 Kusky, T., Wang, J., Wang, L., Huang, B., Ning, W., Fu, D., Peng, H., Deng, H., Polat, A.,
1448 Zhong, Y. and Shi, G. 2020. Mélanges through time: life cycle of the world's largest
1449 Archean mélange compared with Mesozoic and Paleozoic subduction-accretion-

collision. Earth-Science Reviews 209.
Lacroix, S., Sawyer, E.W., 1995. An Archean fold – thrust belt in the northwestern Abitibi Greenstone Belt: structural and seismic evidence. Canadian Journal of Earth Sciences 32, 97-112.
Leclair, A.D., Ernst, R.E., Hattori, K., 1993. Crustal-scale auriferous shear zones in the central Superior province, Canada. Geology 21, 399-402.
Leclerc, F., Houle, P., 2013. Géologie de la region du lac Simon (32G15-200-0102). Ministère des Ressources naturelles, Québec, RP 2013-02.
Leclerc, F., Harris, L.B., Bédard, J.H., van Breemen, O., Goulet, N., 2012. Structural and stratigraphic controls on magmatic, volcanogenic, and shear zone-hosted mineralization in the Chapais-Chibougamau mining camp, Northeastern Abitbi, Canada. Economic Geology 107, 963-989.
Leclerc, F., Bédard, J., Harris, L.B., McNicoll, V.J., Goulet, N., Roy, P., Houle, P., 2011. Tholeiitic to calc-alcaline cyclic volcanism in the Roy Group. Chibougamau area, Abitibi Greenstone Belt – revised stratigraphy and implications for VHMS exploration. Can. J. Earth Sci. 48(3), 661-694.
Leclerc, F., Bédard, J.H., Harris, L.B., Goulet, N., Houle, P., Roy, P., 2008. Nouvelles subdivisions de la Formation de Gilman, Groupe de Roy, region de Chibougamau, sous-province de l'Abitibi, Québec : résultats préliminaires. Commission géologique du Canda, Recherche en cours 2008-7, 20 p.
Legault, M., 2003. Environnement métallogénique du couloir de Fancamp avec emphases sur les gisements aurifères de Chevrier. Région de Chibougamau, Québec. Phd thesis, Université du Québec à Chicoutimi, 488 p.
Lin, S., Parks, J., Heaman, L.M., Simonetti, A., Corkery, M.T., 2013. Diapirism and sagduction as a mechanism for deposition and burial of "Timiskaming-type" sedimentary sequences, Superior Province: Evidence from detrital zircon geochronology and implications for the Borden Lake conglomerate in the exposed meddle to lower crust in the Kapuskasing uplift. Precambrian Research 238, 148-157.
Lister, G.S. and Davis, G.A. 1989. The origin of metamorphic core complexes and detachment faults formed during Tertiary continental extension in the northern Colorado River region, U.S.A. J. Struc. Geol. 11: 65-94.
Lister, G.S., Baldwin, S.L., 1996. Modelling the effect of arbitrary P-T-t histories on Ar diffusion in minerals using the MacArgon program for the Apple Macintosh.

1483 Tectonophys. 253, 83-109.
1484 Ludden, J. and Hynes, A. 2000. The Lithoprobe Abitibi-Grenville transect: two billion years
1485 of crust formation and recycling in the Precambrian shield of Canada. Can. J. Earth
1486 Sci. 37: 459-476.
1487 Ludden, J., Hubert, C., Gariépy, C., 1986. The tectonic evolution of the Abitibi greenstone
1488 belt of Canada: Geological Magazine 123, 153-166.
1489 Mainprice, D., Bouchez, J.L., Blumenfeld, P., Tubia, J.M., 1986. Dominant c-slip in naturally
1490 deformed quartz: implications for dramatic plastic softening at high temperature.
1491 Geology 14, 819-822.
1492 Mathieu, L., Snyder, D.B., Bedeaux, P., Cheraghi, S., Lafrance, B., Thurston, P. and
1493 Sherlock, R. 2020. Deep into the Chibougamau area, Abitibi Greenstone Belt: structure
1494 of a Neoarchean crust revealed by seismic reflection profiling. Tectonics 38.
1495 McDougall, I., Harrison, T.M., 1988. Geochronology and thermochronology by the $^{40}Ar/^{39}Ar$
1496 method. Oxford monographs on geology and geophysics, Oxford Press 9, 212 p.
1497 McNicoll, V.J., Goutier, J., 2008. Trois datations U-Pb de la region du lac au Goéland, Sous-
1498 province de l'Abitibi. Ministère des Ressources naturelles et de la Faune, RP 2008-02,
1499 11 p.
1500 Mole, D.R., Thurston, P.C., Marsh, J.H., Stern, R.A., Ayer, J.A., Martin, L.A.J. Lu, Y.J. 2021.
1501 The formation of Neoarchean continental crust in the south-east Superior Craton by two
1502 distinct geodynamic processes. Precambrian Research 356.
1503 https://doi.org/10.1016/j.precamres.2021.106104.
1504 Montigny, R., 1985. Méthode classique potassium-argon. Méthode de datation par les
1505 phénomènes nucléaires naturels : applications : textes réunis par E. Roth et B. Poty,
1506 Masson, Série Scientifique, 309-340.
1507 Mueller, W.U., 1991. Volcanism and related slope to shallow-marine volcaniclastic
1508 sedimentation: an Archean example near Chibougamau, Quebec, Canada. Precambrian
1509 Research 49, 1-22.
1510 Mueller, W.U., Daigneault, R., Mortensen, J.K., Chown, E.H., 1996. Archean terrane
1511 docking: Upper crust collision tectonics, Abitibi greenstone belt, Quebec, Canada.
1512 Tectonophysics 265, 127-150.
1513 Nadeau, O., Cayer, A., Pelletier, M., Stevenson, R. and Jébrak, M. 2015. The
1514 Paleoproterozoic Montviel carbonatite-hosted REE–Nb deposit, Abitibi, Canada:
1515 Geology, mineralogy, geochemistry and genesis. Ore Geology Rev. 67: 314-335.

1516 Palin, R.M., Santosh, M., Cao, W., Li, S.-S., and Hernandez-Uribe, D. 2020. Secular change
1517 and the onset of plate tectonics on Earth. Earth-Science Reviews 207.
1518 Parmenter, A.C., Lin, S., Corkery, T., 2006. Structural evolution of the Cross Lake greenstone
1519 belt in the northwestern Superior Province, Manitoba: implications for relationship
1520 between vertical and horizontal tectonism. Can J Earth Sci 43, 767-787.
1521 Pedreira-Perez, R., Tremblay, A., Daoudene, Y. and Bandyayera, D. 2020. Étude
1522 géochimique, structurale et géochronologique de la Sous-province de Nemiscau, Baie-
1523 James, Québec : implications quant à l'origine et l'évolution tectonique d'un domaine
1524 sédimentaire archéen. Ministère des Ressources naturelles, MB 2020-07, 82 pages.
1525 Percival, J.A., Skulski, T., Sanborn-Barrie, M, Stott, G.M, Leclair, A., Corkery, M.T., Boily,
1526 M., 2012. Geology and tectonic evolution of the Superior Province, Canada, chapter 6.
1527 In: Percival, J.A., Cook, F.A., Clowes, R.M. (Eds), Tectonic styles in Canada: the
1528 LITHOPROBE perspective. Geological Association of Canda, Special Paper 49, 321-
1529 378.
1530 Percival, J.A., 2007. Geology and metallogeny of the Superior Province, Canada. In:
1531 Goodfellow, W.D. (Ed). Mineral deposits of Canada: a synthesis of major deposit-types,
1532 district metallogeny, the evolution of geological provinces, and exploration methods.
1533 Geol. Ass. Can. Min. Deposit Div. Sp. Pub. 5, 903-928.
1534 Percival, J.A., Sanborn-Barrie, M., Skulski, T., Stott, G.M., Helmstaedt, H., White, D.J.,
1535 2006. Tectonic evolution of the western Superior Province from NatMap and
1536 Lithoprobe studies. Can. J. Earth. Sci. 43:1085-1117.
1537 Piette-Lauzière, N., Guilmette, C., Bouvier, A., Perrouty, S., Pilote, P., Gaillard, N.,
1538 Lypaczewski, P., Linnen, R.L., Olivo, G.R. 2019. The timing of prograde metamorphism in
1539 the Pontiac Subprovince, Superior craton: implications for Archean geodynamics and
1540 gold mineralization. Precambrian Research 320, 111-136.
1541 Pilote, P., Dion, C., Joanisse, A., David, J., Machado, N., Kirkham, R., Robert, F., 1997.
1542 Géochronologie des minéralisations d'affiliation magmatique de l'Abitibi, secteurs de
1543 Chibougamau et de Troilus-Frotet : Implications géotectoniques. In: Vers de
1544 nouvelles découvertes. Séminaire d'information sur la recherche géologique,
1545 Ministère des Ressources naturelles, Programme et résumé 47.
1546 Pitra, P., Ballèvre, M., Ruffet, G., 2010. Inverted metamorphic field gradient towards a
1547 Variscan suture zone (Champtoceaux Complex, Armorican Massif, France). J. Metam.
1548 Geol. 28 (2), 183-208.

1549 Powell, W.G., Hodgson, C.J., Hanes, J.A., Carmichael, D.M., McBride, S., and Farrar, E.
1550 1995. $^{40}Ar/^{39}Ar$ geochronological evidence for multiple post-metamorphic
1551 hydrothermal events focused along faults in the southern Abitibi greenstone belt. Can.
1552 J. Earth Sci. 32: 768-786.
1553 Purdy, J.W., Jäger, E., 1976. K-Ar ages on rock forming minerals from the Central Alps.
1554 Memorie degli Istituti di Geologia e Mineralogia dell'Università di Padova 30, 1-32.
1555 Renne, P.R., Balco, G., Ludwig, R.L., Mundil, R., and Min, K., 2011. Response to the
1556 comment by W.H. Schwarz et al. on "Joint determination of 40K decay constants and
1557 40Ar∗/40K for the Fish Canyon sanidine standard, and improved accuracy for
1558 40Ar/39Ar geochronology" by PR Renne et al. (2010). Geochimica et Cosmochimica
1559 Acta, 75: 5097-5100.
1560 Renne, P.R., Mundil, R., Balco, G., Min, K., and Ludwig, R.L., 2010. Joint determination
1561 of 40K decay constants and 40Ar∗/40K for the Fish Canyon sanidine standard, and
1562 improved accuracy for 40Ar/39Ar geochronology. Geochimica et Cosmochimica Acta
1563 74: 5349–5367.
1564 Revelli, N. 2020. Évolution tectonométamorphique d'un segment de croûte archéenne : le
1565 Complexe d'Attic, Lebel-sur-Quévillon. Ph.D. Thesis, Université du Québec à
1566 Montréal, Montréal, Canada.
1567 Robert, F., Poulsen, K.H., Cassidy, K.F., and Hodgson, C.J. 2005. Gold metallogeny of
1568 the Superior and Yilgarn cratons. Economic Geology 100: 1001–1033.
1569 Roddick, J.C., 1983. High precision intercalibration of ^{40}Ar-^{39}Ar standards. Geochim.
1570 Cosmochim. Acta 51, 2129-2135.
1571 Ross, P.S., Goutier, J., Mercier-Langevin, P., Dubé, B., 2010. Basaltic to andesitic
1572 volcaniclastic rocks in the Blake River Group, Abitibi Greenstone Belt: 1. Mode of
1573 emplacement in three areas. Canadian Journal of Earth Sciences 48, 728-756.
1574 Ruffet, G., Feraud, G., Balèvre, M., Kiénast, J.R., 1995. Plateau ages and excess argon in
1575 phengites: an 40Ar/39Ar laser probe study of Alpine micas (Sezia Zone, Western
1576 Alps, northern Italy). Chem. Geol. 121(1-4), 327-343.
1577 Ruffet, G., Féraud, G., Amouric, M., 1991. Comparison of $^{40}Ar/^{39}Ar$ conventional and laser
1578 dating of biotites from the North Tregor Batholith. *Geochim. Cosmochim. Acta 55*,
1579 1675-1688.
1580 Ruffet G., Perroud H., Féraud G., 1990. ^{40}Ar-^{39}Ar dating of a late Proterozoic paleomagnetic
1581 pole for the Armorican Massif (France). Geophysical Journal International 102; 397-

409.
Sawyer, E.W., 1998. Formation and evolution of granite magmas during crustal reworking: the significance of diatexites. Journal of Petrology 39 (6), 1147-1167.
Sawyer, E.W., Benn, K., 1993. Structure of the high-grade Opatica Belt and adjacent low-grade Abitibi Subprovince, Canada: an Archean mountain front. Journal of Structural Geology 15, 1443-1458.
Schaen, A.J. and 40 others. 2020. Interpreting and reporting $^{40}Ar/^{39}Ar$ geochronological data. Geol. Soc. Am. Bull. 133: 461-487.
Schmid, S.M., Casey, M., 1986. Complete fabric analysis of some commonly observed quartz c-axis pattern. Geophys. Monogr. 36, 263-286.
Simard, M., 1987. Stratigraphie et volcanism dans la partie orientale de la bande volcano-sédimentaire archéenne Frotet-Evans. Ministère de l'Énergie et des Ressources, Québec, MB 87-17, 300 p.
Simpson, C., 1985. Deformation of granite rocks across the brittle-ductile transition. J. Struct. Geol. 7 (5), 503-511.
Simpson, C., Wintsch, R.P., 1989. Evidence for deformation-induced K-feldspar replacement by myrmekite. J. Metamorphic. Geol. 7, 261-275.
Spear, F.S., 1993. Metamorphic phase equilibria and pressure-temperature-time paths. Mineral. Soc. Am., 799 p.
Stern, R.J. 2018. The evolution of plate tectonics. Phil. Trans. of the Royal Soc. Series A.
Stern, R.J. 2008. Modern-style plate tectonics began in Neoproterozoic time: An alternative interpretation of Earth's tectonic history. When did plate tectonics begin on planet Earth, 440, pp 265-280.
Stern, R.J. 2002. Subduction zones. Reviews of Geophysics 40, 38 p.
Stott, G.M., Corkery, M.T., Percival, J.A., Simard, M., Goutier, J., 2010. A revised terrane subdivision of the Superior Province. In: Summary of Field Work and Other Activities 2010, Ontarion Geological Survey, Open File Report 6260 pp. 20-1 to 20-10.
Tartese, R., Ruffet, G., Poujol, M., Boulvais, P., and Ireland, T. R. 2011. Simultaneous resetting of the muscovite K- Ar and monazite U- Pb geochronometers: A story of fluids. Terra Nova 23: 390–398.
Thébaud, N. and Rey, P.F., 2013. Archean gravity-driven tectonics on hot and flooded continents: Controls on long-lived mineralised hydrothermal systems away from continental margins. Precamb. Res. 229, 93-194.

1615 Thibault, P., 1985. Applications à la méthode U-Pb (zircon) à des roches ignées des
1616 ensembles volcano-sédimentaires de l'Abitibi et de Frotet-Evans. Mem. Univ.
1617 Montréal, Montréal, 165 p.
1618 Thurston, P.C., Ayer, J.A., Goutier, J. and Hamilton, M.A., 2008. Depositional gaps in Abitibi
1619 Greenstone Belt stratigraphy: a key to exploration for syngenetic mineralization.
1620 Economic Geology 103: 1097-1134.
1621 Tikoff, B., Teyssier, C. and Waters, Ch. 2002. Clutch tectonics and the partial attachment of
1622 lithospheric layers. EGU Stephen Mueller Special Publication Series 1: 57-73.
1623 Tremblay, A., Ruffet, G, and Lemarchand, J. 2020. Timing and duration of Archean orogenic
1624 gold deposits in the Bourlamaque pluton, Val d'Or mining camp, Abitibi, Canada. Ore
1625 Geology Reviews 127.
1626 Tremblay, A., Ruffet. G. and Bédard. J.H. 2011. Obduction of Tethyan-type ophiolites –
1627 a case-study from the Thetford-Mines ophiolitic Complex, Québec Appalachians,
1628 Canada. Lithos 125: 10-26.
1629 Turner, G., Huneke, J.C., Podosek, F.A., Wasserburg, G.J., 1971. ^{40}Ar-^{39}Ar ages and cosmic
1630 ray exposure age of Apollo 14 samples. Earth Planet. Sci. Lett. 12, 19-35.
1631 Vanderhaeghe, O., Guergouz, C., Fabre, C., Duchêne, S. and Baratoux, D. 2019. Secular
1632 cooling and crystallization of partially molten Archean continental crust over 1 Ga.
1633 Comptes rendus-Geosciences 351: 562-573.
1634 van der Velden, A.J. and Cook, F.A., 2005. Relict subduction zones in Canada. J. Geophys.
1635 Res. 110, doi:10.1029/2004JB003333
1636 Van Hunen, J. and Moyen, J.-F. 2012. Archean subduction: fact or fiction? Annu. Rev. Earth
1637 Planet. Sci 40: 195-219.
1638 Van Kranendonk, M.J. 2011. Archean Tectonics. In: Gargaud M. et al. (eds) Encyclopedia of
1639 Astrobiology. Springer, Berlin, Heidelberg. https://doi.org/10.1007/978-3-642-11274-
1640 4_100.
1641 Villa, I.M., 1998. Isotopic closure. Terra Nova 10, 42-47.
1642 Villa, I. M., Puxeddu, M., 1994. Geochronology of the Larderello geothermal field: new data
1643 and the 'closure temperature' issue. Contrib. Mineral. Petrol. 315, 415-426.
1644 Villa, I.M., Grobéty, B., Kelley, S.P., Trigila, R., Wieler, R., 1996. Assessing Ar transport
1645 paths and mechanisms for McClure Mountains Hornblende. Contrib. Min. Petrol. 126,
1646 67-80.
1647 Wakabayashi, J. 2017. Structural context and variation of ocean plate stratigraphy, Franciscan

Complex, California: insight into mélange origins and subduction-accretion processes. Progress in Earth and Planetary sciences 4 (18). https://progearthplanetsci.springeropen.com/articles/10.1186/s40645-017-0132-y.

Wakabayashi, J., and Dilek, Y., 2011, Introduction: Characteristics and tectonic settings of mélanges, and their significance for societal and engineering problems: in Wakabayashi, J., and Dilek, Y. eds. Mélanges: Processes of Formation and Societal Significance, Geological Society of America Special Paper 480, doi: 10.1130/2011.

Weinberg, R.F. 1997. Diapir-driven crustal convection: decompression melting, renewal of magma source and the origin of nested plutons. Tectonophysics 271: 217-229.

Whitney, D.L., Teyssier, C., and Fayon, A.K. 2004. Isothermal decompression, partial melting and exhumation of deep continental crust, In Grocott, J., McCaffrey, K.J.W., Taylor, G. and Tikoff, B. (eds). Vertical coupling and decoupling in the lithosphere. Geol. Soc. London Sp. Publi. 227: 313-326.

Whitney, D.L., Teyssier, C., Rey, P. and Buck, W.R. 2013. Continental and oceanic core complexes. Geol. Soc. Am. Bull.

Wiemer, D., Schrank, C.E., Murphy, D.T., Wenham, L. and Allen, C.M. 2018. Earth's oldest stable crust in the Pilbara craton formed by cyclic gravitational overturns. Nature Geoscience 11: 357-361.

Wyman, D.A., Kerrich, R., Polat, A., 2002. Assembly of Archean cratonic mantle lithosphere and crust: Plume-arc interaction in the Abitibi-Wawa subductionaccretion complex. Precamb. Res. 115, 37-62.

Figure captions.

Figure 1. a) Principal tectonostratigraphic domains of the Archean Superior Province. Modified from Card (1990) and Benn et al. (1992). **b)** Geological map of the southeastern part of the Superior Province with focus on the Abitibi greenstone belt and the surrounding areas. AC: Attic Complex; BP: Bernetz gneissic pluton; MP: Marest gneissic pluton. Modified from Thurston et al. (2008). See a) for location.

Figure 2. Geological map of the northeastern part of the northeastern part Abitibi Subprovince and the eastern part of the Opatica Subprovince including the eastern portion of the Frotet-Evans greenstone belt. Samples YD101A and YD0100A used for ^{39}Ar-^{40}Ar dating are localized on the map. BSZ, Barlow shear zone; GF, Gwillim fault; KSZ, Kapunapotagen shear zone; LF, Lamarck shear zone; LFSZ, La France river shear zone; LLSZ, La Trève lake

shear zone; LNSZ, Lac à l'Eau-Noire shear zone; LSRSZ, Lucky Strike river shear zone; NRSZ, Nottaway river shear zone. See Fig. 1~~2~~ for location. Modified from Dimroth et al. (1986) and Daigneault et al. (1990).

Figure 3. Geological map of the Lac-au-Goéland area and location of samples used for ^{40}Ar-^{39}Ar for this study. See Fig. 2 for location. Modified from Goutier (2005).

Figure 4. Field photographs of the AGB and OPB rocks. a**)** Amphibolite-grade mafic volcanic rock showing well-preserved pillow structure. b) Strongly deformed gabbro showing quart-feldspar aggregates defining a steeply plunging mineral lineation. c) ~~Un-metamorphosed succession of sandstone and siltstone of the Opémisca Group (Daubrée Formation) in the Chibougamau area~~Typical gneissic tonalite of the OBP characterized by a penetrative S_1 foliation. d) Un-metamorphosed succession of sandstone and siltstone of the Opémisca Group (Daubrée Formation) in the Chibougamau area~~Typical gneissic tonalite of the OBP characterized by a penetrative S_1 foliation~~. e) AGB amphibolite located along the southern boundary of the Noman tonalite (see Fig. 3), showing the S_1 metamorphic layering tightly folded by F2 with an axial-planar S2 foliation. f) Granitic dykes crosscutting amphibolitic horizons within the OPB.

Figure 5. Structural map of the study area showing foliation trajectories and dip directions. Structural data were compiled from the geological mapping data available in SIGEOM information system of the Ministère des Ressources naturelles du Québec (http://sigeom.mines.gouv.qc.ca). Trajectories of regional schistosity/foliation were drawn from structural data acquired in the field and high-resolution magnetic imaging.

Figure 6. Stereographic projections (equal area, lower hemisphere) for dominant planar and linear structural fabric~~s~~ of the Abitibi and Opatica subprovinces. Data for the AGB correspond to S_2 and composite S_{1-2} whereas those from the OPB correspond to S_1.

Figure 7. Field photographs of fabric~~s~~ related to the D_3 deformation event. a) Mylonitic fabric developed in a mafic volcanic rock of the AGB. b) Dextral F_3 fold affecting the regional schistosity S_2 within a mafic volcanic rock. c) Subhorizontal stretching lineation along the Nottaway River shear zone. d) Shear bands indicating dextral shearing in a mylonitized orthogneiss of the Nottaway River shear zone (view perpendicular to the subvertical S_3 foliation and parallel to the subhorizontal lineation). e) Thin section cuts parallel to the XY plane showing dextral mica fish fabric~~s~~ in a felsic mylonite. f) Boudinaged felsic dyke cutting across an amphibolite horizon of the OPB.

Figure 8. Photographs illustrating regional metamorphism and associated deformation

in the study area. a) Low-grade volcanic rocks of the Roy Group showing well-preserved pillow structures. b) Garnet-staurolite micaschist from the northwestern flank of the Waconichi syncline. Staurolite forms large, corroded crystal preferentially aligned along the foliation plane (cross-polarized light). c) Large chloritoid phenocryst overprinting the regional schistosity marked by the preferred orientation of actinolite in the fine-grained matrix (cross-polarized light). d) Outcrop of pillowed basalt showing garnet-rich pillow margins in the vicinity of the AGB-OPB transition. e) Typical lobate boundaries between quartz and feldspar grains in a coarse-grained and weakly-deformed tonalite of the OPB. The foliation is marked by the preferred orientation of biotite (plane-polarized light). f) Field example of migmatitic gneiss of the OPB.

Figure 9. Structural profiles of the study area. See figure 3 for location. East-southeast-looking for profile A-A', East-looking for the other profiles.

Figure 10. Single-grain $^{39}Ar/^{40}Ar$ results for amphiboles and biotites of the AGB. Apparent age error bars are at the 1σ level; errors in the J-parameter are not included. Plateau and pseudo-plateau ages (1σ uncertainties including errors in the J-parameter) are given when applicable. Sample locations are show in Figures 3 and 4. See text for explanations.

Figure 11. Single-grain $^{39}Ar/^{40}Ar$ results for amphiboles and biotites for tonalites of the OPB. See Figures 3 and 4 for locations. Analytical details as for Figure 11. See text for explanations.

Figure 12. Single-grain $^{39}Ar/^{40}Ar$ results for muscovite of quartz-feldspar porphyry dykes of the Lac-au-Goéland area. Analytical details as for Figure 11. See Figure 4 for locations. See text for explanations.

Figure 13. Single-grain $^{39}Ar/^{40}Ar$ results for muscovite, amphibole and biotite from the Nottaway River shear zone. Analytical details as for Figure 11. See Figure 4 for locations. See text for explanations.

Figure 14. Single-grain $^{39}Ar/^{40}Ar$ results for amphibole and biotite from the Montviel Syenite. Analytical details as for Figure 11. See Figure 4 for locations and text for explanations.

Figure 15. Synthesis of the validated ages of the study area (plateau and pseudo-plateau) obtained on amphibole and micas grouped by terranes and/or rock types on probability density diagrams of the resized apparent ages for each group. See text for explanation.

Figure 16. Schematic illustration of a partial crustal overturn model for the OPB-AGB

transition. See text for discussion and details on age constraints for the different panels.

Figure 17. Extract of numerical models performed by Gray and Pysklywec (2010). This model suggests that due to a hot and rheologically-weak lower crust, the mantle and the crust become decoupled at a depth of approximately 50 km and that the lithospheric mantle becomes imbricated along major shear zones whereas the crustal domain itself 2 of Gray and Pysklywec (2010). See text for discussion.

Figure 18. a) Teleseismic imaging of the subduction zone interface of the Cocos slab beneath Mexico. Modified from Kim et al. (2012). b) Alternative interpretation for the AGB showing flat subduction of the Pontiac terrane below a composite AGB-OPB terrane. Note the striking geometrical similarity with the Cocos subduction zone. See text for discussion.

Response to comments

Dear Editor,

We sincerely thank you and the two reviewers for the time you dedicated for critical review of the second version of our manuscript. From these reviews, we made several corrections as detailed below and shown in red in the revised version of the manuscript. We hope that it now responds to the standard quality for publication in Precambrian Research.

Reviewer #1: The final manuscript should mention the fact that some of the 2.6 Ga and 2.5 Ga ages may reflect mid crustal processes as noted in the review by reviewer 1.

The attached Word document lists a small number of strictly grammatical points that should be repaired.

The authors have done a good job of addressing comments by reviewer 2 and there is but one area of reviewer 1's comments needing a response.

To our knowledge, and according to Thurston et al. (2008) and Mole et al. (2021) as well, there are no significant intrusions younger than 2.6 Ga in the Superior Province. 2.6 to 2.5 ages. When present, young Ar-Ar cooling ages can be attributed to progressive exhumation or localized late shearing in both the AGB and OPB (see Tremblay et al. 2020). This being said, we have added much more information regarding 2700-2650 Ma magmatism in the AGB (see revised pages 5-6, 157-188). We also have made all the grammatical corrections listed by the reviewer.

Reviewer #3: General comments.
This is an interesting manuscript which addresses the tectonic history of the Archean Abitibi and Opatica subprovinces by focusing on their complex structural and metamorphic contact relationships. The manuscript is much improved based on the two previous reviews and is in my view publishable with moderate revisions.

The main unresolved issues of the revised version is that it does not address the comment of reviewer #1 in that the AGB's post 2700 Ma geodynamic history is significantly different than from its pre 2700 Ma constructive stage. Pre 2700 Ma the AGB's evolution was clearly autochthonous with the seven major volcanic assemblages developed sequentially over ca. 100 Ma with conformable to disconformable contacts and only minor episodes of chemical or pelagic sedimentation, nor is there any evidence of the development of tectonic fabrics at this time (see Ayer et al., 2002, Thurston et al 2008). However, post 2700 Ma there was a major change in the geodynamic environment with development of numerous sequential compressional episodes of folding and faulting often with associated regional tectonic fabrics developed. This later compressional phase was coeval with emplacement of plutons of various sizes and compositions, but also with a change in the chemical composition of felsic magmatism (in both volcanic and synvolcanic plutons) from the pre-2700 Ma tonalitic plutons being calcium-rich, changing post-2700 Ma to more alkalic compositions of granodiorite, granite and syenite and showing chemical evidence of being sourced from a different, more metasomatised mantle source. This period of transition was also accompanied by the onset of earlier flysch followed by molasse sedimentation, both lying unconformably on the older volcanic and plutonic substrate.

All these features indicate a major geodynamic change occurred around 2700 Ma which suggests a change from early diapirism to later subduction (see Mole et al 2021). The above features need to be better addressed in the manuscript.

Reviewer 3 made very useful and pertinent comments regarding the AGB that help to better focus some sections of our manuscript, to add important lithological information that was lacking and to precise some of our interpretations. In short, these reviewer's comments are:

1- The contrasting pre-2700 Ma and post-2700 Ma magmatic and geodynamic evolution of the AGB as described by Thurston et al. (2008), should be better explained and address in the Ms.

To take account of this issue, we added a better description of the AGB in the revised section 2.2 (see revised page 5, lines 180-188), in order to add information on post-2700 Ma magmatism (essentially characterized by the emplacement of the Preissac-Lacorne batholith) and sedimentation. We now also mention this contrasting pre- vs post-2700 Ma geological evolution on section 6.3 about the significance of the Seismic reflector (see revised lines 1126-1136).

2- The absence of pre-2700 Ma fabric in the AGB.

This is true that there is no occurrences of pre-2700 Ma fabric in most of AGB rocks, but it is consistent with our interpretation; this absence is due to the fact that the AGB exposes the upper crust of an AGB-OPB composition lithosphere and most, if not all, the evidence for early flowage of the lower crust is mostly preserved in OPB gneisses and correlative lower crust rocks in the AGB, such as the Attic Complex, for instance, in which syn-kinematic migmatites yielded ages at ca. 2716 Ma, older than those of the AGB volcanic rocks (see revised lines 980-987).

3- Numerous episodes of sequential folding and faulting in the AGB.

We disagree with that statement. There is only one major event of regional folding and pervasive fabric development in the AGB (i.e. the so-called $D2_{AGB}$ that we suggest is correlative to the $D1\text{-}2_{OPB}$), which is already clearly stated in the manuscript. Younger deformation, that may be locally associated to younger fabrics in both the AGB and OPB are spatially restricted to reverse fault zones (late D2) and strike-slip shears (D3).

4- *Post-2700 Ma deformation associated with extensive magmatism of more alkalic composition in the AGB.*

We agree with the fact that this important magmatic phase has been overlooked in our manuscript. We are now clearly indicating the existence of such magmatism (mostly represented by the Preissac-Lacorne batholith) in lines 157-188 (see comment #1 above) and 1126-1136.

5- The onset of major geodynamic change marked by flysch sedimentation starting during the post-2700 Ma period.

We do not totally agree with that comment, mainly because the occurrence of flysch-like sediments (or turbidites) is not limited to the post-2700 Ma period. It also occurs much earlier, in the Frotet-Evans greenstone belt, for instance, where age constraints for the Broadback Group (resulting from the erosion of underlying volcanic and plutonic rocks, and most likely due to their progressive exhumation) is ca. 2750 Ma or younger, and has likely been a long-lasting process, at least in the OPB. In the revised manuscript, we better described these critical stratigraphic and geochronological constraints in lines 150-154.

Specific comments

Lines 162: remove "separated by the Destor-Porcupine fault zone"
This fault is no longer considered to be the line dividing the Abitibi into northern and southern zones based on evidence that Tisdale and Blake River assemblages occur further to the north, the subdivision was moved northwards to the southern margin of the Scapa metasedimentary belt (see Thurston et al., 2008).

We kept the original reference for that fault zone but added that the Northern-Southern limit of the AGB has been revised by Thurston et al. (2008).

Lines 415-425. This is a long and complicated sentence. Break it up into smaller segments to clarify.
We disagree; we consider that this sentence (even though it is long) remains comprehensive.

Lines 890-900. Remove this paragraph. It is inaccurate and not relevant to your topic. The DPM is no longer considered to mark the contact between the north and south zones (see above).
We agree – this paragraph has been removed.

Highlights :

- The Abitibi-Opatica contact does not show significant shear deformation;
- There is no metamorphic break at the AGB-OPB transition;
- The Opatica exposes the deepest part of a composite Abitibi-Opatica crust;
- $^{40}Ar/^{39}Ar$ ages exhumation of AGB and OPB rocks at c. 2678 Ma and c. 2668 Ma;
- Our model shows the importance of vertical transfer of Archean crustal material.

The Abitibi-Opatica transition, Superior Province, Quebec, Canada: structural analysis, $^{40}Ar/^{39}Ar$ thermochronology and implications for Archean tectonics

Yannick Daoudene[a,*], Alain Tremblay[b], Gilles Ruffet[c], François Leclerc[a]

[a] Ministère de l'Énergie et des Ressources naturelles, 5700, 4e Avenue Ouest, G1H 6R1, Québec, Québec, Canada.
[b] Université du Québec à Montréal, Département des Sciences de la Terre et de l'Atmosphère and GEOTOP, 201 avenue du Président Kennedy, H2X 3Y7, Montréal, Québec, Canada.
[c] CNRS (CNRS/INSU) UMR 6118, Université de Rennes 1, Géosciences Rennes, F-35042 Rennes Cedex, France
* Corresponding author.
E-mail address: Yannick.Daoudene@mern.gouv.qc.ca

ABSTRACT

We present a structural and metamorphic study of the Abitibi greenstone belt (AGB) and Opatica Plutonic Belt (OPB) of the Archean Superior Province. The AGB-OPB contact is considered as an archetype example of Archean subduction, based on a LITHOPROBE seismic profile showing a North-dipping lithospheric-scale reflector interpreted as the vestige of subduction. Our mapping indicates that the AGB overlies the OPB, and that the AGB-OPB contact does not show evidence of significant shear deformation, as expected for a major upper plate-lower plate boundary. There is no metamorphic break at the AGB-OPB transition but rather a progressive increase of metamorphic grade toward the OPB. Therefore, we think that the OPB simply exposes the deepest part of a composite AGB-OPB sequence. $^{40}Ar/^{39}Ar$ ages suggest that the AGB and OPB rocks were exhumed from amphibolite-facies conditions at ~ 2678 Ma and ~ 2668 Ma, respectively, and then that both terranes share the same succession of thermal disturbances at c. 2650 Ma and 2600 Ma, the latter corresponding to shearing along the Nottaway River Shear Zone. We suggest that progressive cooling of both assemblages was accompanied by strain localisation along strike-slip shear zones and occurred when lateral flow of the lower crust became predominant over the convective overturn and vertical crustal material transfer. Comparison with adjacent areas suggests that regional metamorphism has been coeval over a large region, which is consistent with pervasive deformation and slow cooling as expected for vertical tectonic models and diapiric magmagenesis and ascent during the Archean.

Keywords: Abitibi greenstone belt, Opatica plutonic belt, structures, $^{40}Ar/^{39}Ar$ geochronology, Archean tectonism.

1. INTRODUCTION

Orogenic sutures mark the consumption of oceanic plate lithosphere by subduction and of subsequent arc-continent and/or continent-continent collision, if any. In modern plate tectonics, subduction zones are linear and continuous areas of planetary extent where one plate moves under another and is forced to sink due to high gravitational potential energy into the mantle (e.g. Stern, 2002; Bédard, 2018; Brown et al., 2020). Typically, such areas are characterized by an upper plate-lower plate geometry with contrasting geological characteristics. In Phanerozoic belts, subduction sutures are a typical product of plate tectonics. Although their recognition can be sometimes dubious (e.g. Dewey, 1987), they are usually marked by linear belts of intense deformation, where distinct terranes with different magmatic, metamorphic, structural and geochronological histories have been juxtaposed by plate convergence. In the Archean, the nature of global tectonism remains debated, the main problem concerning similarities and differences with present-day plate tectonics (e.g. Stern, 2008; Brown et al., 2020).

Archean cratons largely consist of greenstone belts juxtaposed to deeper crustal rocks dominated by plutonic (TTG's) and orthogneissic rocks, the greenstone belts usually show steep folds and shear zones whereas plutonic belts display large-scale dome-like structures and fabric. These rocks usually preserve MT/HT-LP/MP metamorphism that varies from greenschist- to granulite-facies, from the upper to the lower crustal domains. The most widely used arguments in favor of Archean subduction are the occurrence of calk-alkaline igneous rocks, the structural style of orogenic belts, the nature and asymmetric distribution of metamorphism, and seismic reflection data. In seismic reflection, there are few clear examples of relict slabs beneath Archean collisional belts. An example of it is found in the Lithoprobe seismic transect of the Superior Province (Calvert et al., 1995) at the contact between the Abitibi Greenstone Belt and the Opatica Plutonic Belt. In scientific literature, it has been and is still interpreted as a fossilized subduction zone and a key argument to support Archean plate tectonics (Calvert et al., 1995; Calvert and Ludden, 1999; Ludden and Hynes, 2000; Wyman et al., 2002; van der Velden and Cook, 2005; Cawood et al, 2006; Percival, 2007; van Hunen and Moyen, 2012; among others).

The Archean Superior Province (Fig. 1) consists of a series of volcano-sedimentary and plutonic domains, subprovinces and/or terranes that amalgamated during the Late Archean Kenoran orogeny (e.g. Percival, 2007). The occurrence of unconformable sedimentary rocks as old as 2.48 Ga (i.e. the Huronian Supergroup) over the volcanic and

plutonic rocks indicates that tectonic accretion occurred prior to 2.5 Ga. Although the internal geological characteristics of the domains/subprovinces/terranes are relatively well known, the nature of their boundaries remains poorly constrained and, sometimes, debated. Current views on the tectonic evolution of the Superior Province are that the orogenic collage of Mesoarchean continental fragments and Neoarchean oceanic plates occurred during a complex history of subduction-driven accretionary collision (e.g. Bleeker, 2003; Percival, 2007; Percival et al., 2006; 2012, among others). Hence, several authors have interpreted a series of high-strain deformation corridors and structural lineaments of the Superior Province as the trace of potential orogenic sutures (Ludden et al., 1986; Mueller et al., 1996; Daigneault et al., 2002, 2004). The Abitibi-Opatica contact, for instance, is considered as the surface expression of south-verging crustal-scale thrust faults rooting into an inferred North-dipping subduction zone, the existence of that subduction being attested by a lithospheric-scale seismic reflector extending from c. 40 to c. 70 km-depth.

In this contribution, we present a structural and metamorphic study of rocks lying on both sides of the Abitibi-Opatica contact in northern Quebec for a strike length of c. 300 km, between the Lac-au-Goéland area to the west and the town of Chibougamau to the east (Fig. 2). The main objectives of fieldwork have been to test (1) how the overall geometry of regional structures fits with south-verging collisional tectonism and thrusting of the OPB over the AGB, and (2) if the structural and metamorphic characteristics of both belts are consistent with an upper-lower plate geometry, as inferred by the subduction model. The determination of the age and duration of structural and metamorphic event(s) that have affected both terranes being critical for a better understanding of their respective geological evolution and mutual relationships, we have performed a series of single-grain $^{40}Ar/^{39}Ar$ analyses for representative samples of both belts.

2. GEOLOGICAL SETTING

The Superior Province forms the principal Archean basement of North America (Fig. 1a). It is made up of several tectonostratigraphic terranes or subprovinces grouped into four major tectonostratigraphic types/domains (Card, 1990; Card and Ciesielski, 1986; Hocq, 1994; Stott et al., 2010), (1) metasedimentary rocks, (2) volcanic and plutonic rocks, (3) tonalite-trondjhemite-granite (TTG)-dominated domains, and (4) high-grade metamorphic rocks. Most tectonic models suggest that these tectonostratigraphic terranes were amalgamated, regionally deformed and metamorphosed during multiple episodes of

subduction/collision (e.g. Kimura et al., 1993; Daigneault et al., 2002; Percival et al., 2006, 2012) between ca. 2.72 Ga and 2.68 Ga (Percival, 2007). The southeastern part of the Superior Province comprises, from north to south, the Opatica, Abitibi and Pontiac subprovinces, the former two being designated here as the Opatica Plutonic Belt (OPB) and the Abitibi Greenstone Belt (AGB) (Fig. 1b).

2.1 The Opatica Plutonic Belt

The OPB is located in the northern part of the southeastern Superior Province. It is separated in two structural domains of plutonic rocks, north and south of the Frotet-Evans greenstone belt that extends east-west over a strike length of approximately 250 km (Figs. 1b and 2). The detailed geology of the OPB is poorly documented, mainly due to difficult road access and a limited mineral resources interest as compared to the adjacent Abitibi subprovince. Existing regional studies indicate that the OPB is a large domain of igneous rocks essentially consisting of foliated tonalites and diorites and equivalent gneisses. The latter were designated as «grey gneisses» by Sawyer and Benn (1993). They are characterized by well-developed compositional layering and locally abundant occurrences of diatexite migmatites in their more fractionated members, mainly in the southern part of the belt (Benn et al., 1992; Sawyer and Benn, 1993; Hocq, 1994; Sawyer, 1998). The gneissic tonalites and diorites are intruded by abundant, slightly- to undeformed plutons of granodiorite and granite. The crystallization age of the OPB intrusive rocks is not precisely constrained but the available geochronological data suggest that they formed mostly between 2.83 and 2.68 Ga (Gariépy and Allègre, 1985; Davis et al., 1992; 1994, 1995; Pedreira-Perez et al., 2020). According to Sawyer (1998), partial melting and migmatization occurred at 2.68-2.67 Ga.

In the Lac-au-Goéland area (Fig. 3), the Nomans tonalite, which is surrounded by metavolcanic and metasedimentary rocks of the AGB, possesses petrological and structural characteristics that are identical to those observed in tonalitic rocks of the OPB (Daoudene et al., 2014). It represents an antiformal window of the OPB within the AGB (Goutier, 2005; Daoudene et al., 2014; see below). Previous mapping (i.e. Hocq, 1994), as well as our own observations, shows that the OPB contains km-scale, scattered «lenses» of greenstone-type rocks (Figs. 2 and 3) consisting of amphibolite-grade mafic volcanic rocks and mafic-ultramafic intrusive rocks (Figs. 4a and b). The texture of these mafic volcanic rocks varies from primary, with locally preserved breccia and pillow structures (Fig. 4a), to migmatitic.

The Frotet-Evans greenstone belt (Fig. 2) is a large-scale example of metavolcanic belts surrounded by plutonic rocks of the OPB. It is divided into four segments, from west to east, the Evans-Ouagama, Storm-Evans, Assinica and Frotet-Troilus segments (cf. Boily, 2000). Figure 2 shows the two easternmost segments, the Frotet-Troilus and Assinica segments. The Frotet-Evans greenstone belt has been interpreted as the erosional remnant of an allochthonous thrust sheet by Sawyer and Benn (1993) but it rather represents an autochthonous synformal sequence within the OPB (see below). It preserves evidence for amphibolite-facies metamorphic conditions, except for its central part where greenschist-facies metasedimentary rocks are predominant (Simard, 1987; Brisson et al., 1997a and b). Volcanic and sedimentary rocks of the Frotet-Troilus segment are included into the Frotet Group; U-Pb zircon ages from felsic tuff layers and a felsic dyke yielded crystallization ages of 2780 ± 28 Ma and 2750 ± 28 Ma (Thibault, 1985), and 2782 ± 6 Ma (Pilote et al., 1997), respectively. The Assinica segment represents the western extension of the Frotet-Troilus segment (Fig. 2). It comprises a lower unit of mafic to felsic volcanic rocks, the Assinica Group, and an upper unit of sub-concordant, clastic sedimentary rocks, the Broadback Group. There are currently no isotopic data to constrain the age of the Assinica Group but correlation with the Rabbit Formation of the Evans Group in the Storm-Evans segment to the west, suggests that it is probably ca. 2758 ± 4 Ma (U-Pb on zircon; David, 2018 in Groulier et al., 2020), which indicates that the overlying clastic sequence of the Broadback Group is ca. 2755 Ma or younger.

2.2 The Abitibi Greenstone Belt

The AGB is made up of ultramafic, mafic, felsic volcanic rocks and syn-volcanic intrusions of Late Archean age. It consists of several, east-west-trending assemblages of volcanic, volcanoclastic and sedimentary rocks (Fig. 1b) that have been deformed and metamorphosed at greenschist- to amphibolite-facies conditions (e.g. Daigneault et al., 2002). The volcanic domains are separated by narrow and linear belts of clastic sedimentary rocks that are frequently associated with major fault zones (Ludden et al., 1986; Percival, 2007). The youngest sequence of these clastic sedimentary rocks, the Temiskaming Group, was deposited above angular unconformities between ca. 2679 and ca. 2670 Ma (e.g. Robert et al., 2005). Based on the age of the various volcanic sequences, the AGB is subdivided into the Northern and Southern Volcanic zones originally separated by the Destor-Porcupine fault zone (Ludden et al., 1986; Chown et al., 1992; Daigneault et al., 2004) but relocated

approximately 50 km northward by Thurston et al. (2008; see their Figure 2). In the Southern Volcanic zone, corresponding to the Tisdale (2710-2704 Ma) and Blake River (2704-2695 Ma) assemblages of Thurston et al. (2008; Fig. 1b), peak of regional metamorphism has been bracketed at 2680-2660 Ma by Powell et al. (1995), and at 2665-2660 Ma by Robert et al. (2005) and Tremblay et al. (2020). The volcanic and sedimentary rocks, which together represent about 50-60% of the AGB, bound large plutonic domains dominated by TTG-type plutons (Fig. 1b), and both the volcano-sedimentary assemblages and plutonic domains are intruded by syn- and post-tectonic granite, granodiorite and syenite plutons that span ages as young as ca. 2650 Ma (Feng et al., 1992; Daigneault et al., 2002; Robert et al., 2005). In the Val d'Or area (Fig. 1b), the Preissac-Lacorne batholith is a typical example of these syn- to late-orogenic intrusions. It is made up of a composite series of intrusions in which two distinct types and ages of granitic rocks are present: an early, subalkaline to alkaline, monzodiorite-monzonite-granodiorite-syenite series emplaced between 2690 and 2670 Ma; and a younger, S-type garnet-muscovite granite series dated between 2660 and 2642 Ma, and probably derived from a major metasedimentary source (Feng et al., 1992; Ducharme et al., 1997; Daigneault et al, 2002).

In the study area (Fig. 2), the volcanic rocks of the AGB belong to the Northern Volcanic zone. It mainly consists of two volcanic cycles formed between ca. 2.8 and 2.7 Ga (e.g. Leclerc et al., 2011), and belongs to 2750-2711 Ma volcanic rocks of the Kidd-Monro, Stoughton-Roquemaure, Deloro and Pacaud assemblages with local >2750 Ma occurrences (Fig. 1b; Thurston et al., 2008). In Chibougamau (Fig. 2), the base of the volcanic sequence belongs to the Chrissie Formation, which is currently one of the oldest volcanic units of the AGB at 2791.4 +3.7/-2.8 Ma (U-Pb zircon age; David et al., 2011). It consists of mafic to felsic volcaniclastic rocks, calk-alkaline rhyolites, and tholeiitic-to-andesitic basalts. The Roy Group overlies the Chrissie Formation. It includes two volcanic and sedimentary cycles and is estimated to be up to 13 km-thick (Allard et al., 1985; Dimroth et al., 1984; Daigneault et al., 1990). The lower cycle consists of tholeiitic basalts, the Obatogamau Formation, overlain by tholeiitic rhyolites and calk-alkaline volcaniclastic.rocks of the ca. 2732 Ma to ca. 2726 Ma Waconichi Formation (Daigneault and Allard, 1990; Legault, 2003; Leclerc et al., 2011; David et al., 2012). The upper cycle of the Roy Group comprises, from base to top, the Bruneau, Blondeau, Scorpion and Bordeleau formations, which consist of basalt and andesitic basalt at the base overlain by a well-bedded sequence of volcaniclastic and sedimentary rocks (Leclerc et al., 2011). In the Chibougamau area, a lapilli tuff of the Scorpion Formation

yielded U-Pb crystallization age on zircon of 2716,4 ±1,0 Ma (David et al., 2012). In the Lac-au-Goéland area (Fig. 3), rocks correlatives to the Bordeleau Formation belong to the Bell River and Dussieux formations and yielded zircon U-Pb ages of 2725-2717 Ma (Goutier et al., 2004; David, 2005; David et al., 2006).

The Opémisca Group (Fig. 2) is a sequence of clastic sedimentary and volcanic rocks overlying the Roy Group (Charbonneau et al., 1991; Leclerc et al., 2008; Leclerc and Houle, 2013). From base to top, it consists of the La Trêve, Daubrée, Stella and Haüy formations (Charbonneau et al., 1991). In the Chibougamau area, the Stella Formation has been interpreted as a lateral equivalent to the La Trêve and Daubrée formations (Charbonneau et al., 1991). The La Trêve Formation consists mainly of polygenic conglomerates with heterogeneous clasts, including TTG granitoids and mafic-to-felsic volcanics, whereas the Daubrée Formation is made up of turbidites. The Haüy Formation corresponds to a volcanic sequence mainly composed of K-rich porphyric andesites with lenses of conglomerate. The Haüy lava flows and associated volcaniclastic sediments have been interpreted as the result of evolved arc volcanism and backarc basin sedimentation (Mueller, 1991). In the Stella and Haüy formations, detrital zircons provided maximum ages of deposition of 2704 ± 2 Ma (Leclerc et al., 2012) and 2691.7 ± 2.9 Ma (David et al., 2007), respectively. In the Lac-au-Goéland area (Fig. 3), the Daubrée Formation is intruded by the Inconnue River Diorite, which yielded a U-Pb zircon age of 2693.6 ± 2.9 Ma (McNicoll and Goutier, 2008).

3. REGIONAL STRUCTURES

According to Sawyer and Benn (1993), the OPB records three generations of structures. The oldest is related to D_1 and a penetrative, moderately dipping foliation (S_1) hosting broadly distributed, WSW-ENE-trending mineral and stretching lineations (Fig. 4b). S_1 corresponds to the regional gneissic foliation and defines a metamorphic layering that is axial-planar to intrafolial F_1 folds. D_1 has been attributed to a top-to-the SW verging deformation. Sawyer and Benn (1993) argued that S_1 was folded during a D_2 deformational event, marked by East-West trending, steeply North- or South-dipping compressive shear zones. S_2 is a steeply dipping biotite foliation recording amphibolite-greenschist facies metamorphic conditions, although it may locally attain the amphibolite facies. It frequently forms a composite S_{1-2} fabric with D_1 structures. D_1 and D_2 has been attributed to the progressive development of an overall SSE-verging fold-and-thrust belt (and inferred backthrusting) along the AGB-OPB boundary and southward (Benn et al., 1992; Sawyer and

234 Benn, 1993; Lacroix and Sawyer, 1995). Sawyer and Benn (1993) also recognized a D_3 event,
235 related to NE-SW and NW-SE-trending strike-slip shear zones cutting across both the Frotet-
236 Evans and the Abitibi greenstone belts (see Fig. 2).
237 In the AGB of the study area, existing structural studies of regional extent have
238 documented four deformational phases (e.g. Dimroth et al., 1986, Daigneault et al., 1990;
239 Leclerc et al., 2012; Mathieu et al., 2020), the youngest one (D_4) being related to the
240 Mesoproterozoic Grenvillian orogenic cycle (Daigneault et al., 1990). D_1 has been attributed
241 to an early-formed series of drape folds devoid of axial-planar schistosity (Daigneault et al.,
242 1990). D_2 is related to syn-metamorphic folding and the development of the regional EW-
243 trending schistosity (S_2), it corresponds to F_{2a} and F_{2b} folds as described by Leclerc et al.
244 (2012). D_1 and D_2 of the AGB correlate with the Benn's et al. (1993) $D_{1\text{-}2}$ phase of the OPB.
245 According to Mathieu et al. (2020), the D_3 phase corresponds to the waning stage of the main
246 deformation event that reactivated E- W- striking D_2 reverse faults as transcurrent
247 strike- slip faults. In contrast, Leclerc et al. (2012) described D_3 structures as NE-striking
248 shear zones cutting across earlier E-W trending D_2 shears/faults (Fig. 2).
249 Our comprehension and interpretation of structures in the study area are similar to
250 those described above. We think that $D_{1\text{-}2}$ and D_3 belong to progressive and long-lasting
251 deformational events. In the following sections, we describe fabric and structures related to
252 those $D_{1\text{-}2}$ to D_3 events in both the AGB and the OPB. These descriptions are based on our
253 own field observations and from previous studies.
254
255 **3.1 $D_{1\text{-}2}$ phase of deformation**
256 D_2 deformation structures are regionally-developed and associated with folding of the
257 volcanic and sedimentary rocks of the AGB (Figs. 2 and 3) whereas the D_1 metamorphic
258 layering is restricted to the lowermost stratigraphic part of that belt. Regional folds (F_2) have
259 variable wavelength and their axial traces strike East-West, although they are locally
260 reoriented due to younger D_3 strike-slip shears, such as the Nottaway shear zone (Fig. 2). In
261 the Lac-au-Goéland area (Fig. 3), for instance, to the southwest of the Nottaway shear zone,
262 S_2 trajectories within the AGB are NW-SE trending and define a F_3 syncline, the Maicasagi
263 syncline (Fig. 3; Goutier, 2005). Overall, the regional pattern of folding of the AGB is
264 characterized by a north-south succession of F_2 synclines and anticlines. The core of synclines
265 is usually occupied by the Opémisca Group, whereas the anticline crests expose the

underlying volcanic rocks of the Roy Group which are, locally, crosscut by large pre- to syn-tectonic intrusions such as the Opémisca and Chibougamau plutons (Fig. 2).

The volcanic and sedimentary rocks of the AGB are characterized by a weakly to moderately developed regional schistosity (S_2), although some rock exposures seem to be devoid of structural fabric development (Fig. 4d). When present, S_2 is pervasive, strikes East-West and dips steeply either to the north or the south (Figs 5 and 6a). Towards the contact with the OPB, the volcanic rocks of the Roy Group are more intensely foliated, the dominant foliation (S_1) is there tightly folded by F_2 (Fig. 4e), although that, most of the time, it forms a composite $S_{1\text{-}2}$ fabric and consists of a metamorphic layering marked by metamorphic minerals such as biotite and hornblende (see section 4), that corresponds northward to the flat-lying S_1 gneissic fabric of the OPB gneisses. Our interpretation is that the OPB gneissic foliation is verticalized and transposed into S_2, it forms there a $S_{1\text{-}2}$ metamorphic layering that is subparallel to the contact between the OPB and the AGB (Fig. ~~6~~5) and is absent farther south in the up-stratigraphy, lower-grade rocks of the AGB. The bedding plane, when visible, is usually parallel to the regional S_2 that is marked by the alignment of amphibole and biotite in amphibolite-grade rocks (as for S_1) and by chlorite, epidote and albite in greenschist and sub-greenschist facies rocks of the AGB.

East-West-trending shear zones cut the volcanic and sedimentary sequences of the AGB. These sub-vertical shear zones are poorly exposed. Previous studies (e.g. Dimroth et al., 1986; Daigneault et al., 1990; Leclerc et al., 2012) indicate they are mainly located on the limbs of regional-scale F_2 folds (Fig. 2), some of the latter being synformal troughs occupied by lower grade sedimentary rocks of the Opémisca Group (Fig. 4d). As for F_2 folds, these shear zones are deflected in the vicinity of younger NE- and NW-trending strike-slip shear zones (Figs. 2 and 3). S_2 increases in intensity toward and within these D_2 shear zones and hosts steeply plunging stretching and/or mineral lineation, suggesting significant subvertical elongation (Dimroth et al., 1986; Daigneault et al., 1990). Shear-sense indicators are rare but when present, they suggest that the shear zones correspond to north or south side-up reverse faults.

In the OPB, dominant deformation fabric are attributed to D_1 and expressed by a weakly- to well-developed metamorphic foliation (S_1) showing variable orientations (Fig. 5). S_1 trajectories in the OPB define an East-West trending, elongated dome-and-basin geometry, consistent with the overall trend of D_2 regional folds and structures in the adjacent AGB (Fig. 5). Mineral lineations, defined by the alignment of quartz-feldspar aggregates, are more

discrete and of variable orientation as compared to the AGB (Fig. 6b). These lineations plunge at low angle within the regional foliation. In the area located between the Frotet-Evans and Abitibi greenstone belts (Fig. 2), there are abundant decametre-scale of foliated, amphibolite-grade lenses of basaltic metavolcanic rocks within the OPB gneisses. The foliation in these metavolcanic rocks trends parallel to the S_1 metamorphic layering in the surrounding gneisses.

The AGB-OPB contact is not clearly exposed in the area of Figure 2. Rock exposures are sparse along that contact which is locally masked by syn- and post-orogenic intrusions, such as the Barlow pluton in the Chibougamau area (Fig. 2) and the Canet and Maicasagi plutons (Sawyer and Benn, 1993; Goutier, 2005; Daoudene et al., 2014) in the Lac-aux-Goéland area (Fig. 3). In the latter area, the Nomans tonalite, located to the south of the inferred AGB-OPB contact, shows the same structural style as the gneissic rocks of the OPB. S_1 trajectories within the tonalite (Fig. 5) indicate that it is a D_2-related structural dome that is attached to the OPB at depth (Goutier, 2005; Daoudene et al., 2014). The occurrence of foliation-parallel, amphibolite lenses along the AGB-OPB contact has been considered as evidence for the structural imbrication of both terranes and the allochthonous nature of the AGB (Sawyer and Benn, 1993). We do not think that this boundary corresponds to a major displacement zone (see section 4 below), although S_1 appears there to be more intensely developed in both the metavolcanic rocks of the AGB and the OPB tonalites. S_1 trajectories are parallel to the AGB-OPB contact (Fig. 5), suggesting that it formed, or was transposed, during D_1. There are relatively few lineation measurements in the study area (Fig. 6). Sawyer and Benn (1993) reported SE-plunging mineral lineations in the hanging wall of the Lac Matagami shear zone, a late (D_3) sinistral fault located west of the Lac-au-Goéland area, as well as down-dip lineations along the Barlow fault in the Chibougamau area. In this latter area, stretching lineations plunge moderately to the south, but locally show significant variations of orientation due to the proximity of syn- and post-tectonic intrusions (Bedeaux et al. 2021).

The Abitibi and Frotet-Evans greenstone belts share a similar internal geometry and relationships with the underlying plutonic rocks of the OPB. However, the Frotet-Evans greenstone belt is of higher metamorphic grade and structurally more complex than the AGB (see Gosselin, 1996). It occupies the core of a large-scale series of east-west-trending F_2 synclines (Figs. 2 and 5) within the OPB gneisses, some of them being marked, as for the

AGB, by steeply dipping reverse faults on their limbs (Simard, 1987; Gosselin, 1996; Brisson et al., 1997a and 1997b).

In the study area, we did not observe unambiguous shear-sense criteria within the AGB-OPB contact zone. Along the AGB-OPB contact, there are numerous tonalitic to granitic dykes crosscutting basaltic amphibolites of the AGB (Fig. 4f). Most of these dykes are in irregular and diffuse contacts with the host rocks and are slightly to moderately foliated, suggesting high temperature syntectonic emplacement.

3.2 D_3 structures

The D_3 phase of regional deformation is more localized as compared to D_{1-2}. It is essentially associated with strike-slip displacement along NE- and NW-trending shear zones. The Nottaway River shear zone (Figs 2 and 3) is the largest of the NW-SE-trending D_3 shear zones in the study area. It cuts across the D_{1-2} structures of both the AGB and OPB. It delimits the western boundary of the Frotet-Evans greenstone belt, which is also cut by another major NW-trending shear in its middle part, the Lucky Strike River shear zone (Fig. 2). A mylonitic S_3 schistosity is pervasively developed along these shear zones (Fig. 7a). F_3 dextral folds, with S_3 as an axial-planar foliation, can be observed in the vicinity of D_3 shear zones (Fig. 7b). S_3 hosts a well-developed, sub-horizontal stretching lineation (Fig. 7c), indicating that D_3 is dominated by strike-slip motions. Abundant macroscopic and microscopic shear-sense indicators, such as shear bands, S-C fabric (Fig. 7a and 7d), mica fish (Fig. 7e), drag folds and asymmetrical boudinage (Fig. 7f) are widely present and attest for dextral displacement along the NW-SE-trending shear zones. NE-trending shears, such as the Lac Lamark shear zone (Fig. 2), are characterized by the same type of ductile fabric but are sinistral, as indicated by regional mapping and the offset of marker horizons in the Chibougamau area (e.g. Chown et al., 1992; Daigneault et al., 2002). The two sets of strike-slip shear zones, NW- and NE-trending, form a conjugate system.

4. METAMORPHISM

In this section, we describe the metamorphic characteristics of rocks in the study area, from top to base of the AGB stratigraphy, and from the lower-grade rocks of the AGB towards the high-grade metamorphic units of the OPB.

The sedimentary rocks of the Opémisca Group, which occupy the core of regional F_2 synclines, do not show macroscopic evidence of metamorphic recrystallization. Primary

sedimentary structures, such as bedding (Fig. 4d), and pillow structures in volcanic rocks of the underlying Roy Group are frequently well-preserved (Fig. 8a). Low-grade metamorphic minerals, such as chlorite, sericite, epidote, and actinolite-tremolite progressively appear down into the stratigraphic pile and can be relatively abundant at the margins of synclines, indicating that the lowermost part of the Opémisca Group attained greenschist-facies. The metamorphic grade of these sedimentary rocks even reaches the amphibolite facies towards the AGB-OPB contact, specifically along the northern boundary of the Waconichi Lake syncline (Figs 2) where the Opémisca metapelites contain biotite, garnet, and staurolite (Fig. 8b). Staurolite occurs as mcm-long, oblong-shaped and corroded crystals defining the S_2 foliation. Lithologies of the Opémisca Group also locally contain late- to post-kinematic metamorphic minerals such as, for instance, randomly oriented chloritoïds (Fig. 8c) suggesting late-stage growth.

The mafic rocks of the Roy Group were dominantly metamorphosed to the greenschist-facies (Allard et al., 1985). These rocks are pervasively chloritized and contain typical low-grade metamorphic minerals such as albite, epidote and actinolite-tremolite defining the S_2 schistosity. In the vicinity to the contact with the OPB, they contain, however, metamorphic minerals of higher temperature characteristic of the amphibolite facies. Actinolite-tremolite is there replaced by hornblende and biotite. Garnet is present and usually forms irregular patches that are preferentially distributed along the pillow margins of mafic volcanic flows (Fig. 8d). Garnet is frequently retrogressed into a mixture of epidote, amphibole and chlorite. Some basaltic amphibolites contain epidote porphyroblasts overprinting the composite $S_{1\text{-}2}$ foliation as well as randomly oriented crystals of actinolite, suggesting retrogressive conditions after peak metamorphism.

Metamorphic conditions recorded by the OPB are more difficult to evaluate precisely, mainly because these rocks essentially consist of intermediate and felsic plutonic rocks. However, most of the mafic rocks of the Opatica contain hornblende+andesine assemblages, which, with the occurrence of rare garnet- or clinopyroxene, imply amphibolite-facies conditions (Sawyer, 1998). The intermediate and felsic gneissic rocks are commonly plastically deformed and show coarse-grain recrystallization textures. Feldspar and quartz crystals display evidence for syn-kinematic growth and recrystallization. Grain boundaries are cuspate and undulated (Fig. 8e), which is indicative of extensive high-temperature grain boundary migration during deformation (Gower and Simpson, 1992). Myrmekitic textures preserved in some coarse-grained K-feldspars also indicate metamorphic temperatures in

excess of 500-550°C (Simpson, 1985; Simpson and Wintsch, 1989). All these observations indicate that the regional D_1 deformation structures in the OPB gneisses were acquired at amphibolite-facies conditions of metamorphism, or higher. Some felsic rocks display quartz grains with a chessboard texture, which is typical of intra-crystalline slip textures developed at subsolidus temperatures (i.e. above 600°C; Blumenfeld et al., 1986; Gapais and Barbarin, 1986; Mainprice et al., 1986; Schmid and Casey, 1986). Evidence for anatectic melting is abundant in the deepest crustal domains of the OPB and marked by the occurrence of migmatites (Fig. 8f). Anatectic melt occurs in D_2 shear zones located near to the center of the OPB (Sawyer and Benn, 1993). However, according to Sawyer (1998), melting is late- to post-D_1, as suggested by S_1 disappearing within neosome patches and paleosome material showing remnants of the S_1 foliation.

There are very few pressure-temperature (P-T) studies for metamorphic rocks of the AGB. At the scale of the belt, regional metamorphism ranges in grade from subgreenschist-facies to the greenschist-amphibolite facies transition. In the Blake River and Tisdale assemblages (Fig. 1b), low-pressure regional metamorphism is indicated both by the occurrence of the actinolite-oligoclase zone, and the persistence of pre-regional metamorphism andalusite. According to Powell et al. (1995), pressure of regional metamorphism and of late to post-orogenic contact metamorphism were similar (360-400 MPa), indicating that low-pressure conditions persisted throughout the tectonic evolution of the AGB. Regionally, isograds dip shallowly to the north and trend subparallel to lithological and structural trends (Powell et al., 1995; Faure, 2015). In the Chibougamau area (Fig. 2), Bedeaux et al. (2020) suggested P-T conditions of 550±50ºC and 6±1.2 kbar for basaltic amphibolites of the AGB cropping out in the vicinity of the contact with the OPB. In the OPB, Sawyer (1998) determined a peak metamorphism temperature of 760ºC for the migmatite facies rocks, and pressures of 5.2-6.2 and 6.3-7.1 kbar for diatexite migmatites and adjacent amphibolites, respectively. Pressure measured in the Canet pluton of the Lac-au-Goéland area (Fig. 3) were significantly lower, at 1.7-2.6 kbar (Sawyer, 1998), suggesting that the emplacement of this pluton occurred during exhumation of the OPB gneisses.

Figure 9 presents a series of north-south trending, interpretative structural profiles between the Lac-au-Goéland (profile A-A') and the Chibougamau areas (profile D-D'). These profiles show that the OPB exposes deeper crustal rocks and higher-grade metamorphic rocks as compared to the adjacent and overlying volcanic rocks of both the Frotet-Evans and Abitibi greenstone belts, and that both the OPB and AGB originally constituted an almost continuous

middle-lower (the OPB) to upper crust sequence (the AGB). This contrasts with Sawyer and Benn's (1993) interpretation showing the Frotet-Evans greenstone belt as a far-travelled, south-directed allochthonous nappe thrusted over the OPB gneisses, and both units forming a basement-cored nappe thrusted southward over the AGB (see their figures 6 and 8). We think that their structural interpretation is unlikely for the following reasons, (i) in typical crustal-scale thrust systems (Boyer and Elliott, 2002; Butler and Bond, 2020), older rock units and/or higher grade (deeper) metamorphic rocks are transported over younger and/or lower grade (shallower) metamorphic rocks, which is obviously not the case here, and (ii) it would imply that the Frotet-Evans greenstone belt represents a klippen that roots 50 km, or more to the north, in the Colomb-Chabouillé Group of the Nemiscau subprovince along its southern ~~the~~ boundary with the OPB (see Fig. 2); there are, however, no metamorphic break and major suture between the Nemiscau and Opatica subprovinces, and regional mapping and structural analyses rather suggest the relative exhumation of the OPB as compared to the Nemiscau (Pedreira-Perez et al., 2020), which do~~es~~ not fit the Sawyer and Benn's (1993) thrusting model.

5. $^{40}Ar/^{39}Ar$ GEOCHRONOLOGY

In the following section, we present thirty-one $^{40}Ar/^{39}Ar$ laser probe experiments on single grains of amphibole, biotite and muscovite from eighteen rock samples from both the AGB and OPB.

5.1 Analytical method and procedures

Single grains of amphibole, biotite and muscovite were handpicked under a binocular microscope from 250µm to 1000µm mineral fractions. Separated minerals were irradiated with Cd-shielding, in the 5C high neutron flux facility of the McMaster Nuclear Reactor (Hamilton, Ontario, Canada). This process lasted 298 h with a global efficiency (J/h) of $5.83x10^{-5}$ h^{-1}. The irradiation standard was amphibole Hb3gr (Turner et al. 1971; Roddick 1983, Jourdan et al. 2006; Jourdan and Renne 2007); 1081.0 ± 1.2 Ma according to Renne et al. (2010, 2011).

Single grains of amphibole, biotite and/or white mica were analyzed by the $^{40}Ar/^{39}Ar$ method in step-heating using a CO_2 laser probe coupled with a MAP 215 mass spectrometer. The analytical procedure is described by Ruffet et al. (1991, 1995, 1997). The five argon isotopes and the background baselines were measured in eleven cycles, in peak-jumping

mode. Blanks were performed routinely each first or third/fourth run and subtracted from the subsequent sample gas fractions. All isotopic measurements account for K and Ca isotopic interferences, mass discrimination and atmospheric argon contamination. Apparent age errors are plotted at the 1σ level and do not include the errors on the $^{40}Ar^*/^{39}Ar_K$ ratio, age of the monitor and decay constant.

A plateau is obtained when calculated $^{40}Ar^*/^{39}Ar_K$ ratios of at least three consecutive steps, containing a minimum of 70% of the ^{39}Ar released, agree with the weighted mean calculated $^{40}Ar^*/^{39}Ar_K$ ratio of the plateau segment. This 70% threshold is a requirement criterion that we use in all our geochronological studies, and it is much more restrictive than the 50% threshold set subjectively (in their own words) used by Fleck et al. (1977) and still adopted by most users of the $^{40}Ar/^{39}Ar$ method (e.g. Schaen et al., 2021). Since the amount of $^{39}Ar_K$ released is not a disqualifying criterion, we use the concept of pseudo-plateau (Cheilletz et al., 1999), which meets the same statistical criteria except for the cut-off threshold (<70% of $^{39}Ar_K$), and which is much more efficient for the analysis of complex mineral phases. In our detailed analysis of spectra, we also use a plateau-like descriptive terminology which refers to a weighted average age calculated over segments of apparent ages, not necessarily joined (e.g. edges of a saddle-shaped segment), but which are considered to be geologically significant. The errors on the $^{40}Ar^*/^{39}Ar_K$ ratio and age of the monitor and decay constant are included in the final calculation of the error margins on the pseudo- and plateau ages or for apparent ages individually cited. $^{40}Ar/^{39}Ar$ ages are provided with 1σ errors. Analytical data, parameters used for calculations (isotopic ratios measured on K and Ca pure salts; mass discrimination; atmospheric argon ratios; J parameter; decay constants, etc.) and reference sources are available in the complementary data repository.

5.2 Isotopic closure temperatures

A radiochronological system is the combination of the crystal lattice of a mineral phase and an isotopic pair consisting of a radiogenic element and its radioactive precursor, e.g. $^{40}Ar^*$ and ^{40}K, the latter (K) being or not a constituent of the lattice. The analysis of isotopic systems, particularly those involving noble gases, has long focused on the behaviour of the radiogenic element, in this case $^{40}Ar^*$, the host minerals being themselves considered inert and the fate of the isotopic system being exclusively governed by the diffusion of the gas under temperature control, as described by Fick's laws. This led to the notion of isotopic blocking temperature initially introduced by Jäger et al. (1967), formalized as the isotopic

closure temperature (T_c) by Dodson (1973) and then nuanced with the notion of isotopic closure window by Dunlap (1997). Therefore, during cooling and for a given isotopic system (mineral and isotopic pair), the isotopic chronometer initializes when diffusion becomes negligible because the temperature has dropped below its isotopic closure temperature.

T_c for amphibole is difficult to estimate. In addition to the effect of cooling rate and size of diffusion domains, amphibole diffusivity is influenced by ionic porosity (Fortier and Giletti, 1989; Dahl, 1996). On the basis of natural hornblende compositions, Dahl (1996) suggested a T_c range of 480-550°C, which has been re-evaluated at 550-560°C by Villa (1998) on the basis of Kamber's et al. (1995) experiments suggesting that, depending on the crystal lattice characteristics, hornblende may form a closed system to Ar diffusion at temperature as high as 580°C and a cooling rate of 0.7°K/Ma (Villa et al., 1996). In this study, we will therefore consider a median T_c range value of 550-600°C for amphiboles.

T_c for biotite ranges from 250°C to 400°C (Harrison et al., 1985; Montigny, 1985; McDougall et Harrison, 1988; Spear, 1993). In the absence of deformation and fluid-related recrystallization, it may be at least as high as ~450°C (e.g. Villa and Puxeddu, 1994). With diffusion domains in the range 100-1000 μm and a cooling rate lower than 100°C/Ma, T_c for biotite is ca. 400°C (e.g. Grove and Harrison, 1996). We will here consider a T_c-biotite range value of 350-450°C.

Purdy and Jäger (1976) originally estimated T_c of white micas at 350°C, by calibration of isotopic ages versus metamorphic grade. This estimate was erroneous and underestimated (Villa, 1998). Subsequent studies have shown that in the absence of deformation and fluid-enhanced recrystallisation, T_c for muscovite may reach 500°C (Villa, 1998; Bosse et al., 2005), and even temperatures higher than 550°C for phengite under blueschist facies metamorphic conditions (Lister and Baldwin, 1996). Using experimental muscovite diffusion coefficients yielded by Harrison et al. (2009), Pitra et al. (2010) calculated a 390-590°C isotopic closure temperature range for white micas, using various effective diffusion radii (100 to 1000 μm) and cooling rates (1 to 1000°C/Ma). Considering diffusion domain sizes of 100-1000 μm and cooling rates between 1°C and 10°C/Ma, a more reasonable and realistic assessment for the cooling of Archean rocks (e.g. Chardon et al., 2009), isotopic closure of white micas would occur in the temperature range 400-500°C.

The use of above T_c range estimates should only concern crystals unaffected by deformation and/or recrystallization processes, (e.g.Villa, 1998). In contexts where these phenomena occur, the other component of the radiochronological system, the crystal lattice of

529 the mineral carrying the istopic system, must also be considered because it may no longer
530 remain inert. Deformation can damage crystal lattices, enhances Ar diffusion, and promotes
531 the formation of intra-crystalline domains with lower diffusion length-scales and lower T_c. In
532 the presence of fluids, minerals (or intracrystalline sub-domains) may recrystallize and neo-
533 grains may possibly grow, two configurations which, if they occur at $T \leq T_c$ and after initial
534 isotopic closure, will induce the recording of younger ages. Consequently, distinct intra-
535 crystalline domains with different chemical and isotopic compositions, and thus distinct ages,
536 may coexist within the same mineral/grain.
537 Cheilletz et al. (1999), Alexandrov et al. (2002) or Tartese et al. (2011) identified and
538 detailed a process of sequential fluid-assisted resets of K-Ar isotopic chronometer of white
539 mica from leucogranites. Tremblay et al. (2020) showed that K-Ar isotopic system of white
540 micas from auriferous quartz veins and hosting shear zones of the Bourlamaque pluton (Val
541 d'Or mining district, Abitibi) was driven by sequential dynamic recrystallization
542 (dissolution/recrystallization/neocrystallization/aggregation) linked to successive periods of
543 fluid circulation and deformation which occurred below T_c. Dunlap (1997) suggested that,
544 during ductile deformation, K-Ar isotopic system of white micas from mylonites could also
545 be partly driven by neocrystallization processes below T_c, at 250-350°C. $^{40}Ar/^{39}Ar$ amphibole
546 analyses (e.g. Tremblay et al., 2020) suggest that they also behave in the same way.
547
548 **5.3 Data processing**
549 Metamorphic minerals such as amphiboles and micas extracted from rocks deformed
550 or disturbed by fluids are usually texturally complex (recrystallized, composite grains, etc).
551 The $^{40}Ar/^{39}Ar$ analysis of such crystals is very useful, as information it provides integrates the
552 effects of the disturbing processes and therefore the timing of their occurrence, even if this
553 occurs below Tc (e.g. Cheilletz et al. 1999; Hames et al., 2008; Castonguay et al., 2007;
554 Tremblay et al. 2020). Hence, due to the complexity of $^{40}Ar/^{39}Ar$ results that arise from the
555 analysis of such materials, which are common in old rock series such as the Archean, their
556 processing must go beyond the simple visual examination of age spectra.
557 De Putter et al. (2015), De Putter and Ruffet (2020) and Tremblay et al. (2020)
558 presented and developed tools for the visualization and processing of complex $^{40}Ar/^{39}Ar$
559 systems. Three of these tools are classical: the plateau (Fleck et al., 1977) and pseudoplateau
560 age (PPA) (Cheilletz et al., 1999) concepts, and the probability density diagrams, which have
561 been first used for ^{39}Ar-^{40}Ar data by Deino & Potts (1992). Other tools are more atypical; (i)

562 the degassing and the weighted age spectra, which were designed to visualize Ar degassing
563 kinetics of $^{40}Ar/^{39}Ar$ experiments, and (ii) the resizing of age spectra which was developed to
564 ensure their statistical representativeness.
565 Amphibole $^{37}Ar_{Ca}/^{39}Ar_K$ spectra transcribe the evolution of the Ca/K ratio ($^{37}Ar_{Ca}$ # Ca
566 and $^{39}Ar_K$ # K with $^{37}Ar_{Ca}/^{39}Ar_K = CaO/K_2O$ / 2.179; Deckart et al., 1997) during step-heating
567 (degassing) experiments. Hence, a flat $^{37}Ar_{Ca}/^{39}Ar_K$ segment (homogeneous Ca/K ratio)
568 expresses the degassing of an amphibole component devoid of compositional zoning and/or
569 inclusion of another mineral species.
570
571 **5.4 Sampling strategy**
572 To document and compare the tectonothermal history of the AGB and OPB on both
573 sides of the contact zone, we performed a series of step-heating $^{40}Ar/^{39}Ar$ analyses of micas
574 and amphiboles collected in metamorphic and plutonic units of both terranes. Sixteen samples
575 are from the Lac-au-Goéland area, and two from the AGB-OPB contact in the Chapais-
576 Chibougamau area. Sample locations are shown in figures 3 and 4 whereas their geographic
577 coordinates are in Table 1.
578 Four amphibolite samples (YD0009A, YD0048A, YD0039A, and YD0100A) and a
579 garnet-staurolite micaschist sample (JF4065A) are from the AGB. These rocks show a well-
580 developed S_2 foliation marked by the preferred orientation of amphibole and/or biotite. In thin
581 sections, hornblendes from sample YD0009A and tremolites/actinolites from sample
582 YD0039A are homogeneous and unaltered, whereas dark green hornblendes YD0048A and
583 YD0100A show light-green rims or patches suggesting intracrystalline zonation during crystal
584 growth or recristallization. Biotites from samples YD0009A and YD0100A are green-colored
585 euhedral crystals whereas those from sample JF4065A (a metasedimentary rock) are dark-
586 brown-colored euhedral. There is no optically discernible occurrence of secondary chlorite in
587 these samples. Sample YD0037, from which were extracted amphibole and biotite grains, is a
588 slightly deformed diorite that shows petrographic characteristics similar to the Rivière
589 Inconnue Diorite (Fig. 3), which yielded a U-Pb zircon age of 2693.6 ± 0.6 Ma (McNicolls
590 and Goutier, 2008).
591 YD0018B, YD0020A, YD0063A, YD0035A, JG1245A, and YD0101A are tonalite
592 samples from the OPB. These tonalites are mainly composed of quartz and plagioclase and
593 contain various amounts of amphibole and/or biotite, which mark the regional foliation (S_1).
594 Amphiboles YD0018B, YD0020A, YD0063A and YD0101A are sub-automorphous. All

samples contain green- to brown-colored biotites that are commonly euhedral and only rarely chloritized.

Four samples of quartz-feldspar porphyry dykes were selected in both the AGB (YD0023A, YD0048B, and YD0009B) and the OPB (YD0023A). These dykes contain randomly oriented, coarse-grained muscovite crystals lacking microscopic evidence of recrystallization and/or deformation. A biotite grain from sample YD0009B was also analysed.

Two mylonite rock samples, YD0055A and YD0059A, from the Nottaway River shear zone were analysed. Sample YD0055A is a felsic rock belonging to the AGB. It shows a well-developed mylonitic foliation and contains abundant asymmetric muscovite crystals showing mica fish structures indicative of dextral shearing. These muscovite crystals also show secondary rims of neoformed micas typical of recrystallization. Sample YD0059A is a foliated tonalite from the OPB, it contains coarse-grained biotites that appear slightly altered and corroded. Most of these biotite grains also show fine rims of recrystallization.

Finally, we analyzed one sample of syenite of the Montviel alkaline intrusion (Goutier, 2005), which is associated to a carbonatite facies that has been dated at 1894 ± 4 Ma (U-Pb on zircons; David et al., 2006).

5.5 Results.

The step-heating $^{40}Ar/^{39}Ar$ results are presented on Figures 10 to 14. The distinct age spectra provided by duplicate analyses of amphibole and mica presented in the following sections confirm, as already stressed by Tremblay et al. (2020), that the interpretation of Archean material using the $^{40}Ar/^{39}Ar$ method is challenging and requires a detailed analysis of results.

5.5.1 The Abitibi Greenstone Belt.

The $^{40}Ar/^{39}Ar$ results for the AGB amphiboles and biotites are show in Figure 10. Analysis of amphibole 1 from sample YD0037A provides a rather flat age spectrum, with nevertheless a deflection of apparent ages in the intermediate temperature steps (Fig. 10a). The apparent ages, which are concordant on both sides of that deflection, allow the calculation of a plateau-like age at 2680.1 ± 3.6 Ma (56.3% of the total $^{39}Ar_K$ released), whereas the base of the deflection yields 2637.2 ± 9.0 Ma. The deflection of apparent ages is interpreted as the expression of partial recrystallization due to a disturbing event younger than

c. 2637 Ma of an amphibole grain whose isotopic system initially closed at c. 2680 Ma during cooling of the diorite below Tc. Degassing peaks expressed during this experiment confirm the coexistence of these 2 radiogenic components. The higher degassing rate of the oldest component, at c. 2680 Ma, in the first part of the spectrum and the homogeneous isotopic composition on that segment indicate that it is perfectly individualised, which is, however, apparently not the case for the younger component associated with recrystallization in the intermediate temperature domain of the spectrum where the two radiogenic components overlap. The concomitant decrease of apparent ages (from c. 2749 Ma to c. 2681 Ma), combined with calculated $^{37}Ar_{Ca}/^{39}Ar_K$ (#Ca/K) ratios (from c. 9.7 to 7.2) in the low to intermediate temperature steps of age, the $^{37}Ar_{Ca}/^{39}Ar_K$ spectra of amphibole 2 of sample YD0037A and the overall saddle shape of the age spectrum suggest the incorporation of excess argon. Calcic domains constitute reservoirs for excess argon as shown by Ruffet et al. (1990) for rimmed and patchy-zoned hornblendes. However, the convergence between the pseudo-plateau age calculated for the bottom of the saddle, at 2683.7 ± 4.9 Ma (15.4% of the total $^{39}Ar_K$ released), and the plateau-like age calculated for amphibole 1 supports the above estimated age (c. 2680 Ma) of an initial isotopic closure of amphiboles from YD0037A. The concordant plateau age at 2678.5 ± 2.9 Ma (85.6% of the total $^{39}Ar_K$ released), calculated from age spectrum of a biotite from sample YD0037A (Fig. 10a), is consistent with that interpretation and suggests a fast cooling path for that poorly-deformed diorite.

The two amphiboles of sample YD0039A, although appearing homogeneous and unaltered, also yielded distinct age spectra (Fig. 10b). Amphibole 1 yields a plateau age at 2673.1 ± 4.0 Ma (86.6% of the total $^{39}Ar_K$ released), slightly younger than the inferred age of initial closure for amphibole YD0037A, whereas amphibole 2 yielded a disturbed age spectrum showing an overall increase of apparent ages from c. 2548 Ma to c. 2620 Ma. These discrepancies are reflected in the respective $^{37}Ar_{Ca}/^{39}Ar_K$ spectra of the two experiments, which differ in terms of ratio values and overall trend for low to intermediate temperature steps. Microscopic observations reveal that some amphibole grains of YD0039A contain biotite lamellae along cleavage planes, which is attested by the presence of a small degassing peak in the first heating steps of the staircase-shaped age spectrum (amphibole 2 of Fig. 10b). If these biotite lamellae are as young as the biotite of amphibolite YD0009A (c. 2564 Ma, see below), as suggested by a low temperature pseudo plateau at 2548.3 ± 5.6 Ma, their degassing, partly concomitant with that of amphibole, may account for the staircase shape of the age spectrum. Since amphiboles from sample YD0039A are tremolite/actinolite rather

than hornblende, their calculated $^{37}Ar_{Ca}/^{39}Ar_K$ ratios are significantly higher (>20) than those of the other amphiboles (hornblende), which are usually <10 (Figs. 10a, 10c, 10d and 10e).

Except for a weak deflection of apparent ages in the intermediate to high temperature steps, the age spectrum of amphibole YD0009A (Fig. 10c) yields a plateau-like age of 2677.3 ± 3.6 Ma (77.8% of the total $^{39}Ar_K$ released), which is concordant with the c. 2675-2680 Ma amphibole cooling age calculated for samples YD0037A and YD0039A. A green biotite grain from YD0009A yields a plateau age approximately 110 m.y. younger at 2564.3 ± 3.4 Ma (97.7% of the total $^{39}Ar_K$ released; Fig. 10c). However, the increase of apparent ages of its high temperature steps, up to c. 2571 Ma (Fig. 10c), possibly testifies to a nearly complete reset of its isotopic system at or after c. 2560 Ma and subsequent to its initial closure. The above-mentioned subtle deflection of amphibole age spectrum probably correlates with the younger apparent ages (from c. 2612 to c. 2630 Ma) of the low temperature steps, which are characterized by $^{37}Ar_{Ca}/^{39}Ar_K$ (#Ca/K) ratios lower than those of the main phase at c. 2678 Ma (c. 5 vs. c. 6.5). These low-temperature steps define a specific degassing peak that probably express, as for amphibole YD0039A (see above), the degassing of scarce biotite lamellae plated in amphibole cleavage planes (e.g. Castonguay et al., 2001).

The age spectrum of amphibole YD0048A (Fig. 10d) is consistent with thin section examination which shows light-green rimmed and/or patchy zoned minerals indicative of patchy recrystallisation of amphiboles. The isotopic record of cooling at c. 2675-2680 Ma shown by samples YD0037A, 39A and 0009A was erased, at least locally on a grain scale, during a recrystallisation event at 2643.9 ± 3.5 Ma. The analysis of the degassing rate of amphibole YD0048A supports this interpretation because, unlike amphibole YD0037A, the main radiogenic component (i.e. expressed by the highest degassing rate; Fig. 10d) is the radiogenic component associated with recrystallisation.

The light-green rimmed and/or patchy zoned amphibole from sample YD0100A, texturally similar to those of YD0048A, provides a roughly flat but bumpy age spectrum (Fig. 10e) that yields a plateau-like age at 2598.3 ± 3.0 Ma (67.3% of the total 39ArK released), younger than amphibole cooling and/or disturbance ages of previous samples. It may represent the best estimate of the age of the post-initial cooling disturbance recorded by amphibole 1 from diorite YD0037A. A green euhhedral biotite grain from sample YD0100A provides a hump-shaped age spectrum with maximum apparent ages at c. 2494 Ma. This age spectrum shape indicates that the biotite grain is chloritized (Ruffet et al., 1991), which casts doubt on the reliability of this age.

A brown biotite grain from sample YD4065A yields a staircase-shaped age spectrum whose flat segment defined by high temperature steps provide a pseudo-plateau age at 2644.3 ± 3.6 Ma (Fig. 10f). Such a staircase-shaped age spectrum is typical of $^{40}Ar^*$ loss by volume diffusion induced by a thermal event subsequent to initial crystallization and/or cooling (e.g. Turner, 1968). The apparent age at 2571.8 ± 9.4 Ma of the low-temperature step provides a maximum estimate for the age of that $^{40}Ar^*$ loss event. Its concordance with the plateau age yielded by biotite from sample YD0009A suggests that $^{40}Ar^*$ loss most likely occurred around c. 2560 Ma. In this scenario of $^{40}Ar^*$ loss, the age at c. 2644 Ma calculated from the high-temperature steps should only be a minimum estimate of the age of isotopic closure during initial cooling. Nevertheless, its perfect agreement with the recrystallization age of amphibole YD0048A, also at c. 2644 Ma, argues for its validity.

5.5.2 The Opatica Plutonic Belt.

Amphibole and biotite age spectra from the OPB are show in Figure 11. All samples were collected in tonalites.

Amphibole age spectra of samples YD0018B, YD0020A, YD0063A, and YD0101A are more disturbed than those of the AGB. The effects of thermal disturbances following initial isotopic closure appear to be quite significant, especially those related to an event equivalent to the c. 2644 Ma disturbance recorded by the AGB amphiboles. The analysis of degassing patterns of amphiboles YD0020A and YD0063A (Figs. 11a and b) indicates that the radiogenic component associated with partial recrystallization induced by this disturbing event constitutes the main radiogenic component of these amphiboles. Related segments of age spectra allow the calculation of concordant plateau ages at 2644.5 ± 3.8 Ma (72.6 % of the total $^{39}Ar_K$ released) and 2648.4 ± 3.0 Ma (69.6 % of the total $^{39}Ar_K$ released), respectively.

Several elements of the $^{40}Ar/^{39}Ar$ experiments suggest that this latter event affected amphiboles with initial ages of 2670-2665 Ma, which correspond to the apparent age bracket yielded by high-temperature steps of amphiboles YD0020A and YD0063A (Figs. 11a and b), at 2668.8 ± 8.9 Ma and 2672.3 ± 8.9 Ma, respectively. The validity of these high temperature apparent ages is supported by consistencies with pseudo-plateau ages at 2665.6 ± 4.4 Ma and 2668.9 ± 5.3 Ma calculated from the disturbed age spectra of amphiboles YD0018B and YD0101A (Figs. 11c and d). The degassing patterns of the latter amphiboles, especially YD0101A (Fig. 11d), indicate that the related radiogenic component is a major component of

their respective isotopic system. However, some aspects of the age spectrum shapes of YD0018B and YD0101A remain enigmatic; for instance, the breakdown of the high-temperature apparent ages of amphibole YD0018B (down to 2588.8 ± 9.2 Ma, Fig. 11c) coinciding with an abrupt and unusual drop of the $^{37}Ar_{Ca}/^{39}Ar_K$ ratio (down to c. 2.69), which may be due to the degassing of a non-amphibolitic component. In addition, the concomitant increase of the high temperature $^{37}Ar_{Ca}/^{39}Ar_K$ (#Ca/K) ratios of amphibole YD0101A and decrease of apparent ages (Fig.11d) are unexpected. Such unusual behaviours may be due to a younger disturbing event, as suggested by biotite plateau ages at 2600.3 ± 3.0 Ma (94.8 % of the total $^{39}Ar_K$ released), 2583.4 ± 4.5 Ma (70.7 % of the total $^{39}Ar_K$ released) and 2588.2 ± 3.5 Ma (96.3 % of the total $^{39}Ar_K$ released) yielded by samples YD0020A, YD0063A and YD0035A, respectively (Figs. 11a, b and e). The existence of even younger disturbing events is suggested by biotites YD1245A (pseudo-plateau age at 2544.3 ± 3.5 Ma) and YD0101A (plateau age at 2525.4 ± 3.1 Ma) (Figs. 11d and f). However, the chlorite alteration of some biotite grains (hump-shaped age spectrum YD1245A) and/or the apparent occurrence of $^{40}Ar^*$ loss (staircase-shaped age spectrum YD0101A) makes these latter age estimates hazardous.

5.5.3 Granitic dykes.

Three muscovite single grains from quartz-feldspars granitic dykes collected in the Lac-au-Goéland area, YD0009B, YD0023A and YD0048B, provided rather disparate results (Fig. 12). The saddle-shaped age spectrum of muscovite YD0009B (Fig. 12a) suggests the presence of two radiogenic components whose coexistence probably relates to a fluid-induced partial recrystallization, (e.g. Cheilletz et al., 1999; Alexandrov et al., 2002; Castonguay et al., 2007; Tartèse et al., 2011; Tremblay et al., 2011; 2020). In such type of spectra, the plateau-like age at 2602.1 ± 4.5 Ma (85.6 % of the total $^{39}Ar_K$ released; Fig. 12a) yields a minimum age estimate of the former muscovite, which was partially recrystallized at or after 2567.2 ± 6.2 Ma, i.e. the apparent age yielded by the base of the saddle. The degassing pattern and the weighting of this age spectrum indicate that the older component is overwhelmingly the main radiogenic component to which it is reasonable to attribute an age of c. 2603 Ma. (Fig. 12a).

Muscovite YD0048B provides a plateau age at 2517.2 ± 2.4 Ma (93% of the total $^{39}Ar_K$ released; Fig. 12b) but a detailed examination of that age spectrum reveals a complex thermal history for this mineral. Apparent ages increase steadily from low to high temperature steps, suggesting the occurrence, around 2500 Ma, of a disturbing event which induced $^{40}Ar^*$

loss by volume diffusion (Turner, 1968) on a muscovite grain older than c. 2524 Ma (Fig. 12b).

The first 30% of the $^{39}Ar_K$ degassing of muscovite YD0023A is highly disturbed (Fig. 12c) with erratic apparent ages which could result from the occurrence of interfoliar chlorite. Overall, this age spectrum shows a saddle shape, as for muscovite YD0009B, which allows the calculation of pseudo-plateau ages at 2603.2 ± 4.3 Ma (21.6% of the total $^{39}Ar_K$ released) for the base of the saddle and at 2627.1 ± 3.7 Ma (47.4% of the total $^{39}Ar_K$ released) for the high temperature steps (Fig. 12c). Our preferred interpretation is that muscovite YD0023A crystallized at the latest at c. 2627 Ma and has been affected by a fluid-induced partial recrystallization event at c. 2603 Ma, which has been coeval with initial crystallization of muscovite YD0009B (Fig. 12a).

5.5.4 The Nottaway River shear zone.

The analyzed muscovite of sample YD0055A belongs to a population of mica-fish muscovite grains (Fig. 7e) extracted from a felsic mylonite of the Nottaway River shear zone. As for muscovite YD0023A, the first 20% of the degassing spectra of YD0055A is highly disturbed (Fig. 13a), which can also reflect the occurrence of interfoliar chlorite. The remaining 80% of the degassing produces a multi-stepped age spectrum with a global staircase shape interspersed with three flat segments. Similar muscovite age spectra have been described by Tremblay et al. (2020) for Archean rocks of the southern Abitibi suprovince; they were interpreted as the result of the aggregation, via dissolution/recrystallization/ neocrystallization of increasingly younger white mica sub-grains as deformation increments and coeval fluid inflows progress. Pseudo-plateau ages calculated from the flat segments suggest periods of aggregation/remobilisation of muscovite YD0055A at 2565.2 ± 3.7 Ma and 2504.0 ± 5.0 Ma, at the expense of a muscovite grain that would have initially crystallized at 2595.6 ± 5.4 Ma (Fig. 13a). These aggregation/remobilisation processes, which partially preserve the previous or initial states of white micas, occur below their isotopic closure temperature, at temperatures as low as 250-350°C.

Despite a possible plateau age at 2527.8 ± 2.9 Ma (76.2% of the total $^{39}Ar_K$ released), the age spectrum of biotite YD0059A, with recrystallized rims (Fig. 13b), shows a regular increase of apparent ages from low to high temperature steps, suggesting the occurrence of a disturbing event at c. 2505.5 ± 8.5 Ma of an initial grain that would be older than c. 2531 Ma. The highly disturbed age spectrum of an amphibole from that sample is useless (Fig. 13b).

792

793 ***5.5.5 The Montviel Syenite.***

794 Two amphiboles and a biotite from sample YD5143A from the Montviel Syenite (see
795 Fig. 3 for location) provide highly contrasted but significant results (Fig. 14). The age
796 spectrum of amphibole 1, a hornblende according to its $^{37}Ar_{Ca}/^{39}Ar_K$ ratio values of 4.0-4.2,
797 allows the calculation of a plateau age at 2653.9 ± 2.7 Ma (83.6% of the total $^{39}Ar_K$ released;
798 Fig. 14). The age and $^{37}Ar_{Ca}/^{39}Ar_K$ spectra of amphibole 2 are clearly different in the sense
799 that, from low to high temperature steps, both the apparent ages and $^{37}Ar_{Ca}/^{39}Ar_K$ ratios
800 increase in unusual proportions, from c. 1934.4 ± 7.3 to 2911.4 ± 10.8 Ma and 2.1 to 101.6,
801 respectively, which is not complying with what can be expected for hornblendes. The
802 unrealistic age of the fusion step (at c. 2911 Ma) and its $^{37}Ar_{Ca}/^{39}Ar_K$ ratio higher than 100
803 suggest the incorporation of excess argon, most likely by a calcic component resulting from
804 the alteration of the amphibole during a disturbing event which would have occurred at c.
805 1934 Ma or after (Fig. 14).

806 The age spectrum of biotite YD5143A is also strongly discordant with that of
807 amphibole 1. However, apparent ages of the base of its saddle shape, in the range c.1967-
808 1940 Ma (Fig. 14), are consistent with the timing of the disturbance that presumably
809 destabilized amphibole 2. The destabilisation process possibly results from the emplacement
810 of the nearby Montviel Carbonatite, whose age is constrained by a U–Pb zircon age of 1894 ±
811 4 Ma (David et al., 2006).

812

813 **5.6 Interpretation and significance of $^{40}Ar/^{39}Ar$ ages**

814 A synthetic compilation of all $^{40}Ar/^{39}Ar$ ages measured during this study is show in
815 Figure 15.

816 The probability density diagram established from resized age spectra for amphiboles
817 and biotites of the AGB (Fig. 15a) allows a synthetized interpretation of analytical results. On
818 Figure15a, the principal age peak is at 2678.1 ± 1.7 Ma, as defined by amphiboles YD0009A
819 and YD0039A, as well as amphibole and biotite of sample YD0037A. The concordance of
820 biotite and amphibole ages suggests that they are cooling ages, and that this cooling has been
821 relatively fast between 600°C and 400°C. The asymmetrical and stepped base of that peak
822 toward younger ages reflects the impact of subsequent disturbing events on amphiboles after
823 initial cooling. The first of these events occurs around c. 2644 Ma. It induced a partial
824 recrystallization of amphibole YD0048A and probably the total reset of biotite YD4065A

(Fig. 10f). The second disturbing event occurred around c. 2598 Ma (Fig. 15a) and induced the complete recrystallization of amphibole YD0100A (Fig. 10e). It would have been followed by a third event (with a frequency peak at c. 2564 Ma) that would have caused an almost complete age resetting of biotite YD0009A and a partial reset for micaschist biotite YD4065A (Figs. 10c, f and 15a).

Figure 15b suggests that OPB amphiboles initially cooled down to Tc at c. 2668 Ma, before a partial recrystallization event that occurred at c. 2647 Ma. Hence, there seems to be a ca. 10 m.y. time lag between the AGB and the OPB for initial cooling below Tc for amphiboles, at approximately 2678 Ma and 2668 Ma, respectively (Figs. 15a and b). The OPB tonalites also record a younger disturbing event around c. 2593 Ma (Fig. 15b). These two latter post-cooling events correlate within errors to those recorded by the AGB amphiboles at c. 2644 Ma and c. 2598 Ma (compare Fig. 15a and b).

The three analyzed muscovite grains from granitic porphyry dykes (Fig. 15c) are indicative of a complex and polyphased thermal history that can not be precisely understood here due to the small number of analyses. This thermal evolution may have started earlier than c. 2627 Ma and ended around c. 2495-2500 Ma (Fig. 15c). The effective occurrence of a disturbing event at c. 2602.7 ± 3.1 Ma, as reported on the probability density diagram of Figure 15c, remains however proven.

The initial crystallisation of muscovite YD0055A, around 2600 Ma (Figs. 13a and 15d), can be confidently attributed to shear deformation along the Nottaway River Shear Zone. $^{40}Ar/^{39}Ar$ age data suggest that the shear zone was discontinuously active for, at least, ca. 100 m.y., from 2595.6 ± 5.4 Ma, the minimum age estimate for white mica initial crystallisation (or the complete resetting of the Ar «clock» of pre-existing muscovites) to final shear increments around c. 2500 Ma. However, this does not exclude the possible initiation of the Nottaway River Shear Zone before 2600 Ma.

$^{40}Ar/^{39}Ar$ analyses suggest that the Montviel Syenite (Figs. 14 and 15e) and the nearby carbonatite represent two different magmatic pulses, an older one related to syenite emplacement at c. 2654 Ma and a younger one corresponding to the carbonatite intrusion at c. 1894 Ma. This is, however, in contradiction with a model proposed by Nadeau et al. (2014) in which both the syenite and the carbonatite are attributed to a single phase of magmatism at 1894 Ma.

6. DISCUSSION

The tectonic evolution of Archean terranes involves extensive rifting/plume/arc magmatism and multiple, or progressive phases of deformation and metamorphism (e.g. Cawood et al., 2009; Bédard, 2018; Brown et al., 2020; Palin et al., 2020). Understanding the nature of the related geodynamic regime(s), and identifying the various alternative model(s) to the classical plate tectonics interpretation, if any, has important implications for a better comprehension of the early Earth dynamics, the processes that led to continental crust formation and structural evolution, including the mineral deposit potential of Archean orogenic belts (e.g. Thébaud and Rey, 2013).

6.1 The AGB-OPB contact – not a subduction suture.

Subduction is a geological process by which the lithosphere is recycled into the Earth's mantle at convergent plate margins, creating an upper plate-lower plate (UP-LP) boundary. Among the different mountain belts generated by plate convergence and collision during the Phanerozoic, a significant number took place in an environment of continuing subduction and accretion along sites of oceanic lithosphere consumption. These belts are known as accretionary orogens, zones of type-B subduction, or Cordilleran-, Pacific- and Andean-type collisions (see Cawood et al., 2009 for a review). A similar type of plate setting has been suggested for the AGB-OPB boundary, with the AGB acting as the down-going plate. Phanerozoic accretionary orogens are variably deformed and metamorphosed, and characteristically occur as paired and parallel high-temperature (HT) and high-pressure (HP) belts with metamorphic grade up to granulite and blueschist-to-eclogite facies, respectively (e.g. Brown, 1993; 2010; Ernst et al., 1994). Such orogens typically include wedge-shaped accretionary prisms (or subduction mélanges) that formed at the UP-LP interface. These accretionary prisms are organized in thrust sheets and attributed to the offscraping and underplating of material from the descending oceanic plate and of subduction-related volcanic-magmatic arc system in the upper plate (e.g. Ernst et al., 1994; Cawood et al., 2009; Wakabayashi and Dilek, 2011; Kusky et al., 2020; Palin et al., 2020; among many others). A fore-arc basin generally occurs in between. Accretionary prisms are usually elongated and depending on the plate velocity, the dip of the subduction zone, the backstop geometry of the wedge and the volume of sediments on the down-going plate, they can be relatively voluminous. The Franciscan subduction complex, for instance, is at least 50 km-wide along a strike-length of c. 900 km (e.g. Ernst et al., 1994; Wakabayashi, 2017). Accretionary prisms are essentially made up of tectonic slices of island-arcs, backarcs, forearcs, dismembered

ophiolites, granulite-facies and/or ultrahigh-pressure (UHP)-HP metamorphic rocks, and pre- to syn-accretion clastic sedimentary sequences. Thrusting and reverse faulting usually led to the imbrication of the upper plate rocks with those of the lower plate, leading to complex field relationships.

The subduction model proposed for the AGB-OPB boundary is mainly based on the Lithoprobe seismic profile (e.g. Calvert and Ludden, 1999) and field structures attributed to a south-verging fold-and-thrust belt in the AGB (Sawyer and Benn, 1993; Lacroix and Sawyer, 1995). However, the AGB-OPB transition does not show any of the characteristic features of UP-LP boundary as expected for a subduction suture. There are no accretionary prism and no metamorphic break along the AGB-OPB contact. Metamorphism varies progressively from low- to high-grade from the uppermost units of the AGB toward the plutonic rocks of the OPB (Fig. 9). There are, obviously, local fault contacts between greenschist- and amphibolite-grade rocks of the AGB, such as the Barlow fault in the Chibougamau area (Bedeaux et al., 2020), but these are late reverse faults related to regional folding. Our field observations and structural analysis indicate that the volcanic and sedimentary sequences of the AGB overly the TTG-type orthogneisses of the OPB (Fig. 9), suggesting that both domains likely formed a single structural unit prior to regional deformation (e.g. Benn, 2006; Benn and Moyen, 2008). Hence, we do not think that the AGB-OPB transition represents a subduction-related, upper plate-lower plate boundary.

6.2 The formation of composite OPB-AGB – speculative models.

The structural relations and metamorphic characteristics of the AGB and OPB are reminiscent of various tectonic settings such as (i) metamorphic core complexes (MCC, Lister and Davies, 1989; Whitney et al., 2013), (ii) suprastructure-infrastructure transition (e.g. Culshaw et al., 2006; Stern, 2017), two models in which the upper crust is tectonically juxtaposed to the deep crust and/or upper mantle, and (iii) the convective overturn of crustal material (Collins et al, 1998; van Kranendonk, 2011; Bédard, 2018; Wiemer et al., 2018; Vanderhaeghe et al., 2019).

6.2.1 The OPB as a metamorphic core complex.

As compared to MCC's, the OPB shares similar features: (1) synkinematic granitoids, pegmatites and migmatites restricted to domal core domains; (2) sheet-like granitoids and discontinuous high-strain migmatites towards the contact with the overlying upper crust; (3) a

décollement horizon (i.e. potentially, the OPB-AGB contact) between lower crustal gneisses and the upper crust; and (4) a normal metamorphic zonation. However, MCC's are generally less than 10 km in diameter, asymmetrical (e.g. the detachment being folded due to the bowing upward of the lower crust) and usually related to major continental extension (see Lister and Davies, 1989). In contrast to detachments of typical MCC's, the OPB-AGB contact has been involved in progressive reorientation and repeated late-intrusion. Moreover, the ductility and metamorphic contrasts across the OPB-AGB interface are not extreme as in typical MCC's in which the detachment separates rocks of highly contrasting structural and metamorphic character, with deformation in the cover rocks being typically brittle. Finally, the abundant syn-tectonic granitoids of the OPB-AGB are not confined to the proximity of the detachment, as for MCC's, but extend into the interior of both the OPB and the AGB.

6.2.2 Superstructure-infrastructure transition.

In superstructure-infrastructure (S-I) transition zones, superstructure represents a low-grade upper crust level with early, typically upright structures, whereas infrastructure constitutes a high-grade migmatitic lower crust level with late, gently inclined structures overprinting the early structures of the overlying upper crust (Culshaw et al., 2006). In typical examples, a crustal-scale detachment shear zone is observed between the upper and lower tectonic levels (Tikoff et al., 2002; Culshaw et al., 2006; Stern, 2017). The infrastructure gneissic rocks generally yield radiometric ages younger than superstructure rocks, indicating that the infrastructure was hot, partially molten and weak during the deformation of the superstructure above it (e.g. Culshaw et al., 2006; Stern, 2017). The OPB presents evidence for anatectic melting and syn-kinematic migmatites formation at ca. 2.68-2.67 Ma (Sawyer, 1998), a melting event that, according to our $^{40}Ar/^{39}Ar$ data (Figs. 15a and b), has been almost coeval with or slightly followed the ca. 2680 Ma metamorphism in the AGB. This suggests a maximum time lapse of 10 m.y. for metamorphic conditions between upper (AGB) and lower (OPB) crustal levels, which could fit with the S-I model data presented by Culshaw et al. (2006) for the Western Superior Province. In such interpretation, the amphibolite-facies rocks occurring towards the base of the AGB would define a low-angle detachment fault at the contact with deeper and hotter rocks of the OPB, a detachment that would has been subsequently folded and verticalized. In the study area, these amphibolites are several km-thick (Bedeaux et al., 2020), and may thus reasonably represent a mid-crustal decoupling zone between a ca. 15 km-thick superstructure (the AGB) and a plutonic, TTG-rich infrastructure

(the OPB). However, the occurrence of F_2 folds affecting the low-angle metamorphic S_1 layering in the OPB gneisses invalidates a typical S-I transition model. The metamorphic age variations can be simply related to the differential uplift and exhumation of both belts (the ABG first and then the underlying OPB). A S-I transition model is also inconsistent with age constraints from the Attic Complex (located in the southern part of the AGB; see Fig. 1b) where U-Pb zircon dating suggests a 20 m.y gap between the formation of migmatites in tonalitic gneisses (TTG's) of the lower crust (at ca. 2716.1 ± 2.9 Ma) and those in adjacent mafic volcanic rocks (at ca. 2695 ± 1 Ma) (Revelli, 2020). This has been attributed to the diapiric ascent and crustal melting of lower crustal intrusive material and the related burial (and prograde metamorphism) of cold and dense greenstones of the upper crust (Revelli, 2020), which agrees with a convective crustal overturn as described below.

6.2.3 Convective crustal overturn.

The third tectonic setting involves the partial convective overturn of the crust (Fig. 16). It was originally proposed by Collins et al. (1998) for Archean rocks of the Pilbara craton (Australia). In such a setting, the OPB gneissic domes represent the diapiric response of density inversion created by the accumulation of a thick (ca. 15 km) greenstone cover (the AGB) erupted over a previously stable and more-or-less continuous sialic crustal basement ≥ 2.80 Ga, both domains being intruded by syn-volcanic and syn-tectonic TTG plutons ranging from c. 2.76 to c. 2.65 Ga (Davis et al. 1995; Sawyer, 1998; Daoudene et al., 2015~~5~~6, Pedreira-Perez et al., 2020) (Figs. 16a and b). Diapirism is considered here as part of a larger process involving the partial convective overturn of the crust (Collins et al., 1998; Wiemer et al., 2018). We suggest that deformation initiated by sinking and subsidence of the thick cover of greenstones within a hot and weak (ductile), laterally flowing sialic lower crust that generated the S_1 metamorphic layering both in the OPB and the lowermost part of the AGB (Fig. 16a). This produced strong horizontal temperature gradients and related changes of metamorphic facies as, for instance, in thermal models of Thébaud and Rey (2013). Due to density contrasts, both the gneissic lower crust and crosscutting TTG's ultimately migrated upward passively as accommodation structures. Material flow into the AGB synclines would has been compensated by lateral and vertical migration of the less dense sialic substrate into the domal crests of the OPB (Fig. 16b), generating a pattern of partial convective overturns in the crust (Collins et al., 1998; Weinberg, 1997). The downflow of greenstones would has been almost entirely compensated by TTG uprises (Fig. 16c). Shallow interdome depressions developed

and progressively filled with clastic sediments, such clastic sequences occupying the core of greenstone synclines and being represented by sedimentary rocks of the Opémisca and Broadback groups within the Abitibi and Frotet-Evans belts, respectively. Some of these clastic sequences possibly formed as early as ca. 2750 Ma, as suggested by stratigraphic relationships between the Broadback Group and the underlying Frotet-Evans volcanics (Brisson et al., 1998; see section 2.1). In the Opémisca Group, maximum sedimentation age of the Haüy Formation ($\leq 2691.7 \pm 2.9$ Ma; David et al., 2007) is coeval, at least in part, with regional metamorphism in the AGB (see section 5.5). Part of the Opémisca Group therefore deposited during regional deformation, as proposed for most sedimentary sequences of the Superior Province (e.g. Leclair et al., 1993; Parmenter et al., 2006; Lin et al., 2013). As the greenstones and overlying sedimentary rocks progressively flow deeper into the synclines, strain intensity increased and was accommodated by horizontal shortening, the S_2 foliation became more pervasive and faults and shear zones with down-dip lineations developed (Fig. 16b). The Barlow fault (Bedeaux et al., 2021) is one of these; in the Chibougamau area, it is located along the northern flank of the Waconichi F_2 syncline (Waconichi basin on Fig. 2) and marked by upper crustal, south-dipping seismic reflectors (Mathieu et al., 2020). The Barlow fault is interpreted as a reactivated structure (Bedeaux et al., 2021), and it possibly belongs to a series of basin-bounding faults that accommodated the exhumation of the OPB gneisses and inverted during the following contraction (e.g. Mathieu et al., 2020), which is consistent with the interpretation shown on Figure 16. With time, the early generation of TTG's were progressively deformed and rotated into subconcordance with the steepening domal boundaries (Fig. 16c). Other TTG's were syn-kinematic and formed sheeted intrusions. Some of these did not move far from their source, remained heterogeneous, and can be better described as `intrusive diatexites' (Sawyer, 1998), whereas later intrusions tend to be larger, more discordant, less strongly foliated bodies and are more obvious near the AGB-OPB boundary, where they cut the OPB-AGB interface. Such an interpretation fits well with (1) the relative downflow of the AGB volcanic rocks as compared to the OPB gneisses (Fig. 9), (2) the distribution of S_1 foliations and lineations in the OPB domes (Fig. 2 and Fig. 6b), (3) the up-stratigraphy increasing proportion of plutonic clasts in polygenic conglomerates of both the Broadback and Opémisca groups (Brisson et al., 1997a; 1998; Charbonneau et al., 1991), which reflects the progressive erosion of volcanic cover rocks and underlying plutonic rocks in the source area, and (4) slightly higher pressure and temperature preserved in the OPB migmatites and amphibolites (6.3-7.1 kb and 750^{o}C, Sawyer, 1998) as compared to the

amphibolite facies rocks of the AGB (c. 6 kb and c. 550ºC, Bedeaux et al., 2021).

$^{40}Ar/^{39}Ar$ age measurements performed during our study are in good agreement with that model. Amphibole ages suggest that the lowermost part of the AGB exhumed around 2678.1 ± 1.7 Ma (Fig. 15a). Ages from the OPB, at 2667.8 ± 3.0 Ma (Fig. 15b), suggest that it was more-or-less coeval with, or quickly followed the exhumation of the AGB, an event that we suggest has been coeval with decompression melting (Weinberg, 1997; Whitney et al., 2004) and the genesis of syn- to late-D_1 migmatites in the cores of OPB gneiss domes at 2.67-2.68 Ga (Sawyer, 1998; Fig. 16c). Then, both terranes share the same succession of thermal disturbances at c. 2650-2645 Ma and 2600-2590 Ma, including the inferred onset of shearing along the Nottaway River Shear Zone at ca. 2600 Ma, as recorded by related mylonites (Fig. 15d) and quartz-feldspar porphyry dykes (Fig. 15c). Such a series of events is also documented in the Val d'Or mining district of the Abitibi subprovince (Tremblay et al., 2020). Besides, at the scale of the Superior Province, there is accumulating geochronological evidence for major crustal deformation event(s) and related metamorphism spreading over a timeframe much larger than suggested in literature (e.g. Percival, 2007). Easton (2000), for instance, argued that the distribution of metamorphic grade and age of metamorphism in the western Superior reflect a series of tectonic events between 2710 and 2640 Ma, which is in agreement with U-Pb zircon age constraints for metamorphism, syn-orogenic magmatism and deformation in the southern Abitibi subprovince (see Tremblay et al., 2020 for a review). North of the OPB, in the Opinaca subprovince, granulite-facies metamorphism spreads over ages varying from c. 2666 Ma to 2636 Ma (Morfin et al., 2013) whereas it even lasted down to ca. 2620–2600 Ma in supracrustal rocks of the La Grande subprovince (Fontaine et al., 2017, 2018). Combined with geochronological data from our study, this is a strong indication that peak and duration of regional metamorphism have been more-or-less coeval and long-lasting over a large region of the Superior Province, if not all over the Pontiac, Abitibi and Opatica subprovinces and beyond.

6.3 Significance of the Lithoprobe seismic reflector.

Seismic profiles showing shallow sub-horizontal to slightly dipping reflectors beneath Archean and/or Paleoproterozoic greenstone belts are relatively common. Some of these reflectors may be due, obviously, to tectonic events that are younger than, and not directly related to, the formation of the greenstone belts and, until the age of such reflectors can be determined, their bearing on the greenstone belt evolution remains speculative. However,

assuming that the Lithoprobe seismic reflector of the Superior Province is an Archean artefact (e.g. Cawood et al., 2006) and that our interpretation of the AGB-OPB relations is correct, what can be the origin and significance of that reflector then? We envision two possibilities that we briefly discuss below, (i) mantle lithosphere imbrication (Fig. 17), and (ii) bending of a flat subduction rooted southward at the Pontiac-Abitibi interface (Fig. 18).

Gray and Pysklywec (2010) performed a series of forward numerical modeling of the thermo- mechanical evolution of continental lithosphere undergoing collision and orogenesis under Neoarchean- like conditions for stratified mafic-to-felsic crustal domains overlying the mantle lithosphere. They have identified three dominant modes of mantle lithosphere deformation, (1) pure- shear thickening; (2) mantle imbrication; (3) and underplating. Their result for the mantle imbrication mode is reproduced on Figure 18. For that mode, numerical modeling shows that, due to a «hot» and weak lower crust, there is a decoupling between the mantle and the crust at a depth of approximately 40 km. The model shows that the lithospheric mantle becomes imbricated along major shear zones along which slices of crustal eclogites may occur, whereas the crustal domain itself essentially absorbs deformation by pure-shear thickening and folding. Gray and Pysklywec (2010) inserted a weak zone in the initial configuration of their numerical experiments to favor the onset and localization of deformation, and to mimic an original plate boundary (see their Figure 1) as well. Although that such a weak zone may has influenced the location of some shear zones within the mantle lithosphere, it did not lead to the formation of any shear zones (that could have been interpreted as a nascent subduction plane) in the upper crust. The modeled imbrication shown on Figure 17 is obviously unrelated to subduction since the crustal part of the lithosphere is not recycled into the mantle as in typical subduction settings. We think that mantle imbrications as shown by these results likely formed during the Archean and can account for deep seismic reflectors such as the Abitibi-Opatica Lithoprobe transect.

An alternative hypothesis that cannot be ignored is that the Lithoprobe seismic reflector may not represent the original location of an Abitibi-Opatica subduction zone, but the trace of a Pontiac-Abitibi subduction zone interface that flattened for several hundreds of km at depth and steepen at or close to the Abitibi-Opatica contact. Such shallow subduction flattening has been already invoked as a predominant tectonic regime during the Archean due to thicker and more buoyant oceanic lithosphere (e.g. Cawood et al., 2006). Flat subduction is documented on modern Earth. A typical example of it is the Mexican subduction zone where the young Cocos plate is shallowly subducting beneath central Mexico (Fig. 18a; Kim et al.,

2012). This is well illustrated by the teleseismic imaging of a 500 km long transect between the Middle America trench to the south, and the Trans-Mexican volcanic belt (TMVB, the continental volcanic arc) to the north (Fig. 18b). This shows that subduction of the Cocos oceanic plate dips c. 15º north for about 80 km along the coast, and then horizontally underplates the continental crust at c. 50 km-depth for c. 250 km northward. The slab then abruptly changes to a steeply dipping geometry at approximately 75º as it bends right below the TMVB. The similarity of the geometry of the Cocos plate subduction zone and the reinterpreted Abitibi segment of the Grenville-Abitibi seismic transect is striking (Fig. 18c), both in terms of depth and lateral extent of seismic reflectors. Hence, it is possible that the steeply north-dipping seismic reflector of the Abitibi Lithoprobe transect roots into the Pontiac-Abitibi interface rather than the AGB-OPB. The Pontiac-Abitibi contact would be then interpreted as a surface of former subduction and recycling of the oceanic crust that originally existed between the Pontiac and Opatica «basements», causing the underthrusting and burial of the Pontiac block below the Abitibi subprovince and accounting for ensuing tectono-metamorphism and magmatism (e.g. Dimroth et al., 1983; Card, 1990; Camiré and Burg, 1993; Davies, 2002; Frieman et al., 2017, among many others). This may possibly explain the contrasting pre-2700 Ma plume-driven constructive stage of the AGB as compared to its post-2700 Ma geodynamic evolution as depicted by Thurston et al. (2008) and Mole et al. (2021); the latter stage being mainly characterized, according to these authors, by subduction-related compressional lithospheric deformation, flysch sedimentation and more-or-less coeval emplacement of alkalic granodiorite, granite and syenite plutons (such as in the Preissac-Lacorne batholith). However, such an uniformitarian interpretation for the Pontiac-Abitibi relations has been ~~recently~~ disputed by Piette-Lauzière et al. (2019) that argue for a multi-stage tectono-metamorphic evolution involving extensional tectonism and crustal delamination followed by re-accretion and subcretion of ribbon~~s~~ continents as suggested by Bédard (2018) for the Northern Superior.

CONCLUSION

Our structural and metamorphic analysis of the transition between the Abitibi and Opatica subprovinces does not confirm the former existence of north-dipping subduction between these two lithological assemblages, despite the occurrence of a major seismic reflector at depth. We think that both terranes originally formed a single and composite crustal sequence, the Abitibi and Frotet-Evans greenstone belts and associated sedimentary

rocks representing the upper crust and the Opatica Plutonic Belt being the remnant of middle-lower crust plutonic domains. This implies that the Frotet-Evans belt originally formed an upper crust sequence that was continuous with the AGB. Although there is a lack of precise geochronological constraints for the Frotet-Evans belt, such an interpretation is consistent with available U-Pb age data from both greenstone belts. However, it does not mean that the Frotet-Evans belt has ever been as thick as the AGB (c. 10-15 km), since there are erosional unconformities on top of each volcanic sequences that may has removed more volcanic material from the former belt (due to the progressive exhumation of the OPB; see Fig. 16) as compared to the AGB. Our interpretation also means that OPB-like orthogneissic massifs are likely to be exposed south of the OPB-AGB transition. We are not saying here that OPB gneisses are systematically present at depth below the AGB but that discontinuous masses of orthogneissic TTGs, more-or-less attached to each other and to the Opatica, are likely to occur and to be expose along the crest of antiformal/domal culminations within the Abitibi belt. Examples of such metamorphic domes may be represented by the Marest and Bernetz gneissic plutons in central Abitibi (Faure, 2015), which are currently interpreted as the crustal roots of volcanic arc(s) (Chown et al., 2002), and by the Attic Complex in the Lebel-sur-Quévillon area (Fig. 1b) that has been recently interpreted as the result of diapiric and sagduction-related processes (Revelli, 2020).

As for most Archean cratons, the structural evolution of the Opatica and Abitibi belts is the result of several episodes of regional deformation and metamorphism that spans several tens, if not hundred's, of million years. The main events, D_1 and D_2, are predominantly developed in the OPB and the AGB, respectively. S_1 is a penetrative amphibolite-grade foliation in the OPB gneisses and in metavolcanic rocks lying at the base of both the Frotet-Evans and Abitibi greenstone belts whereas S_2 is a medium- to low-grade regional schistosity of variable intensity in both the AGB and OPB. S_1 is subparallel to the OPB-AGB contact although it is frequently transposed into a composite $S_{1\text{-}2}$ fabric within the AGB. S_1 trajectories in the OPB define a dome-and-basin geometry that is the result of vertical transfert of middle- to lower-crustal material. The counterpart progressive burial of the AGB into synformal troughs generated the abrupt EW-trending S_2 schistosity and related down-dip mineral and stretching lineations. Amphiboles and micas $^{40}Ar/^{39}Ar$ ages measured in both the OPB and AGB suggest that exhumation of the latter started at $\geq$ 2678 Ma and was almost coeval with, or slightly followed, by the uplift and related migmatization of OPB gneisses at c. 2668 Ma or earlier. This is consistent with a diapiric convective overturn of the crust as

illustrated on Figure 16. Both the OPB and AGB then shared the same magmatic and structural evolution, including the onset of dextral and sinistral transcurrent shearing and faulting at ca. 2600 Ma that may have lasted for c. 100 m.y. Comparison with adjacent areas suggests that magmatism and metamorphism have been coeval over a large region (Easton, 2000), which is consistent with pervasive deformation and slow cooling as expected for vertical tectonic models and diapiric magmagenesis and ascent during the evolution of the Archean Superior Province (e.g. Bédard and Harris, 2014; Bédard, 2018).

Declaration of Competing Interest.

The authors declare that they have no known competing financial interests or personal relationships that could have appeared to influence the work reported in this paper.

ACKNOWLEDGEMENTS

Y.D. benefited of a financial support from Mitacs-Acceleration and the *Ministère de l'Énergie et des Ressources* (MERN) du Québec for a postdoctoral fellowship at UQAM in 2014-16. The Natural Science and Engineering Council of Canada (NSERC) has provided research grants to A.T. (NSERC-PG105669). Thanks to A. Chabot-Bergeron, A.-S. Corriveau, P. Lamontagne-Hallé, A. Moïse, A. Nolet-Regaudie, T. Plasmodon-Tremblay, and C. Vézina for help and support during field work. Thanks are also due to Michèle Laithier for drawing some of the figures. We thank Dr Phil Thurston and three anonymous reviewers for thoughtful comments that significantly improved the manuscript.

REFERENCES

Alexandrov, P., Ruffet, G., Cheilletz, A., 2002. Muscovite recrystallization and saddle-shaped $^{40}Ar/^{39}Ar$ age spectra: Example from the Blond granite (Massif Central, France). Geochim. Cosmochim. Acta 66, 1793-1807.

Allard, G.O., Caty, J.-L., and Gobeil, A. 1985. The Archean supracrustal rocks of the Chibougamau area. *In* Evolution of Archean Supracrustal Sequences. Ayres, L.D., Thurston, P.D., Card, K.D. and Weber, W. (eds). Geological Association of Canada; Special Paper 28, p. 55–63.

Bédard, J.H. 2018. Stagnant lids and mantle overturns: implications for Archean tectonics, magmagenesis, crustal growth, mantle evolution, and the start of plate tectonics. Geoscience Frontiers 9: 19-40.

1188 Bédard, J.H. and Harris, L. 2014. Neoarchean disaggregation and reassembly of the Superior
1189 Craton. Geology 42: 951-954.
1190 Bedeaux, P., Brochu, A, Mathieu, L., Gaboury, D. and Daigneault, R. 2020. Structural
1191 analysis and metamorphism of the Barlow Fault Zone, Chibougamau area, Neoarchean
1192 Abitibi Subprovince: implications for gold mineralization. Can. J. Earth Sci. 58.
1193 Benn, K., 2006. Tectonic delamination of the lower crust during late Archean collision of the
1194 Abitibi-Opatica and Pontiac terranes, Superior Province, Canada. In: Benn K et al.
1195 (Eds) Archean geodynamics and environments: American Geophysical Union,
1196 Geophysical Monograph 164, 267-282.
1197 Benn, K., Moyen, J.F., 2008. The late Archean Abitibi-Opatica terrane, Superior Province: a
1198 modified oceanic plateau. In: Condie KC, Pease V (Eds). When didi palte tectonics
1199 begin on Planet Earth? Geological Society of America Special Paper 440, 173-197.
1200 Benn, K., Sawyer, E.D., Bouchez, J.L., 1992. Orogen parallel and transverse shearing in the
1201 Opatica belt, Quebec: implications for the structure of the Abitibi Subprovince.
1202 Canadian Journal of Earth Sciences 29, 2429-2444.
1203 Bleeker, W. 2003, The late Archean record: A puzzle in ca. 35 pieces. Lithos, 71, 99 – 134.
1204 Blumenfeld, P., Mainprice, D., Bouchez, J.L., 1986. C-slip in quartz from subsolidu deformed
1205 granite. Tectonophysics 127, 97-115.
1206 Boily, M., 2000. Géochimie des volcanites des ceintures volcano-sédimentaires de Frotet-
1207 Evans (CVFE) et de la Moyenne-Eastmain. Ministère des Ressources naturelles,
1208 MB 2000-12.
1209 Bosse, V., Féraud, G., Ballèvre, M., Peucat, J.-J., Corsini, M., 2005. Rb-Sr and $^{40}Ar/^{39}Ar$ ages
1210 in blueschists from the Île de Groix (Armorican Massif, France): implications for
1211 closure mechanisms in isotopic systems. Chem. Geol. 220, 21-45.
1212 Bosse, V., Féraud, G., Ruffet, G., Ballèvre, M., Peucat, J.J., de Jong, K., 2000. Late Devonian
1213 subduction and early-orogenic exhumation of eclogite-facies rocks from the
1214 Champtoceaux Complex (Variscan belt, France). Geol. J. 35, 297-325.
1215 Boyer S.E.& Elliott D., 1982. Thrust systems. Bulletin of the American Association of
1216 Petroleum Geologists 66 (9), 1196-1230.
1217 Brisson, H., Gosselin, C., Fallara, F, Gaulin, R., Dion, D.-J., 1998. Géologie de la région du
1218 Lac Evans. Ministère des Ressources naturelles, RG 98-06, 23 p.
1219 Brisson, H., Gosselin, C., Baumier, M., Dion, D.J., Gaulin, R., Lefebvre, D.L., 1997a.
1220 Géologie de la région du lac Assinica (SNRC 32J/11). Ministère des Ressources

1221 naturelles, RG 96-11, 28 p.
1222 Brisson, H., Gosselin, C., Baumier, M., Dion, D.J., Gaulin, R., Lefebvre, D.L., 1997b.
1223 Géologie de la région du ruisseau Lucky Strike (SNRC 32J/12). Ministère des
1224 naturelles, RG 96-10, 21 p.
1225 Brown, M. 2010. Paired metamorphic belts. Gondwana Research 18: 46-59.
1226 Brown, M. 1993. P-T-t evolution of orogenic belts and the cause of regional metamorphism.
1227 Journal of the Geological Society, London 150: 227-241.
1228 Brown, M., Johnson, T., and Gardiner, N.J. 2020. Plate tectonics and the Archean Earth. Ann.
1229 Rev. Earth Planet. Sc. 48: 291-320.
1230 Butler, R. and Bond, C. 2020. Thrust systems and contractional tectonics, *in* N. Scarselli, J.
1231 Adam and D. Chiarella, *eds,* Regional Geology and Tectonics: Principles of Geologic
1232 Analysis - Volume 1: Principles of Geologic Analysis, Elsevier, Netherlands, pp. 149-
1233 167.
1234 Calvert, A.J., Ludden, J.N., 1999. Archean continental assembly in the southeastern Superior
1235 Province of Canada. Tectonics 18 (3), 412-429.
1236 Calvert, A.J., Sawyer, E.W., Davis, W.J., Ludden, J.N., 1995. Archean subduction inferred
1237 from seismic images of a mantle suture in the Superior Province. Nature 375, 670-674.
1238 Camiré, G.E., and Burg, J.P., 1993. Late Archaean thrusting in the northwestern Pontiac
1239 Subprovince, Canadian Shield: Precambrian Research, v. 61, no. 1–2, p. 51–66, doi:
1240 10.1016/0301-9268(93)90057-9.
1241 Card, K.D., 1990. A review of the Superior Province of the Canadian Shield, a product of
1242 Archean accretion. Precambrian Research 48, 99-156.
1243 Card, K.D., Ciesielski, A., 1986. DNAG N°1 Subdivisions of the Superior Province of the
1244 Canadian Shield. Geoscience Canada 13, pp 5-13.
1245 Castonguay, S., Ruffet, G., Tremblay, A., 2007. Dating polyphase deformation across low-
1246 grade metamorphic belts: An exemple based on $^{40}Ar/^{39}Ar$ muscovite age constraints
1247 from the southern Quebec Appalachians, Canada. Geol. Soc. Am. Bull. 119, 978-992.
1248 Cawood, P.A., Kroner, A., Collins, W.J., Kusky, T.M., Mooney, W.D. and Windley, B.F.
1249 2009. Accretionary orogens through Earth history, *in* Cawood, P.A. and Kroner, A.
1250 (eds) *Earth accretionary systems in space and time.* The Geological Society, London,
1251 Special Publications, 318, p. 1-36.
1252 Cawood, P.A., Kröner, A., Pisarevsky, S., 2006. Precambrian plate tectonics: Criteria and
1253 evidence. GSA Today 16(7), 1-11.

1254 Charbonneau, J.-M., Picard, C., Dupuis-Hébert, L., 1991. Synthèse géologique de la région de
1255 Chapais-Branssat, Abitibi. Ministère des Ressources naturelles, MM 88-01, 189 p.
1256 Chardon, D., Gapais, D., Cagnard, F., 2009. Flow of ultra-hot orogens: A view from the
1257 Precambrian, clues for the Phanerozoic. Tectonophysics 477, 105-118.
1258 Cheilletz, A., Ruffet, G., Marignac, C., Kolli, O., Gasquet, D., Féraud, G., 1999. $^{40}Ar/^{39}Ar$
1259 dating of shear zones in the Variscan basement of Greater Kabyllia (Algeria). Evidence
1260 of an Eo-Alpine event at 128 Ma (hauterivian-Barremian boundary): Geodynamic
1261 consequences. Tectonophysics 306, 97-116.
1262 Chown, E.H., Daigneault, R., Mueller, W., Mortensen, J.K., 1992. Tectonic evolution of the
1263 Northern Volcanic Zone, Abitibi belt, Quebec. Can. J. Earth Sci. 29, 2211-2225.
1264 Collins, W.J., Van Kranendonk, J., and Teyssier, C. 1998. Partial convective overturn of
1265 Archean crust in the east Pilbara Craton, Western Australia: driving mechanism and
1266 tectonic implications. J. Struc. Geol. 20:
1267 Culshaw, N.G., Beaumont, C. and Jamieson, R.A. 2006. The orogenic superstructure-
1268 infrastructure concept: revisited, quantified and revived. Geology 34: 733-736.
1269 Dahl, P.S., 1996. The effects of composition on retentivity of argon and oxygen in hornblende
1270 and related amphiboles: a field-tested empirical model. Geochim. Cosmochim. Acta
1271 60, 3687-3700.
1272 Daigneault, R., Allard, G.O., 1990. Le Complexe du lac Doré et son environnement
1273 géologique (region de Chibougamau - Sous-province de l'Abitibi). Ministère de
1274 l'Énergie, des Mines et des Ressources, Québec, MM 89-03, 275 p.
1275 Daigneault, R.A., Mueller, W.U, and Chown, E.H. 2004. Abitibi greenstone belt platte
1276 tectonics: the diachronous history of arc development, accretion and collision, *in*
1277 Erikkson, P., Altermann, W., Nelson, D., Mueller, W., Catumeanu,O. and Strand, K.,
1278 eds. Developments in Precambrian geology/tempos of events in Precambrian time:
1279 Amsterdam, Elsevier, p. 85-103.
1280 Daigneault, R., Mueller, W.U., Chown, E.H., 2002. Oblique Archean subduction: accretion
1281 and exhumation of an oveanic arc during dextral transpression, Southern Volcanic
1282 Zone, Abitibi Subprovince Canada. Precambrian Research 115, 261-290.
1283 Daigneault, R., St Julien, P., Allard, G.O., 1990. Tectonic evolution of the northeast portion
1284 of the Archean Abitibi greenstone belt, Chibougamau area, Quebec. Can. J. Earth Sci.
1285 27, 1714-1736.
1286 Daoudene, Y., Tremblay, A., Ruffet, G., Leclerc, F., 2014. Étude structurale et

métamorphique de la bordure nord-est de la ceinture de roches vertes de l'Abitibi, Québec, Canada : apport de la thermochronologie $^{40}Ar/^{39}Ar$ et implications tectoniques. Ministère des Ressources naturelles, Québec, MB 2014-04, 55 pages.

Daoudene, Y., Leclerc, F., Tremblay, A., 2016. Une histoire tectono-métamorphique commune et de longue durée pour les sous-provinces d'Abitibi et d'Opatica, Province du Supérieur, Québec, Canada. Ministère des Ressources naturelles, Québec, MB 2016-01, 41 pages.

David, J., Davis, D.W., Dion, C., Goutier, J., Legault, M., Roy, P., 2007. U-Pb age dating in the Abitibi Subprovince in 2005-2006. Ministère des Ressources naturelles et de la Faune, RP 2007-01(A), 17 pages.

David, J., Dion, C., Goutier, J., Roy, P., Bandyayera, D., Legault, M., Rhéaume, P., 2006. Datations U-Pb effectuées dans la Sous-province de l'Abitibi à la suite des travaux de 2004-2005. Ministère des Ressources naturelles et de la Faune, RP 2006-04, 22 pages.

David, J. 2005. Rapport préliminaire sur des travaux de géochronologie U-Pb, année 2004-2005. Ministère des Ressources naturelles et de la Faune, Québec, GM :62069, 31 pages.

David, J. 2012. Datations isotopiques effectuées dans le nord-est de la Province du Supérieur, Travaux de 2001, 2002 et 2003. Ministère des Ressources naturelles et de la Faune, Québec, DV 2012-05, 82 pages.

David, J., 2018. Datations U-Pb dans la Province du Supérieur effectuées au GEOTOP en 2015-2016. Ministère de l'Énergie et des Ressources naturelles du Québec. MB 2018-16, 24 pages.

David, J., McNicoll, V., Simard, M., Bandyayera, D., Hammouche, H., Goutier, J., Pilote, P., Rhéaume, P., Leclerc, F. et Dion, C. (2011). Datations U-Pb effectuées dans les provinces du Supérieur et de Churchill en 2009-2010. Ministère des Ressources naturelles et de la Faune, Québec. RP 2011-02, 37 pages.

Davis, D.W., 2002. U–Pb geochronology of Archean metasedimentary rocks in the Pontiac and Abitibi subprovinces, Quebec, constraints on timing, provenance and regional tectonics: Precambrian Research, v. 115, no. 1–4, p. 97–117, doi: 10.1016/S0301-9268(02)00007-4.

Davis, D.W., Simard, M., Hammouche, H,, Bandyayera, Goutier, J., Pilote, P. 2014. Datations U-Pb effectuées dans les Provinces du Supérieur et de Churchill en 2011-12. MERN report RP 2014-05 : Ministère de l'Énergie et des Ressources naturelles,

Québec, RP 2014-05, 61 pages.
Davis, D.W. and Dion, C. 2012. Datations ID-TIMS d'échantillons recueillis en 2011-2012 par Géologie Québec. Ministère de l'Énergie et des Ressources naturelles, Québec, GM 66443, 26 pages.
Davis, W.J., Sawyer, E., Machado, N., Gariépy, C., Benn, K., 1992. U-Pb Geochronology of plutonism and metamorphism in the Opatica Belt : initial Results. Lithoprobe Report 33, 147-149.
Davis, W.J., Machado, N., Gariépy, C., Sawyer, E.W., Benn, K., 1995. U-Pb geochronology of the Opatica tonalite-gneiss belt and its Relationship to the Abitibi greenstone belt, Superior Province, Quebec. Canadian Journal of Earth Sciences 32, 113-127.
Davis, W.J., Gariépy, C., Sawyer, E.W., 1994. Pre-2.8 Ga crust in the Opatica gneiss belt : A potential source of detrital zircons in the Abitibi and Pontiac subpriovince, canada. Geology 22, 1111-1114.
Deino, A., and Potts, R. 1992. Age-probability spectra for examination of single-crystal 40Ar/39Ar dating results: examples from Olorge sailie, southern Kenya Rift. Quat Int 13/14:47–53
De Putter, T. and Ruffet, G., 2020. Supergene manganese ore records 75 Myr-long Campanian to Pleistocene geodynamic evolution and weathering history of the Central African Great Lakes region - Te–tonic drives, climate assists. Gondwana Research 83: 96-117.
De Putter, T., Ruffet, G., Yans, J., and Mees, F. 2015. The age of supergene manganese deposits in Katanga and its implications for the Neogen evolution of African Great Lakes Region. Ore Geology Reviews 71: 350-362.
Dewey J.F., 1987. Suture. In: Structural Geology and Tectonics. Encyclopedia of Earth Science. Springer, Berlin, Heidelberg. https://doi.org/10.1007/3-540-31080-0_115.
Dimroth, E., Mueller, W., Daigneault, R., Brisson, H., Poitras, A., Rocheleau, M., 1986. Diapirism during regional compression: the structural pattern in the Chibougamau region of the Archean Abitibi belt, Québec. Geologische Rundschau 75(3), 715-736.
Dimroth, E., Rocheleau, M., Mueller, W., 1984. Paleogeography. Isostasy and crustal evolution of the Archean Abitibi belt: a comparison between the Rouyn-Noranda and Chibougamau-Chapais areas. In: Guha, J., and Chown. E.H. (Eds) Chibougamau.
Dimroth, E., Imreh, L., Goulet, N., and Rocheleau, M., 1983. Evolution of the south-central segment of the Archean Abitibi Belt, Quebec. Part II: Tectonic evolution and

1353 geomechanical model. Canadian Journal of Earth Sciences, v. 20, no. 9, p. 1374–1388.
1354 Dodson, M.H., 1973. Closure temperatures in cooling geochronological and petrological
1355 systems. Contribution to Mineral Petrology 40, 259-274.
1356 Ducharme, Y., Stevenson, R.K., Machado, N., 1997. Sm-Nd geochemistry and U-Pb
1357 geochronology of the Preissac and La Motte leucogranites, Abitibi Subprovince.
1358 Canadian Journal of Earth Sciences 34, 1059–1071.
1359 Ernst, G.W., Liou, J.G. and Hacker, B.R. 1994. Petrotectonic significance of high and
1360 ultrahigh-pressure metamorphic belts: inferences from subduction-zone histories.
1361 International Geology Review 36: 213-237.
1362 Faure, S., 2015. Relations entre les minéralisations aurifères et les isogrades métamorphiques
1363 en Abitibi. Rapport, Projet CONSOREM 2013-03, 52 p.
1364 Feng, R., Kerrich, R., McBride, S. and Farrar, E. 1992. 40Ar/39Ar age constraints on the
1365 thermal history of the Archean Abitibi greenstone belt and the Pontiac subprovince:
1366 implications for terrane collision, differential uplift, and overprinting of gold deposits.
1367 Candian Journal of Earth Sciences 29: 1389-1411.
1368 Fleck, R.J., Sutter, J.F., and Elliot, D.H., 1977. Interpretation of discordant 40Ar/39Ar age
1369 spectra of Mesozoic tholeiites from Antarctica. Geochimica Cosmochimica Acta 41:
1370 15-32.
1371 Fortier, S.M., Giletti, B.J., 1989. An empirical model for predicting diffusion coefficients in
1372 silicate minerals. Science 245, 1481-1484.
1373 Frieman, B.M., Kuiper, Y.D., Kelly, N.M., Monecke, T., and Kylander-Clark, A., 2017.
1374 Constraints on the geodynamic evolution of the southern Superior Province: U-Pb LA-
1375 ICP-MS analysis of detrital zircon in successor basins of the Archean Abitibi and
1376 Pontiac subprovinces of Ontario and Quebec, Canada: Precambrian Research, v. 292,
1377 p. 398–416, doi: 10.1016/j.precamres.2017.01.027.
1378 Gapais, D., Barbarin, B., 1986. Quartz fabric transition in cooling syntectonic granite
1379 (Hermitage massif, France). Tectonophysics 124, 357-370.
1380 Gariépy, C., Allègre, C.J., 1985. The lead isotope geochemistry and geochronology of late
1381 kinematic intrusives from the Abitibi greenstone belt, and the implications for late
1382 Archean crustal evolution. Geochim. Cosmochim. Acta 49, 2371-2383.
1383 Gosselin, C., 1996. Synthèse géologique de la région de Frotet-Troilus. Ministère des
1384 Resssources Naturelles du Québec, ET-96-02, 21 p.
1385 Goutier, J., 2005. Géologie de la région du lac au Goéland (32F/15). Ministère des

1386 Ressources naturelles et de la Faune, Québec. RG 2005-05, 39 pages.
1387 Goutier, J., Rhéaume, P., Davis, D.W., 2004. Géologie de la région du lac Olga (32F14).
1388 Géologie Québec, RG 2003-09, 42 p.
1389 Gower, R.J.W, Simpson, C., 1992. Phase boundary mobility in naturally deformed, high-
1390 grade quartzofeldspathic rocks: evidence for diffusional creep. J. Struct. Geol 14 (3),
1391 301-313.
1392 Gray, R. and Pysklywec, R.N., 2010. Geodynamic models of Archean continental
1393 collision and the formation of mantle lithosphere keels. Geophysical Research Letters
1394 37: 1-5.
1395 Groulier, P.A., De Souza, S., Daoudene, Y. et Massei, F., 2020. Synthèse gîtologique de la
1396 ceinture de roches vertes de Frotet-Evans, segments Evans-Ouagama et Storm-Evans.
1397 Ministère de l'Énergie et des Ressources naturelles, Québec. MB 2020-14, 128 pages.
1398 Grove, M., Harrison, T.M., 1996. ^{40}Ar diffusion in Fe-rich biotite. Am. Min. 81, 940-951.
1399 Hames, W. E., Cheney, J. T., Tracy, R. J., 2008. Single-crystal ^{40}Ar/^{39}Ar age variation in
1400 muscovite of the Gassetts Schist and associated gneiss, Vermont Appalachians. Am.
1401 Mineral. 93, 384-395.
1402 Harrison, T.M, Celerier, J., Aikman, A.B, Hemaqnn, J., Heizler, M.T., 2009. Diffusion of 40Ar
1403 in muscovite. Geochim. Cosmochim. Acta. 73, 1039-1051.
1404 Harrison, T.M., Duncan, I., McDougall, I., 1985. Diffusion of 40Ar in biotite: temperature,
1405 pressure and compositional effects. Geochim. Cosmochim, Acta 55, 1435-1448.
1406 Hocq, M., 1994. La Province du Supérieur. In: Géologie du Québec. Ministère des
1407 Ressources naturelles, Québec, MM94-01, 7-20.
1408 Jäger, E., 1967. Die Bedeutung des Biotit-Aterswerte. In: Jäger, E., Niggli, E., Wenk, E.
1409 (Eds), Rb-Sr Alersbestimmugen an Glimmern der Zentralalpen. Beitr. Geol. Karte
1410 Scweiz, NF 134, 28-31.
1411 Kamber, B.S., Blenkinsop, T.G., Villa, I.M., Dahl, P.S., 1995. Proterozoic transpressive
1412 deformation in the Northern Marginal Zone, Limpopo Belt, Zimbabwe. J. Geol. 103,
1413 493-508.
1414 Kim, Y.H., Miller, M.S., Pearce, F. and Clayton, R.W. 2012. Seismic imaging of the Cocos
1415 plate subduction zone system in central Mexico. Geochem. Geophys. Geosyst. 13, doi:
1416 10.1029/2012GC004033.
1417 Kimura, G., Ludden, J.N., Desrochers, J.P., Hori, R., 1993. A model of ocean-crust accretion
1418 for the Superior province, Canada. Lithos 30, 337-355.

Kusky, T., Wang, J., Wang, L., Huang, B., Ning, W., Fu, D., Peng, H., Deng, H., Polat, A., Zhong, Y. and Shi, G. 2020. Mélanges through time: life cycle of the world's largest Archean mélange compared with Mesozoic and Paleozoic subduction-accretion-collision. Earth-Science Reviews 209.

Lacroix, S., Sawyer, E.W., 1995. An Archean fold – thrust belt in the northwestern Abitibi Greenstone Belt: structural and seismic evidence. Canadian Journal of Earth Sciences 32, 97-112.

Leclair, A.D., Ernst, R.E., Hattori, K., 1993. Crustal-scale auriferous shear zones in the central Superior province, Canada. Geology 21, 399-402.

Leclerc, F., Houle, P., 2013. Géologie de la region du lac Simon (32G15-200-0102). Ministère des Ressources naturelles, Québec, RP 2013-02.

Leclerc, F., Harris, L.B., Bédard, J.H., van Breemen, O., Goulet, N., 2012. Structural and stratigraphic controls on magmatic, volcanogenic, and shear zone-hosted mineralization in the Chapais-Chibougamau mining camp, Northeastern Abitbi, Canada. Economic Geology 107, 963-989.

Leclerc, F., Bédard, J., Harris, L.B., McNicoll, V.J., Goulet, N., Roy, P., Houle, P., 2011. Tholeiitic to calc-alcaline cyclic volcanism in the Roy Group. Chibougamau area, Abitibi Greenstone Belt – revised stratigraphy and implications for VHMS exploration. Can. J. Earth Sci. 48(3), 661-694.

Leclerc, F., Bédard, J.H., Harris, L.B., Goulet, N., Houle, P., Roy, P., 2008. Nouvelles subdivisions de la Formation de Gilman, Groupe de Roy, region de Chibougamau, sous-province de l'Abitibi, Québec : résultats préliminaires. Commission géologique du Canda, Recherche en cours 2008-7, 20 p.

Legault, M., 2003. Environnement métallogénique du couloir de Fancamp avec emphases sur les gisements aurifères de Chevrier. Région de Chibougamau, Québec. Phd thesis, Université du Québec à Chicoutimi, 488 p.

Lin, S., Parks, J., Heaman, L.M., Simonetti, A., Corkery, M.T., 2013. Diapirism and sagduction as a mechanism for deposition and burial of "Timiskaming-type" sedimentary sequences, Superior Province: Evidence from detrital zircon geochronology and implications for the Borden Lake conglomerate in the exposed meddle to lower crust in the Kapuskasing uplift. Precambrian Research 238, 148-157.

Lister, G.S. and Davis, G.A. 1989. The origin of metamorphic core complexes and detachment faults formed during Tertiary continental extension in the northern

Colorado River region, U.S.A. J. Struc. Geol. 11: 65-94.

Lister, G.S., Baldwin, S.L., 1996. Modelling the effect of arbitrary P-T-t histories on Ar diffusion in minerals using the MacArgon program for the Apple Macintosh. Tectonophys. 253, 83-109.

Ludden, J. and Hynes, A. 2000. The Lithoprobe Abitibi-Grenville transect: two billion years of crust formation and recycling in the Precambrian shield of Canada. Can. J. Earth Sci. 37: 459-476.

Ludden, J., Hubert, C., Gariépy, C., 1986. The tectonic evolution of the Abitibi greenstone belt of Canada: Geological Magazine 123, 153-166.

Mainprice, D., Bouchez, J.L., Blumenfeld, P., Tubia, J.M., 1986. Dominant c-slip in naturally deformed quartz: implications for dramatic plastic softening at high temperature. Geology 14, 819-822.

Mathieu, L., Snyder, D.B., Bedeaux, P., Cheraghi, S., Lafrance, B., Thurston, P. and Sherlock, R. 2020. Deep into the Chibougamau area, Abitibi Greenstone Belt: structure of a Neoarchean crust revealed by seismic reflection profiling. Tectonics 38.

McDougall, I., Harrison, T.M., 1988. Geochronology and thermochronology by the $^{40}Ar/^{39}Ar$ method. Oxford monographs on geology and geophysics, Oxford Press 9, 212 p.

McNicoll, V.J., Goutier, J., 2008. Trois datations U-Pb de la region du lac au Goéland, Sous-province de l'Abitibi. Ministère des Ressources naturelles et de la Faune, RP 2008-02, 11 p.

Mole, D.R., Thurston, P.C., Marsh, J.H., Stern, R.A., Ayer, J.A., Martin, L.A.J. Lu, Y.J. 2021. The formation of Neoarchean continental crust in the south-east Superior Craton by two distinct geodynamic processes. Precambrian Research 356. https://doi.org/10.1016/j.precamres.2021.106104.

Montigny, R., 1985. Méthode classique potassium-argon. Méthode de datation par les phénomènes nucléaires naturels : applications : textes réunis par E. Roth et B. Poty, Masson, Série Scientifique, 309-340.

Mueller, W.U., 1991. Volcanism and related slope to shallow-marine volcaniclastic sedimentation: an Archean example near Chibougamau, Quebec, Canada. Precambrian Research 49, 1-22.

Mueller, W.U., Daigneault, R., Mortensen, J.K., Chown, E.H., 1996. Archean terrane docking: Upper crust collision tectonics, Abitibi greenstone belt, Quebec, Canada. Tectonophysics 265, 127-150.

1485 Nadeau, O., Cayer, A., Pelletier, M., Stevenson, R. and Jébrak, M. 2015. The
1486 Paleoproterozoic Montviel carbonatite-hosted REE–Nb deposit, Abitibi, Canada:
1487 Geology, mineralogy, geochemistry and genesis. Ore Geology Rev. 67: 314-335.
1488 Palin, R.M., Santosh, M., Cao, W., Li, S.-S., and Hernandez-Uribe, D. 2020. Secular change
1489 and the onset of plate tectonics on Earth. Earth-Science Reviews 207.
1490 Parmenter, A.C., Lin, S., Corkery, T., 2006. Structural evolution of the Cross Lake greenstone
1491 belt in the northwestern Superior Province, Manitoba: implications for relationship
1492 between vertical and horizontal tectonism. Can J Earth Sci 43, 767-787.
1493 Pedreira-Perez, R., Tremblay, A., Daoudene, Y. and Bandyayera, D. 2020. Étude
1494 géochimique, structurale et géochronologique de la Sous-province de Nemiscau, Baie-
1495 James, Québec : implications quant à l'origine et l'évolution tectonique d'un domaine
1496 sédimentaire archéen. Ministère des Ressources naturelles, MB 2020-07, 82 pages.
1497 Percival, J.A., Skulski, T., Sanborn-Barrie, M, Stott, G.M, Leclair, A., Corkery, M.T., Boily,
1498 M., 2012. Geology and tectonic evolution of the Superior Province, Canada, chapter 6.
1499 In: Percival, J.A., Cook, F.A., Clowes, R.M. (Eds), Tectonic styles in Canada: the
1500 LITHOPROBE perspective. Geological Association of Canda, Special Paper 49, 321-
1501 378.
1502 Percival, J.A., 2007. Geology and metallogeny of the Superior Province, Canada. In:
1503 Goodfellow, W.D. (Ed). Mineral deposits of Canada: a synthesis of major deposit-types,
1504 district metallogeny, the evolution of geological provinces, and exploration methods.
1505 Geol. Ass. Can. Min. Deposit Div. Sp. Pub. 5, 903-928.
1506 Percival, J.A., Sanborn-Barrie, M., Skulski, T., Stott, G.M., Helmstaedt, H., White, D.J.,
1507 2006. Tectonic evolution of the western Superior Province from NatMap and
1508 Lithoprobe studies. Can. J. Earth. Sci. 43:1085-1117.
1509 Piette-Lauzière, N., Guilmette, C., Bouvier, A., Perrouty, S., Pilote, P., Gaillard, N.,
1510 Lypaczewski, P., Linnen, R.L., Olivo, G.R. 2019. The timing of prograde metamorphism in
1511 the Pontiac Subprovince, Superior craton: implications for Archean geodynamics and
1512 gold mineralization. Precambrian Research 320, 111-136.
1513 Pilote, P., Dion, C., Joanisse, A., David, J., Machado, N., Kirkham, R., Robert, F., 1997.
1514 Géochronologie des minéralisations d'affiliation magmatique de l'Abitibi, secteurs de
1515 Chibougamau et de Troilus-Frotet : Implications géotectoniques. In: Vers de
1516 nouvelles découvertes. Séminaire d'information sur la recherche géologique,
1517 Ministère des Ressources naturelles, Programme et résumé 47.

1518 Pitra, P., Ballèvre, M., Ruffet, G., 2010. Inverted metamorphic field gradient towards a
1519 Variscan suture zone (Champtoceaux Complex, Armorican Massif, France). J. Metam.
1520 Geol. 28 (2), 183-208.
1521 Powell, W.G., Hodgson, C.J., Hanes, J.A., Carmichael, D.M., McBride, S., and Farrar, E.
1522 1995. $^{40}Ar/^{39}Ar$ geochronological evidence for multiple post-metamorphic
1523 hydrothermal events focused along faults in the southern Abitibi greenstone belt. Can.
1524 J. Earth Sci. 32: 768-786.
1525 Purdy, J.W., Jäger, E., 1976. K-Ar ages on rock forming minerals from the Central Alps.
1526 Memorie degli Istituti di Geologia e Mineralogia dell'Università di Padova 30, 1-32.
1527 Renne, P.R., Balco, G., Ludwig, R.L., Mundil, R., and Min, K., 2011. Response to the
1528 comment by W.H. Schwarz et al. on "Joint determination of 40K decay constants and
1529 40Ar∗/40K for the Fish Canyon sanidine standard, and improved accuracy for
1530 40Ar/39Ar geochronology" by PR Renne et al. (2010). Geochimica et Cosmochimica
1531 Acta, 75: 5097-5100.
1532 Renne, P.R., Mundil, R., Balco, G., Min, K., and Ludwig, R.L., 2010. Joint determination
1533 of 40K decay constants and 40Ar∗/40K for the Fish Canyon sanidine standard, and
1534 improved accuracy for 40Ar/39Ar geochronology. Geochimica et Cosmochimica Acta
1535 74: 5349–5367.
1536 Revelli, N. 2020. Évolution tectonométamorphique d'un segment de croûte archéenne : le
1537 Complexe d'Attic, Lebel-sur-Quévillon. Ph.D. Thesis, Université du Québec à
1538 Montréal, Montréal, Canada.
1539 Robert, F., Poulsen, K.H., Cassidy, K.F., and Hodgson, C.J. 2005. Gold metallogeny of
1540 the Superior and Yilgarn cratons. Economic Geology 100: 1001–1033.
1541 Roddick, J.C., 1983. High precision intercalibration of ^{40}Ar-^{39}Ar standards. Geochim.
1542 Cosmochim. Acta 51, 2129-2135.
1543 Ross, P.S., Goutier, J., Mercier-Langevin, P., Dubé, B., 2010. Basaltic to andesitic
1544 volcaniclastic rocks in the Blake River Group, Abitibi Greenstone Belt: 1. Mode of
1545 emplacement in three areas. Canadian Journal of Earth Sciences 48, 728-756.
1546 Ruffet, G., Feraud, G., Balèvre, M., Kiénast, J.R., 1995. Plateau ages and excess argon in
1547 phengites: an 40Ar/39Ar laser probe study of Alpine micas (Sezia Zone, Western
1548 Alps, northern Italy). Chem. Geol. 121(1-4), 327-343.
1549 Ruffet, G., Féraud, G., Amouric, M., 1991. Comparison of $^{40}Ar/^{39}Ar$ conventional and laser
1550 dating of biotites from the North Tregor Batholith. *Geochim. Cosmochim. Acta 55*,

1675-1688.

Ruffet G., Perroud H., Féraud G., 1990. ^{40}Ar-^{39}Ar dating of a late Proterozoic paleomagnetic pole for the Armorican Massif (France). Geophysical Journal International 102; 397-409.

Sawyer, E.W., 1998. Formation and evolution of granite magmas during crustal reworking: the significance of diatexites. Journal of Petrology 39 (6), 1147-1167.

Sawyer, E.W., Benn, K., 1993. Structure of the high-grade Opatica Belt and adjacent low-grade Abitibi Subprovince, Canada: an Archean mountain front. Journal of Structural Geology 15, 1443-1458.

Schaen, A.J. and 40 others. 2020. Interpreting and reporting $^{40}Ar/^{39}Ar$ geochronological data. Geol. Soc. Am. Bull. 133: 461-487.

Schmid, S.M., Casey, M., 1986. Complete fabric analysis of some commonly observed quartz c-axis pattern. Geophys. Monogr. 36, 263-286.

Simard, M., 1987. Stratigraphie et volcanism dans la partie orientale de la bande volcano-sédimentaire archéenne Frotet-Evans. Ministère de l'Énergie et des Ressources, Québec, MB 87-17, 300 p.

Simpson, C., 1985. Deformation of granite rocks across the brittle-ductile transition. J. Struct. Geol. 7 (5), 503-511.

Simpson, C., Wintsch, R.P., 1989. Evidence for deformation-induced K-feldspar replacement by myrmekite. J. Metamorphic. Geol. 7, 261-275.

Spear, F.S., 1993. Metamorphic phase equilibria and pressure-temperature-time paths. Mineral. Soc. Am., 799 p.

Stern, R.J. 2018. The evolution of plate tectonics. Phil. Trans. of the Royal Soc. Series A.

Stern, R.J. 2008. Modern-style plate tectonics began in Neoproterozoic time: An alternative interpretation of Earth's tectonic history. When did plate tectonics begin on planet Earth, 440, pp 265-280.

Stern, R.J. 2002. Subduction zones. Reviews of Geophysics 40, 38 p.

Stott, G.M., Corkery, M.T., Percival, J.A., Simard, M., Goutier, J., 2010. A revised terrane subdivision of the Superior Province. In: Summary of Field Work and Other Activities 2010, Ontarion Geological Survey, Open File Report 6260 pp. 20-1 to 20-10.

Tartese, R., Ruffet, G., Poujol, M., Boulvais, P., and Ireland, T. R. 2011. Simultaneous resetting of the muscovite K- Ar and monazite U- Pb geochronometers: A story of fluids. Terra Nova 23: 390–398.

Thébaud, N. and Rey, P.F., 2013. Archean gravity-driven tectonics on hot and flooded continents: Controls on long-lived mineralised hydrothermal systems away from continental margins. Precamb. Res. 229, 93-194.

Thibault, P., 1985. Applications à la méthode U-Pb (zircon) à des roches ignées des ensembles volcano-sédimentaires de l'Abitibi et de Frotet-Evans. Mem. Univ. Montréal, Montréal, 165 p.

Thurston, P.C., Ayer, J.A., Goutier, J. and Hamilton, M.A., 2008. Depositional gaps in Abitibi Greenstone Belt stratigraphy: a key to exploration for syngenetic mineralization. Economic Geology 103: 1097-1134.

Tikoff, B., Teyssier, C. and Waters, Ch. 2002. Clutch tectonics and the partial attachment of lithospheric layers. EGU Stephen Mueller Special Publication Series 1: 57-73.

Tremblay, A., Ruffet, G, and Lemarchand, J. 2020. Timing and duration of Archean orogenic gold deposits in the Bourlamaque pluton, Val d'Or mining camp, Abitibi, Canada. Ore Geology Reviews 127.

Tremblay, A., Ruffet. G. and Bédard. J.H. 2011. Obduction of Tethyan-type ophiolites – a case-study from the Thetford-Mines ophiolitic Complex, Québec Appalachians, Canada. Lithos 125: 10-26.

Turner, G., Huneke, J.C., Podosek, F.A., Wasserburg, G.J., 1971. ^{40}Ar-^{39}Ar ages and cosmic ray exposure age of Apollo 14 samples. Earth Planet. Sci. Lett. 12, 19-35.

Vanderhaeghe, O., Guergouz, C., Fabre, C., Duchêne, S. and Baratoux, D. 2019. Secular cooling and crystallization of partially molten Archean continental crust over 1 Ga. Comptes rendus-Geosciences 351: 562-573.

van der Velden, A.J. and Cook, F.A., 2005. Relict subduction zones in Canada. J. Geophys. Res. 110, doi:10.1029/2004JB003333

Van Hunen, J. and Moyen, J.-F. 2012. Archean subduction: fact or fiction? Annu. Rev. Earth Planet. Sci 40: 195-219.

Van Kranendonk, M.J. 2011. Archean Tectonics. In: Gargaud M. et al. (eds) Encyclopedia of Astrobiology. Springer, Berlin, Heidelberg. https://doi.org/10.1007/978-3-642-11274-4_100.

Villa, I.M., 1998. Isotopic closure. Terra Nova 10, 42-47.

Villa, I. M., Puxeddu, M., 1994. Geochronology of the Larderello geothermal field: new data and the 'closure temperature' issue. Contrib. Mineral. Petrol. 315, 415-426.

Villa, I.M., Grobéty, B., Kelley, S.P., Trigila, R., Wieler, R., 1996. Assessing Ar transport

paths and mechanisms for McClure Mountains Hornblende. Contrib. Min. Petrol. 126, 67-80.

Wakabayashi, J. 2017. Structural context and variation of ocean plate stratigraphy, Franciscan Complex, California: insight into mélange origins and subduction-accretion processes. Progress in Earth and Planetary sciences 4 (18). https://progearthplanetsci.springeropen.com/articles/10.1186/s40645-017-0132-y.

Wakabayashi, J., and Dilek, Y., 2011, Introduction: Characteristics and tectonic settings of mélanges, and their significance for societal and engineering problems: in Wakabayashi, J., and Dilek, Y. eds. Mélanges: Processes of Formation and Societal Significance, Geological Society of America Special Paper 480, doi: 10.1130/2011.

Weinberg, R.F. 1997. Diapir-driven crustal convection: decompression melting, renewal of magma source and the origin of nested plutons. Tectonophysics 271: 217-229.

Whitney, D.L., Teyssier, C., and Fayon, A.K. 2004. Isothermal decompression, partial melting and exhumation of deep continental crust, In Grocott, J., McCaffrey, K.J.W., Taylor, G. and Tikoff, B. (eds). Vertical coupling and decoupling in the lithosphere. Geol. Soc. London Sp. Publi. 227: 313-326.

Whitney, D.L., Teyssier, C., Rey, P. and Buck, W.R. 2013. Continental and oceanic core complexes. Geol. Soc. Am. Bull.

Wiemer, D., Schrank, C.E., Murphy, D.T., Wenham, L. and Allen, C.M. 2018. Earth's oldest stable crust in the Pilbara craton formed by cyclic gravitational overturns. Nature Geoscience 11: 357-361.

Wyman, D.A., Kerrich, R., Polat, A., 2002. Assembly of Archean cratonic mantle lithosphere and crust: Plume-arc interaction in the Abitibi-Wawa subductionaccretion complex. Precamb. Res. 115, 37-62.

Figure captions.

Figure 1. a) Principal tectonostratigraphic domains of the Archean Superior Province. Modified from Card (1990) and Benn et al. (1992). **b)** Geological map of the southeastern part of the Superior Province with focus on the Abitibi greenstone belt and the surrounding areas. AC: Attic Complex; BP: Bernetz gneissic pluton; MP: Marest gneissic pluton. Modified from Thurston et al. (2008). See a) for location.

Figure 2. Geological map of the northeastern part of the northeastern part Abitibi Subprovince and the eastern part of the Opatica Subprovince including the eastern portion of

the Frotet-Evans greenstone belt. Samples YD101A and YD0100A used for ^{39}Ar-^{40}Ar dating are localized on the map. BSZ, Barlow shear zone; GF, Gwillim fault; KSZ, Kapunapotagen shear zone; LF, Lamarck shear zone; LFSZ, La France river shear zone; LLSZ, La Trève lake shear zone; LNSZ, Lac à l'Eau-Noire shear zone; LSRSZ, Lucky Strike river shear zone; NRSZ, Nottaway river shear zone. See Fig. 1~~2~~ for location. Modified from Dimroth et al. (1986) and Daigneault et al. (1990).

Figure 3. Geological map of the Lac-au-Goéland area and location of samples used for ^{40}Ar-^{39}Ar for this study. See Fig. 2 for location. Modified from Goutier (2005).

Figure 4. Field photographs of the AGB and OPB rocks. a**)** Amphibolite-grade mafic volcanic rock showing well-preserved pillow structure. b) Strongly deformed gabbro showing quart-feldspar aggregates defining a steeply plunging mineral lineation. c) Typical gneissic tonalite of the OBP characterized by a penetrative S_1 foliation. d) Un-metamorphosed succession of sandstone and siltstone of the Opémisca Group (Daubrée Formation) in the Chibougamau. e) AGB amphibolite located along the southern boundary of the Noman tonalite (see Fig. 3), showing the S_1 metamorphic layering tightly folded by F2 with an axial-planar S2 foliation. f) Granitic dykes crosscutting amphibolitic horizons within the OPB.

Figure 5. Structural map of the study area showing foliation trajectories and dip directions. Structural data were compiled from the geological mapping data available in SIGEOM information system of the Ministère des Ressources naturelles du Québec (http://sigeom.mines.gouv.qc.ca). Trajectories of regional schistosity/foliation were drawn from structural data acquired in the field and high-resolution magnetic imaging.

Figure 6. Stereographic projections (equal area, lower hemisphere) for dominant planar and linear structural fabric of the Abitibi and Opatica subprovinces. Data for the AGB correspond to S_2 and composite S_{1-2} whereas those from the OPB correspond to S_1.

Figure 7. Field photographs of fabric related to the D_3 deformation event. a) Mylonitic fabric developed in a mafic volcanic rock of the AGB. b) Dextral F_3 fold affecting the regional schistosity S_2 within a mafic volcanic rock. c) Subhorizontal stretching lineation along the Nottaway River shear zone. d) Shear bands indicating dextral shearing in a mylonitized orthogneiss of the Nottaway River shear zone (view perpendicular to the subvertical S_3 foliation and parallel to the subhorizontal lineation). e) Thin section cuts parallel to the XY plane showing dextral mica fish fabric in a felsic mylonite. f) Boudinaged felsic dyke cutting across an amphibolite horizon of the OPB.

Figure 8. Photographs illustrating regional metamorphism and associated deformation

in the study area. a) Low-grade volcanic rocks of the Roy Group showing well-preserved pillow structures. b) Garnet-staurolite micaschist from the northwestern flank of the Waconichi syncline. Staurolite forms large, corroded crystal preferentially aligned along the foliation plane (cross-polarized light). c) Large chloritoid phenocryst overprinting the regional schistosity marked by the preferred orientation of actinolite in the fine-grained matrix (cross-polarized light). d) Outcrop of pillowed basalt showing garnet-rich pillow margins in the vicinity of the AGB-OPB transition. e) Typical lobate boundaries between quartz and feldspar grains in a coarse-grained and weakly-deformed tonalite of the OPB. The foliation is marked by the preferred orientation of biotite (plane-polarized light). f) Field example of migmatitic gneiss of the OPB.

Figure 9. Structural profiles of the study area. See figure 3 for location. East-southeast-looking for profile A-A', East-looking for the other profiles.

Figure 10. Single-grain $^{39}Ar/^{40}Ar$ results for amphiboles and biotites of the AGB. Apparent age error bars are at the 1σ level; errors in the J-parameter are not included. Plateau and pseudo-plateau ages (1σ uncertainties including errors in the J-parameter) are given when applicable. Sample locations are show in Figures 3 and 4. See text for explanations.

Figure 11. Single-grain $^{39}Ar/^{40}Ar$ results for amphiboles and biotites for tonalites of the OPB. See Figures 3 and 4 for locations. Analytical details as for Figure 11. See text for explanations.

Figure 12. Single-grain $^{39}Ar/^{40}Ar$ results for muscovite of quartz-feldspar porphyry dykes of the Lac-au-Goéland area. Analytical details as for Figure 11. See Figure 4 for locations. See text for explanations.

Figure 13. Single-grain $^{39}Ar/^{40}Ar$ results for muscovite, amphibole and biotite from the Nottaway River shear zone. Analytical details as for Figure 11. See Figure 4 for locations. See text for explanations.

Figure 14. Single-grain $^{39}Ar/^{40}Ar$ results for amphibole and biotite from the Montviel Syenite. Analytical details as for Figure 11. See Figure 4 for locations and text for explanations.

Figure 15. Synthesis of the validated ages of the study area (plateau and pseudo-plateau) obtained on amphibole and micas grouped by terranes and/or rock types on probability density diagrams of the resized apparent ages for each group. See text for explanation.

Figure 16. Schematic illustration of a partial crustal overturn model for the OPB-AGB

transition. See text for discussion and details on age constraints for the different panels.

Figure 17. Extract of numerical models performed by Gray and Pysklywec (2010). This model suggests that due to a hot and rheologically-weak lower crust, the mantle and the crust become decoupled at a depth of approximately 50 km and that the lithospheric mantle becomes imbricated along major shear zones whereas the crustal domain itself 2 of Gray and Pysklywec (2010). See text for discussion.

Figure 18. a) Teleseismic imaging of the subduction zone interface of the Cocos slab beneath Mexico. Modified from Kim et al. (2012). b) Alternative interpretation for the AGB showing flat subduction of the Pontiac terrane below a composite AGB-OPB terrane. Note the striking geometrical similarity with the Cocos subduction zone. See text for discussion.

Figure 1 (color)

Click here to access/download;Figure;Figure 1.jpg

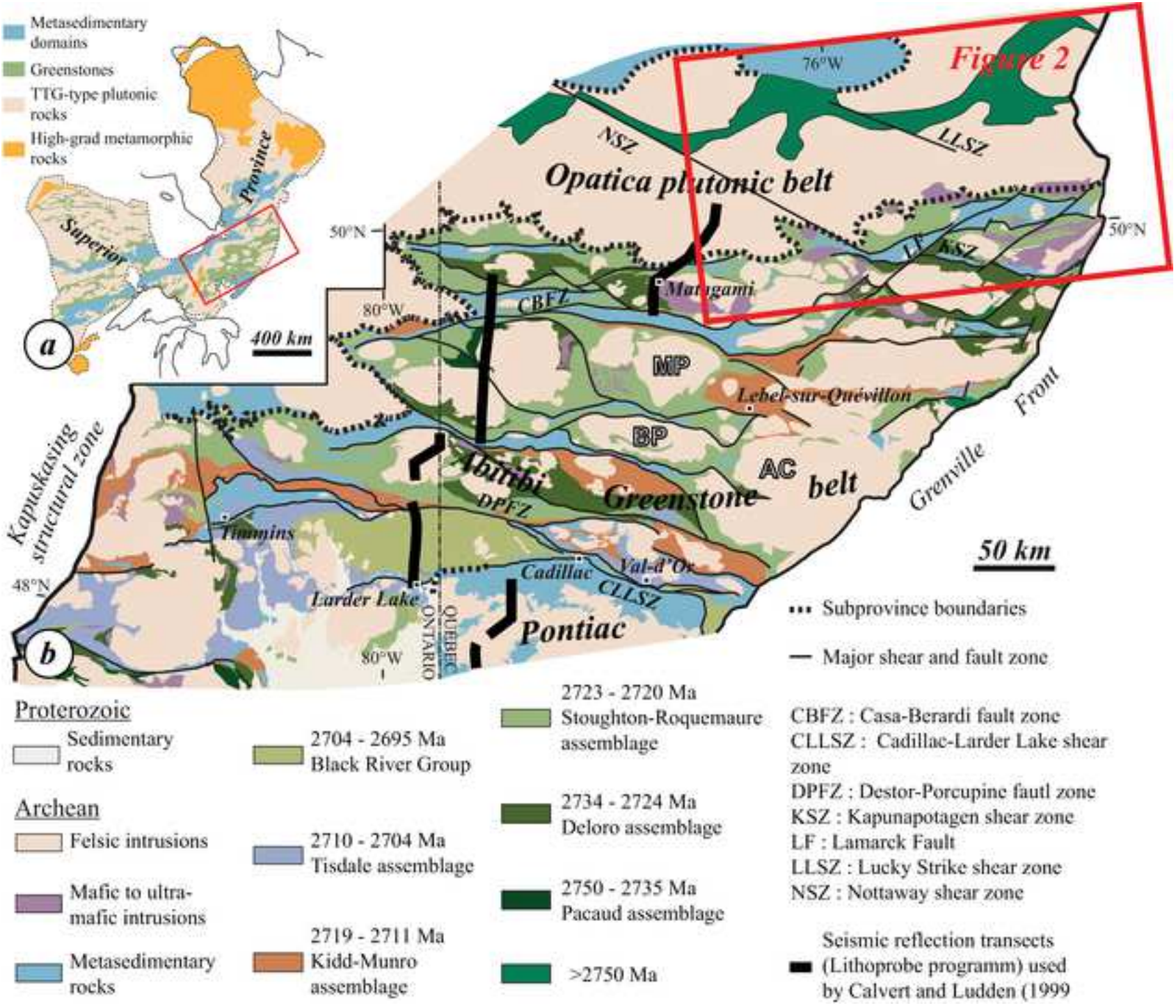

Figure 2 (color)

Click here to access/download;Figure;Figure 2.jpg

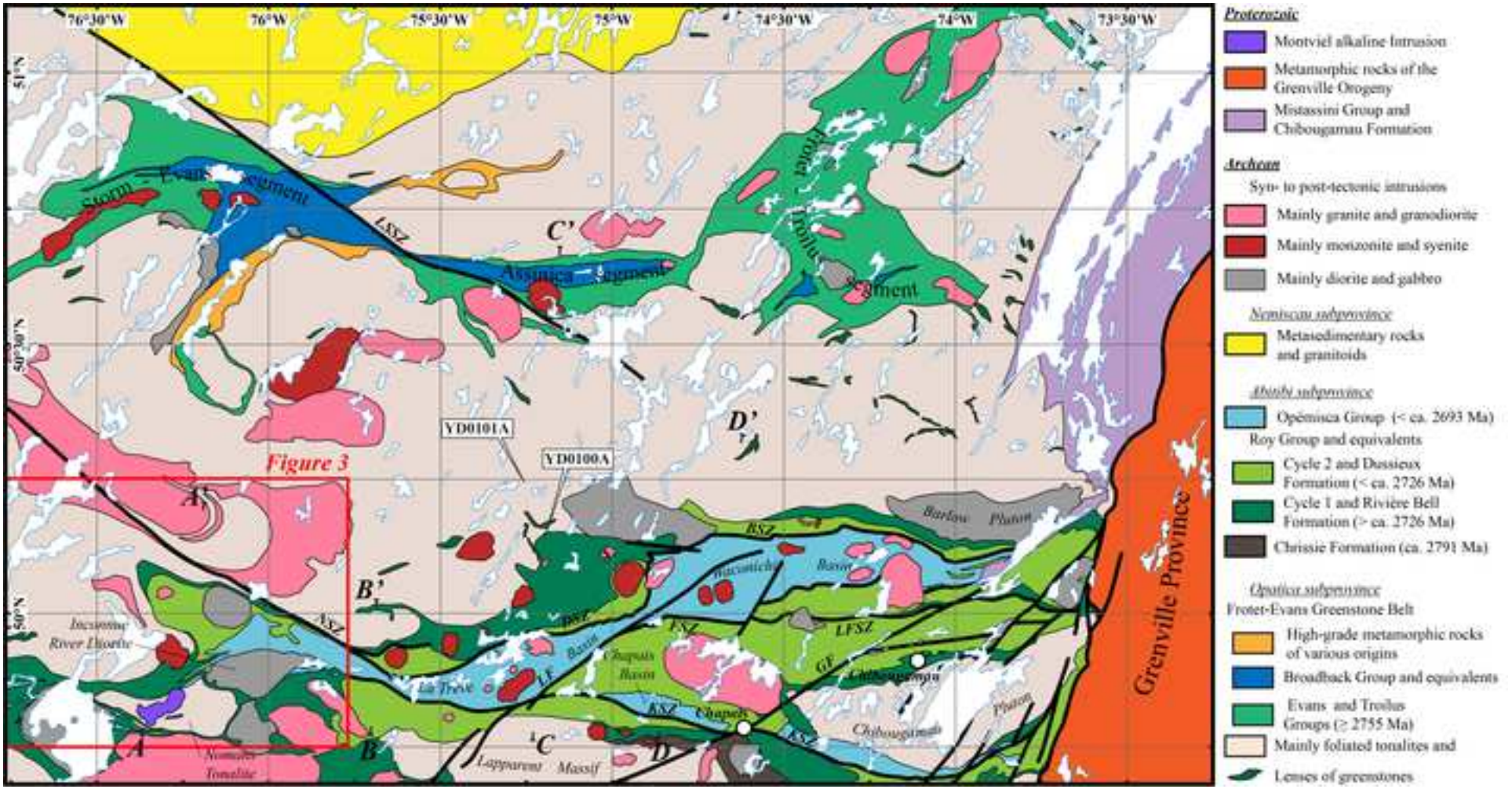

Figure 3 (color)

Click here to access/download;Figure;Figure 3.jpg

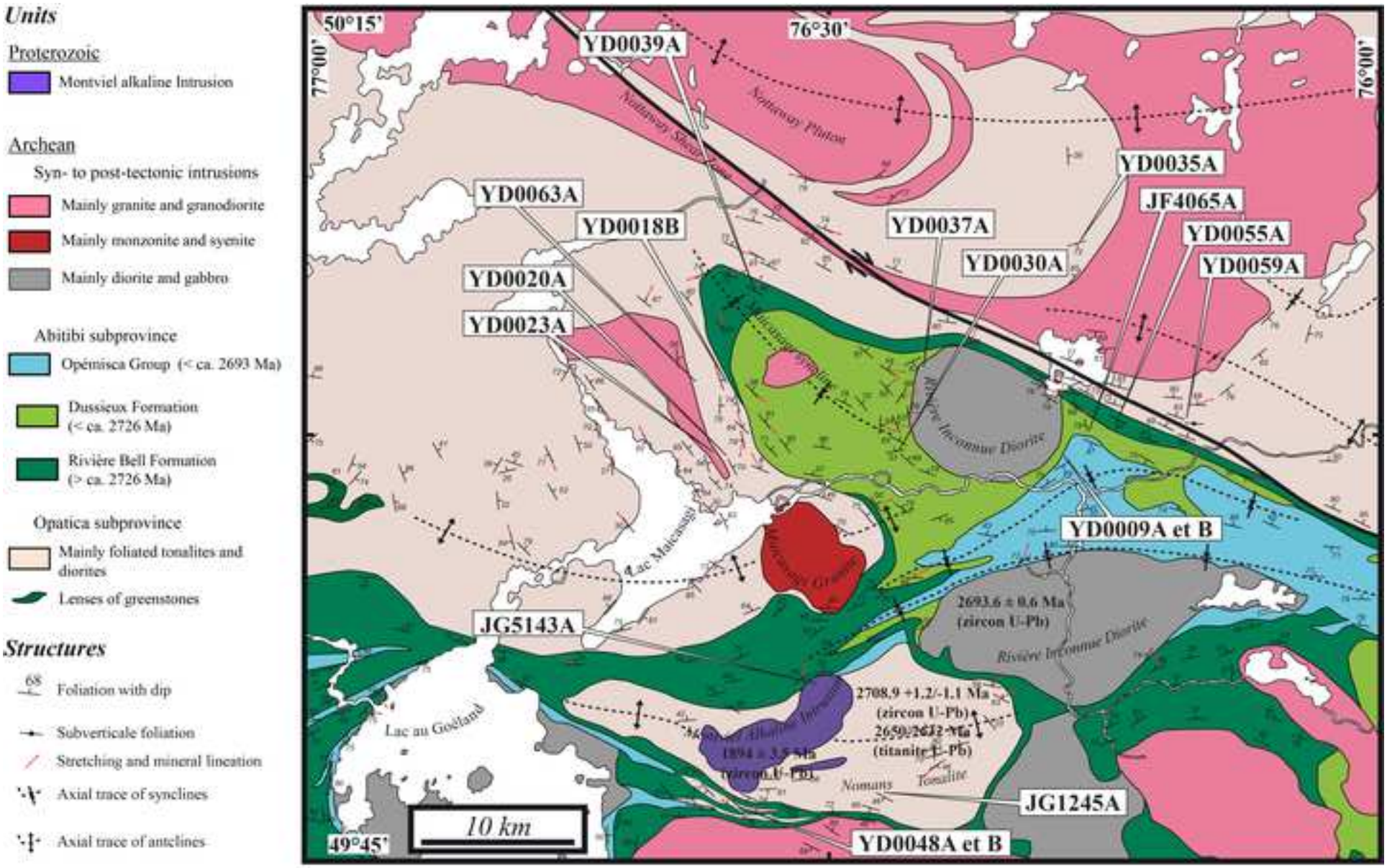

Figure 4 (color)

Click here to access/download;Figure;Figure 4.jpg

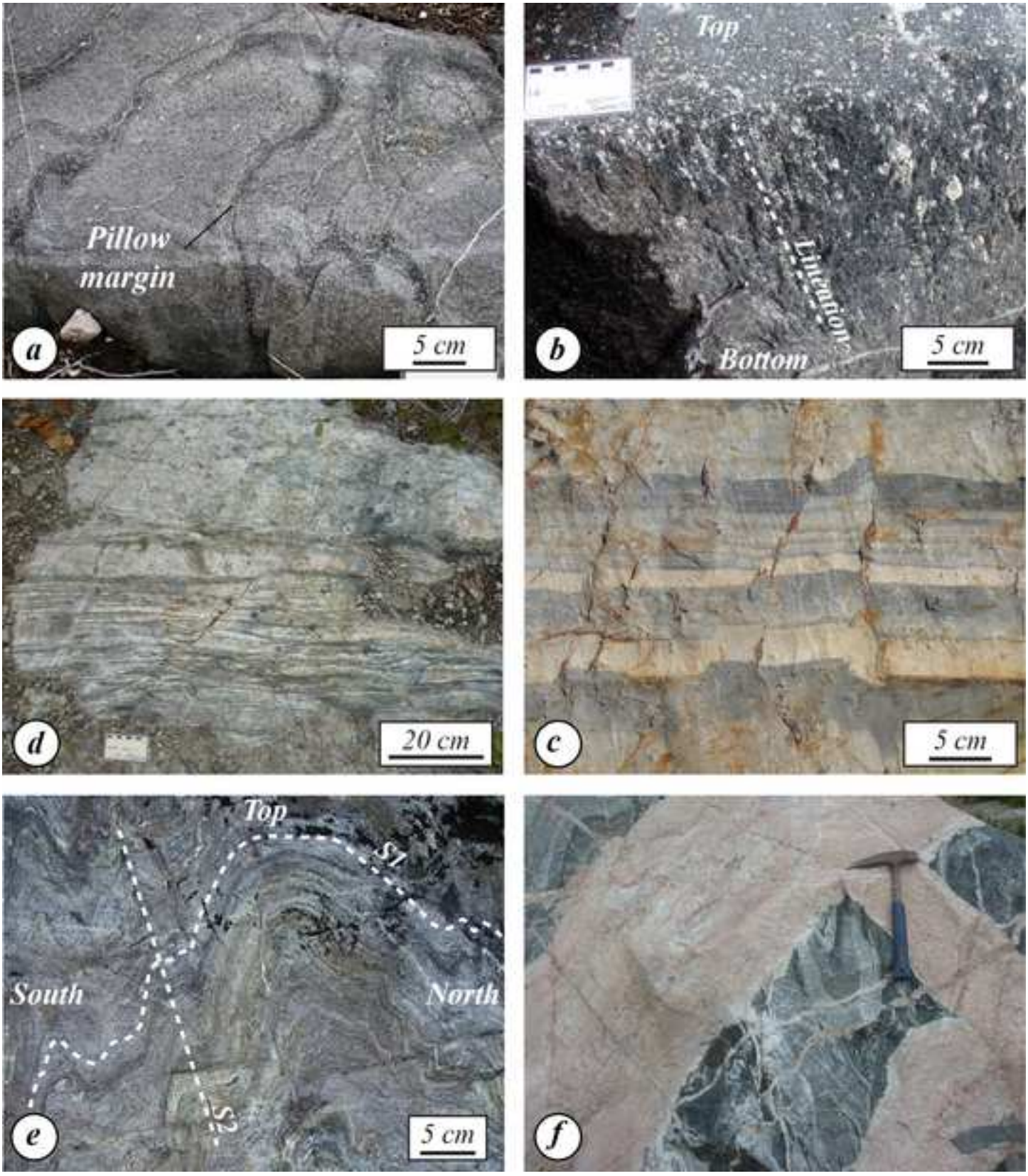

Figure 5 (color)

Click here to access/download;Figure;Figure 5.jpg

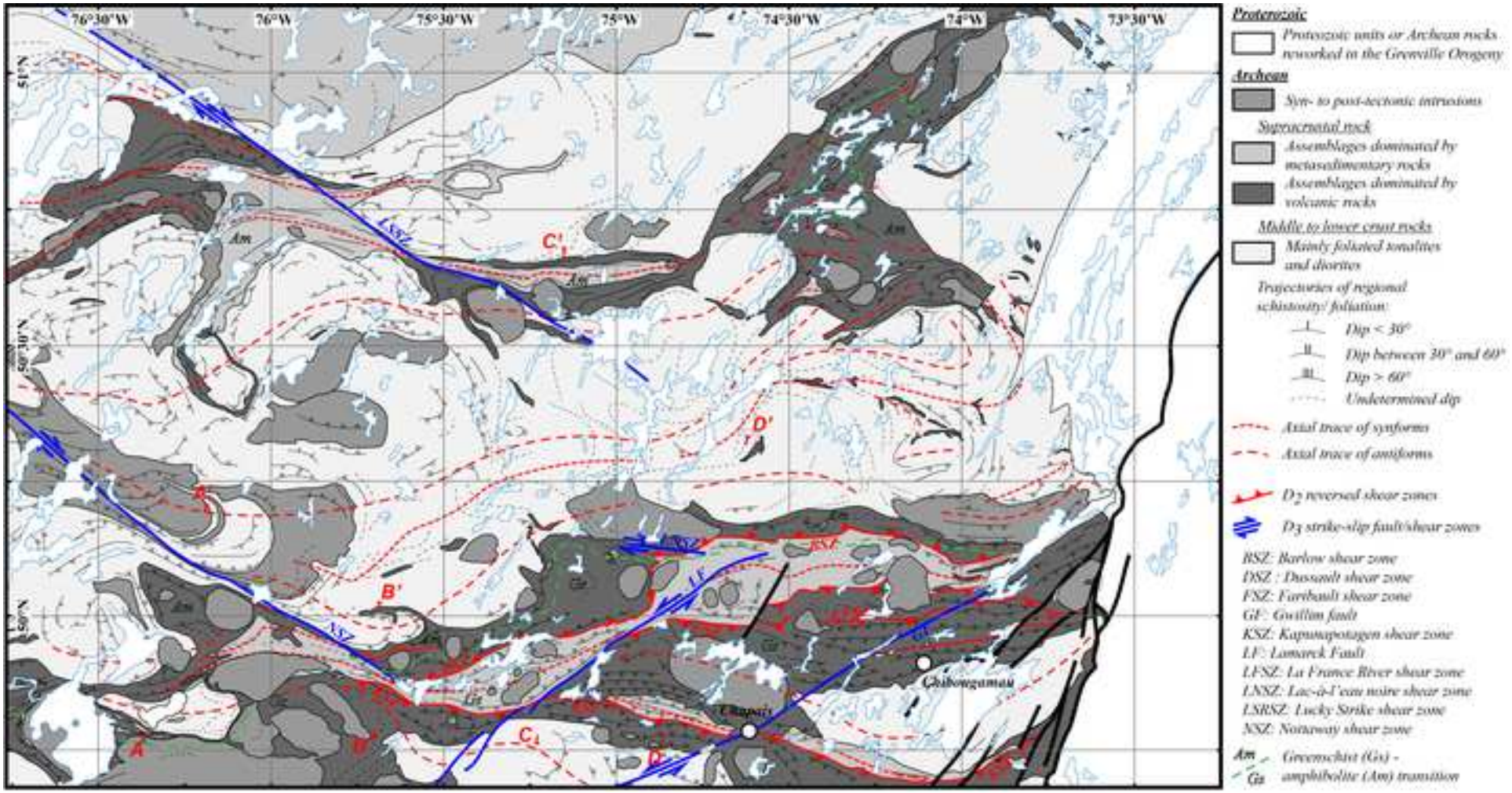

Figure 6

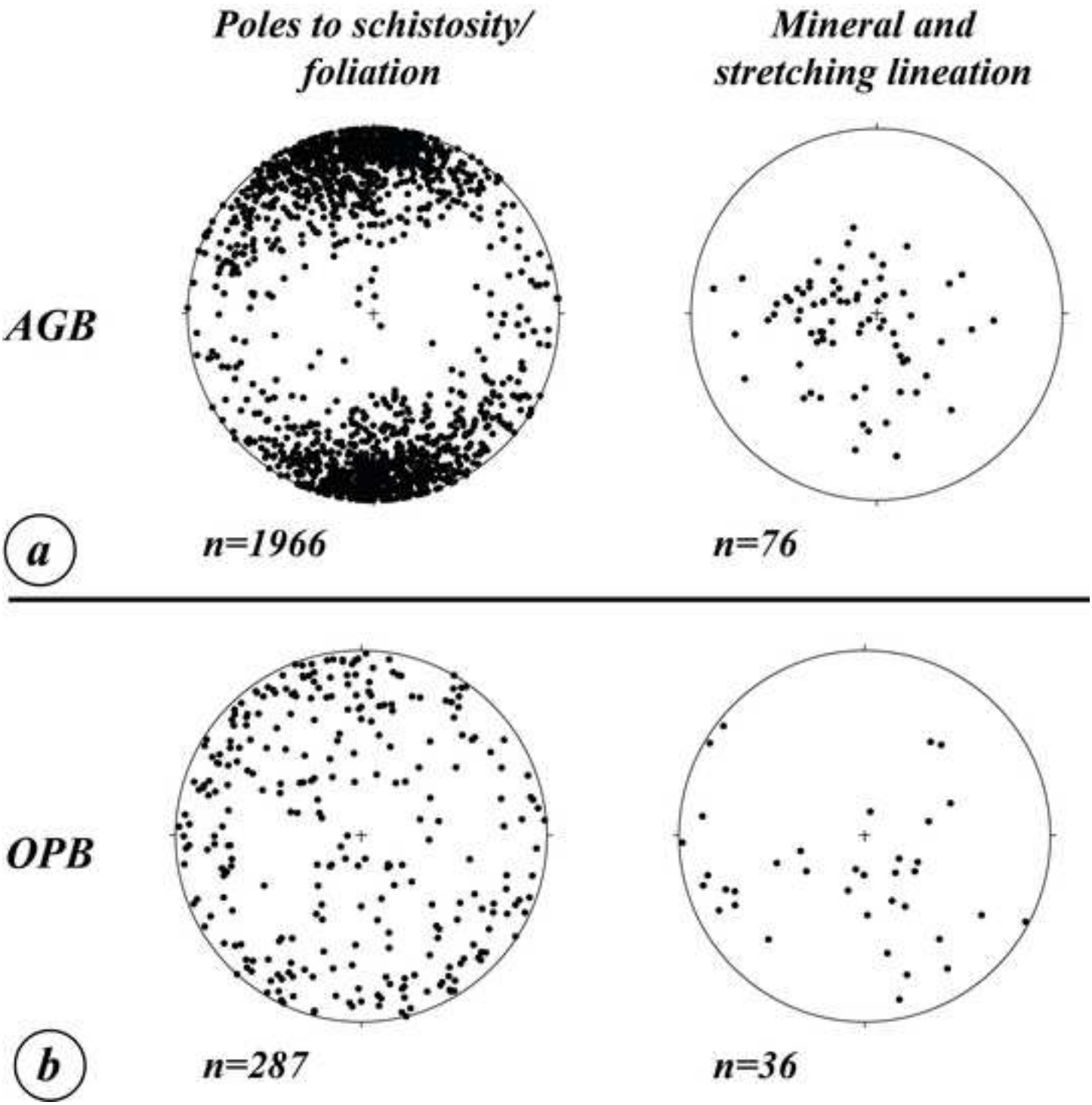

Figure 7 (color)

Click here to access/download;Figure;Figure 7.jpg

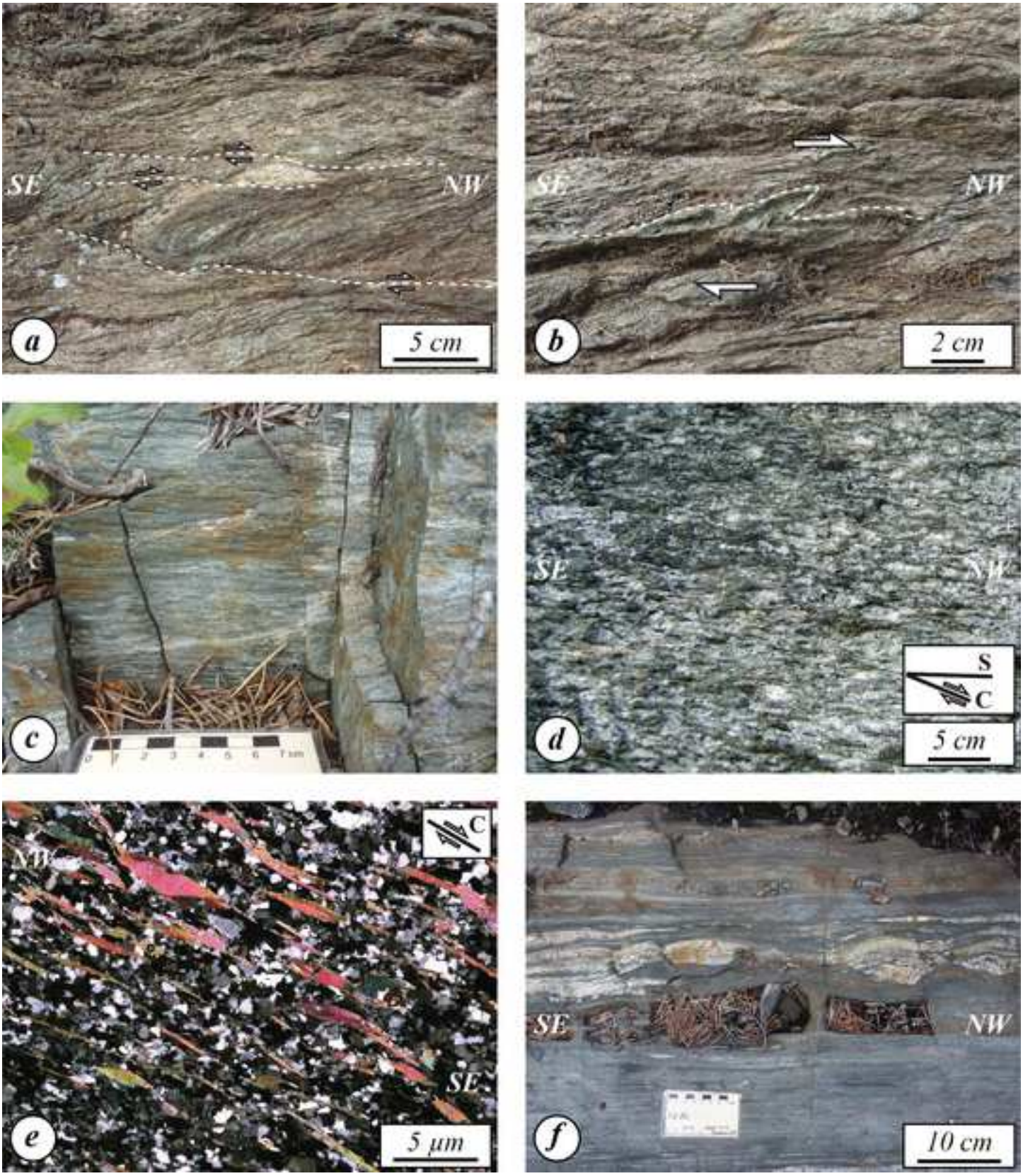

Figure 8 (color)

Click here to access/download;Figure;Figure 8.jpg

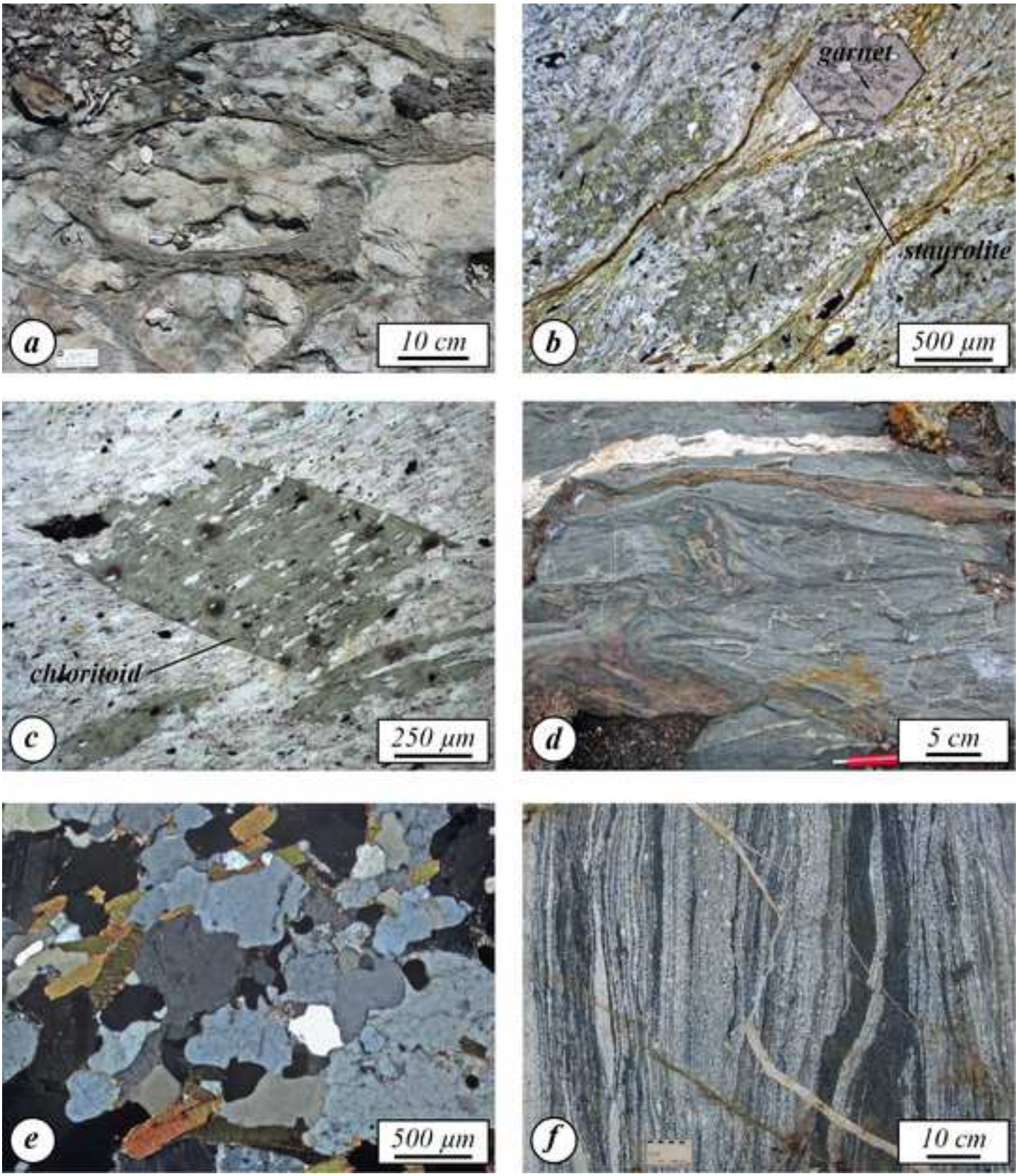

Figure 9 (color)

Click here to access/download;Figure;Figure 9.jpg

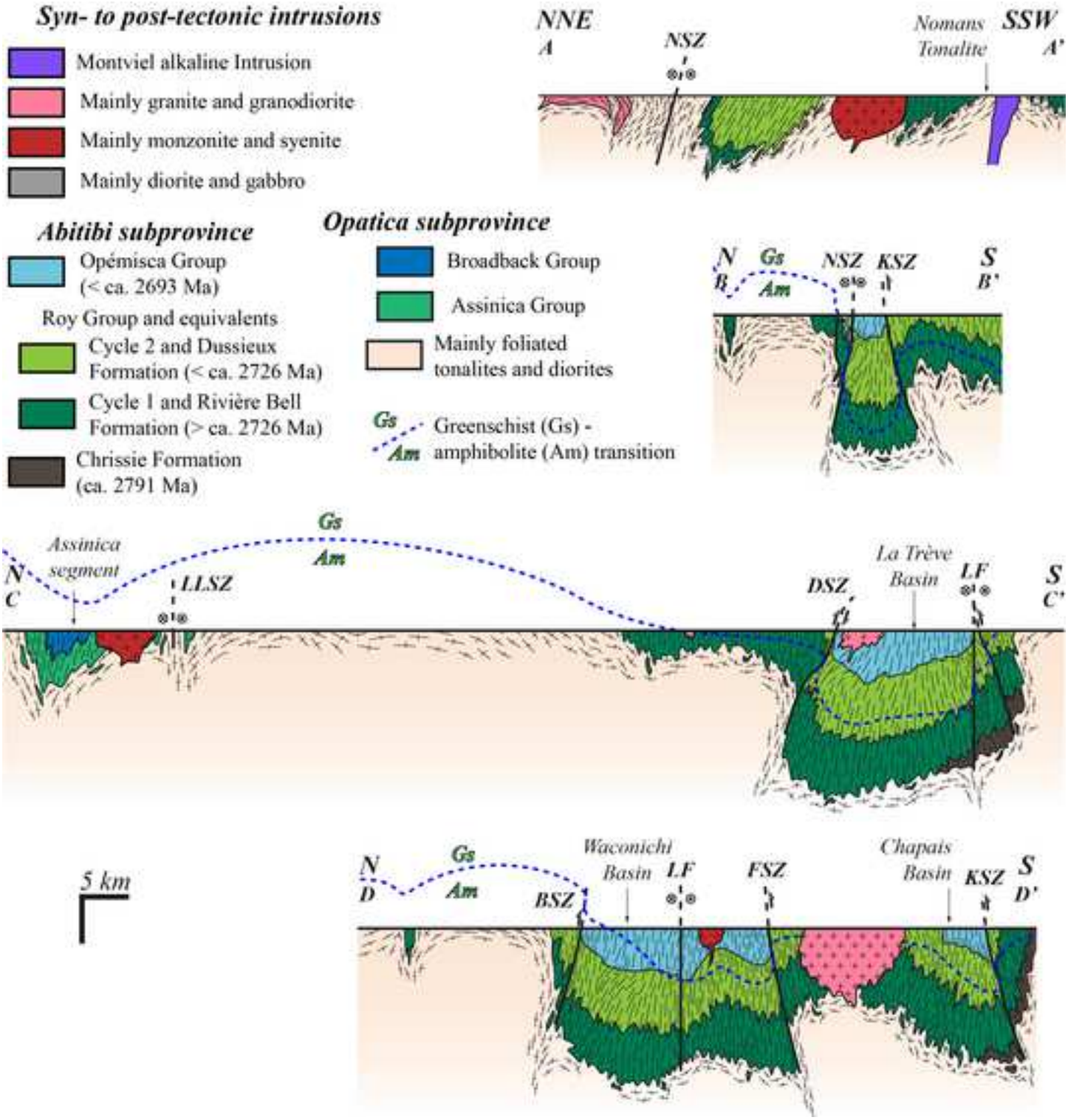

Figure 10 (color)

Click here to access/download;Figure;Figure 10.jpg

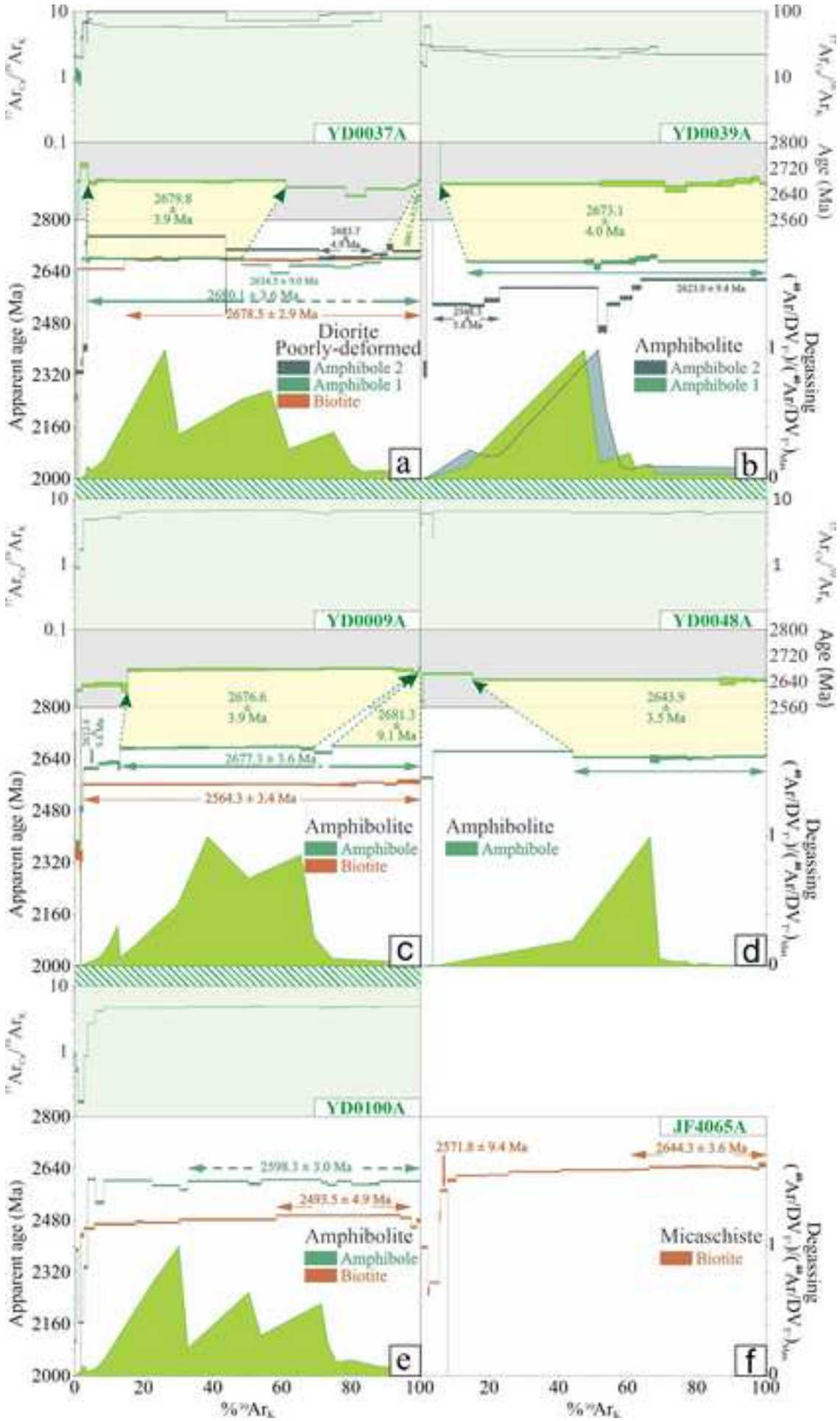

Figure 11 (color)

Click here to access/download;Figure;Figure 11.jpg

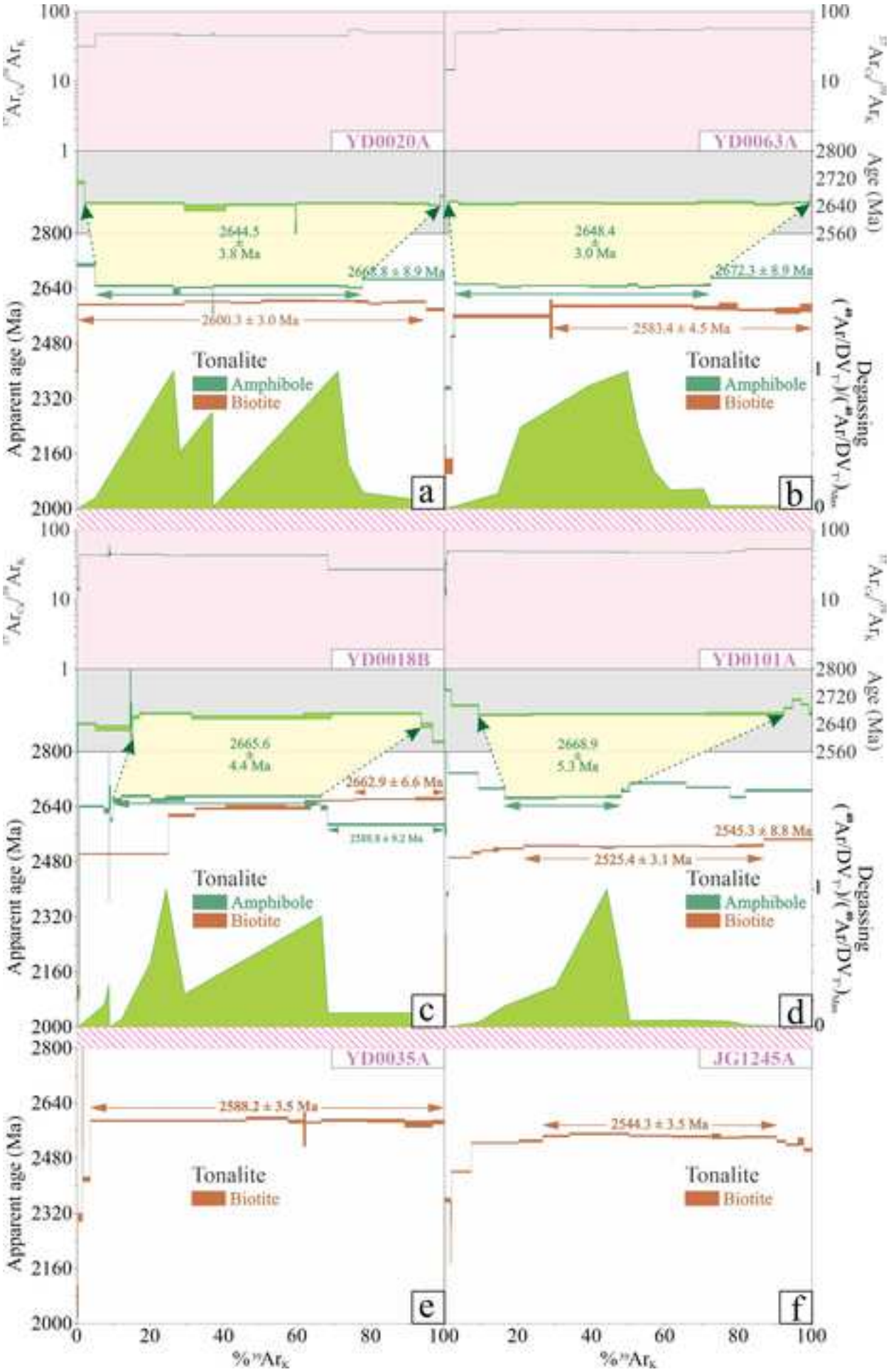

Figure 12 (color)

Click here to access/download;Figure;Figure 12.jpg

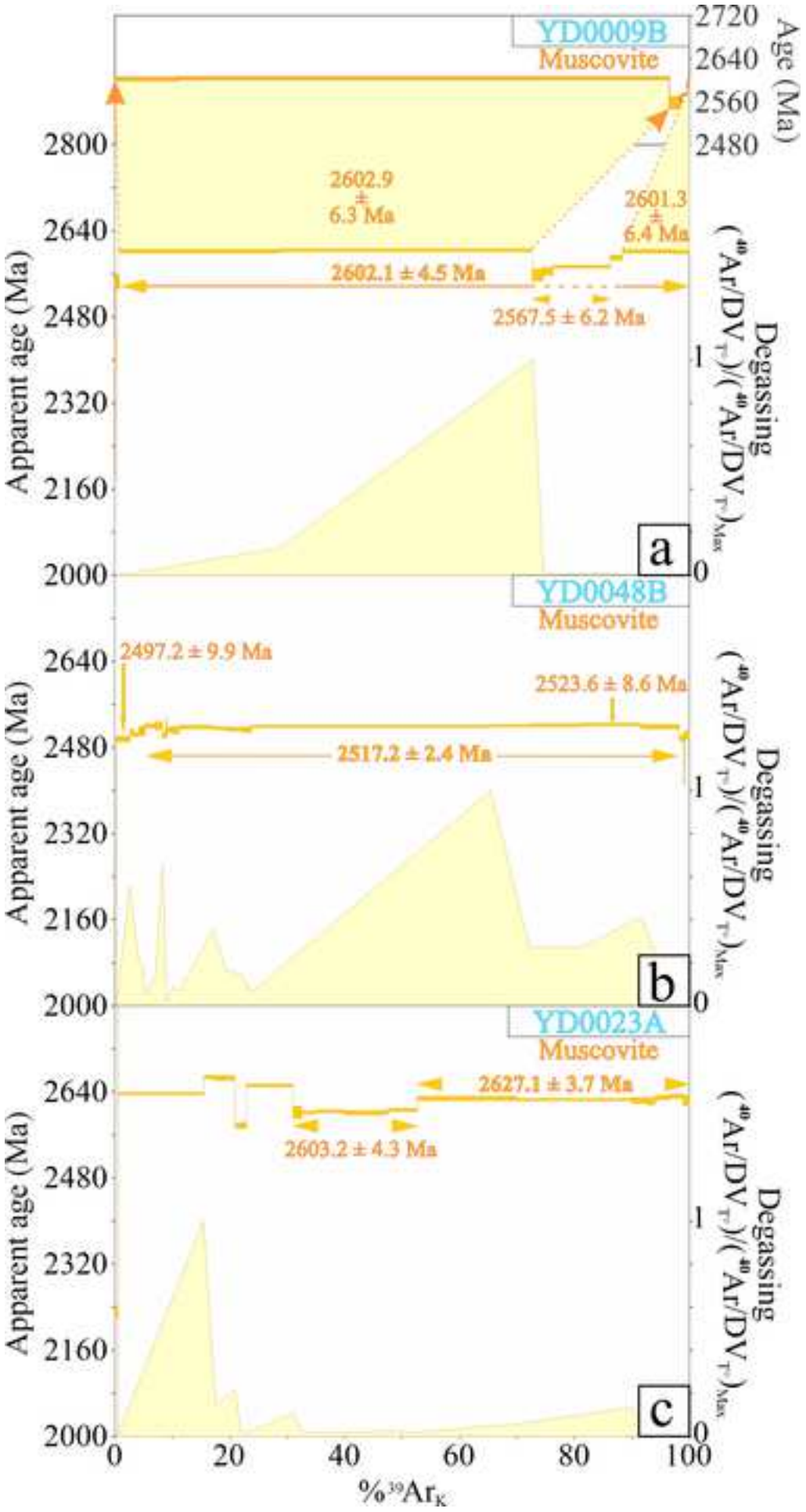

Figure 13 (color)

Click here to access/download;Figure;Figure 13.jpg

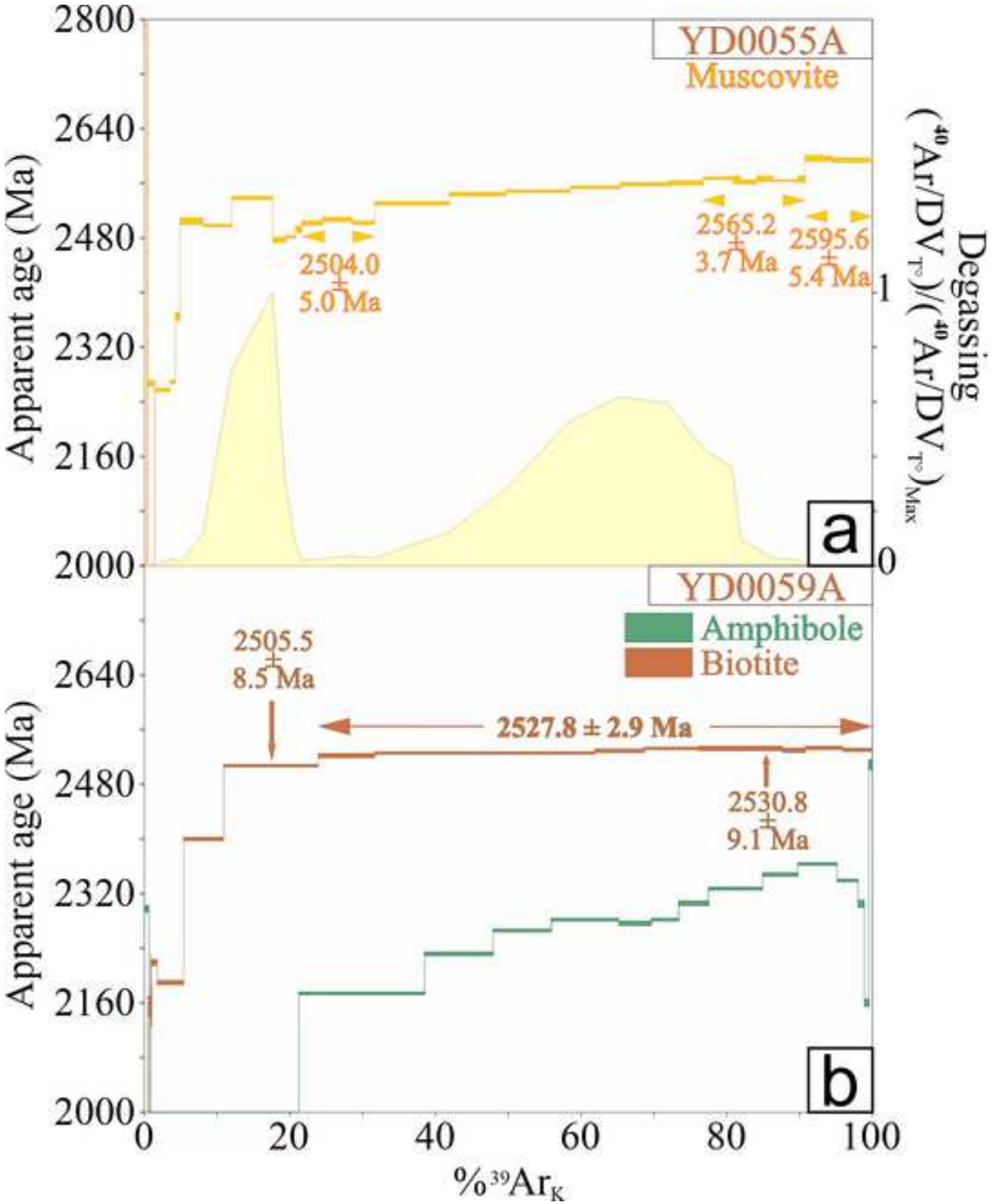

Figure 14 (color)

Click here to access/download;Figure;Figure 14.jpg

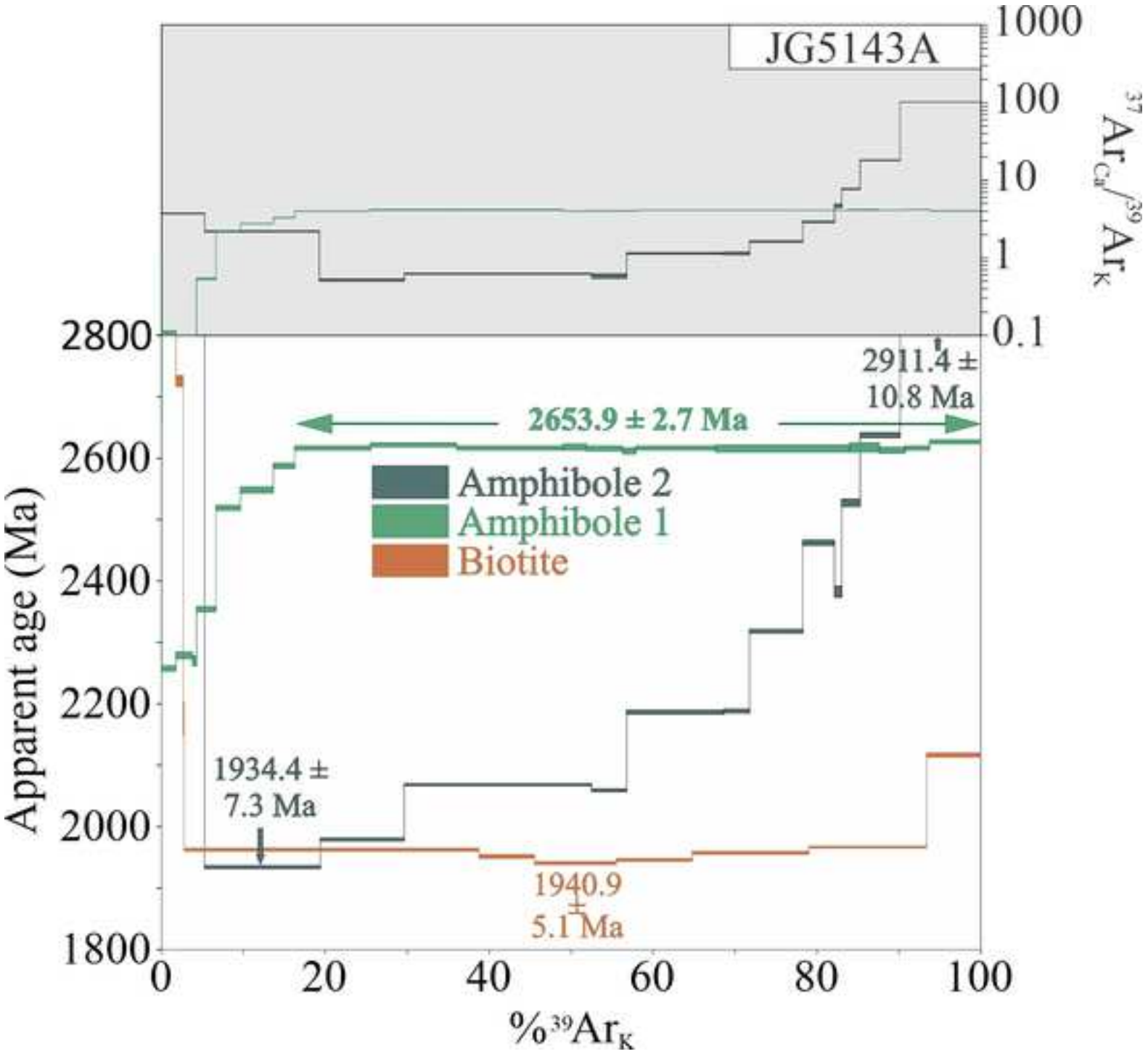

Figure 15 (color)

Click here to access/download;Figure;Figure 15.jpg

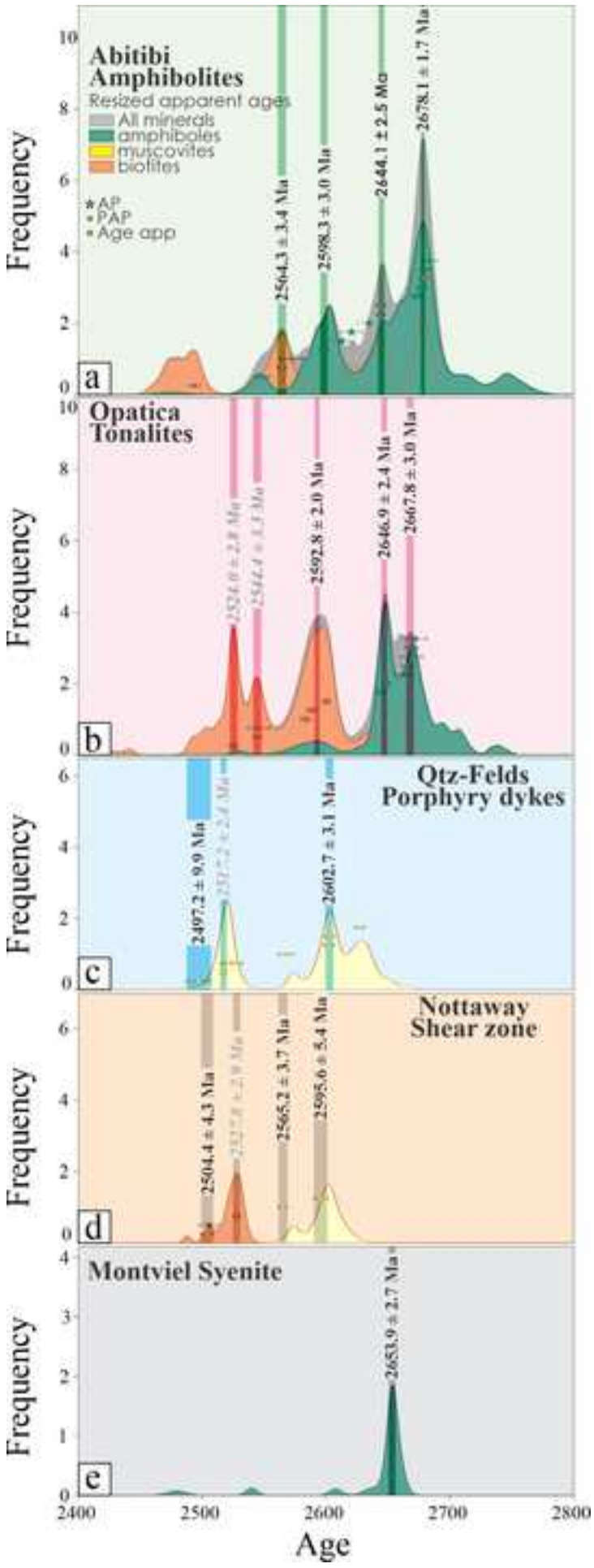

Figure 16 (color)

Click here to access/download;Figure;Figure 16.jpg

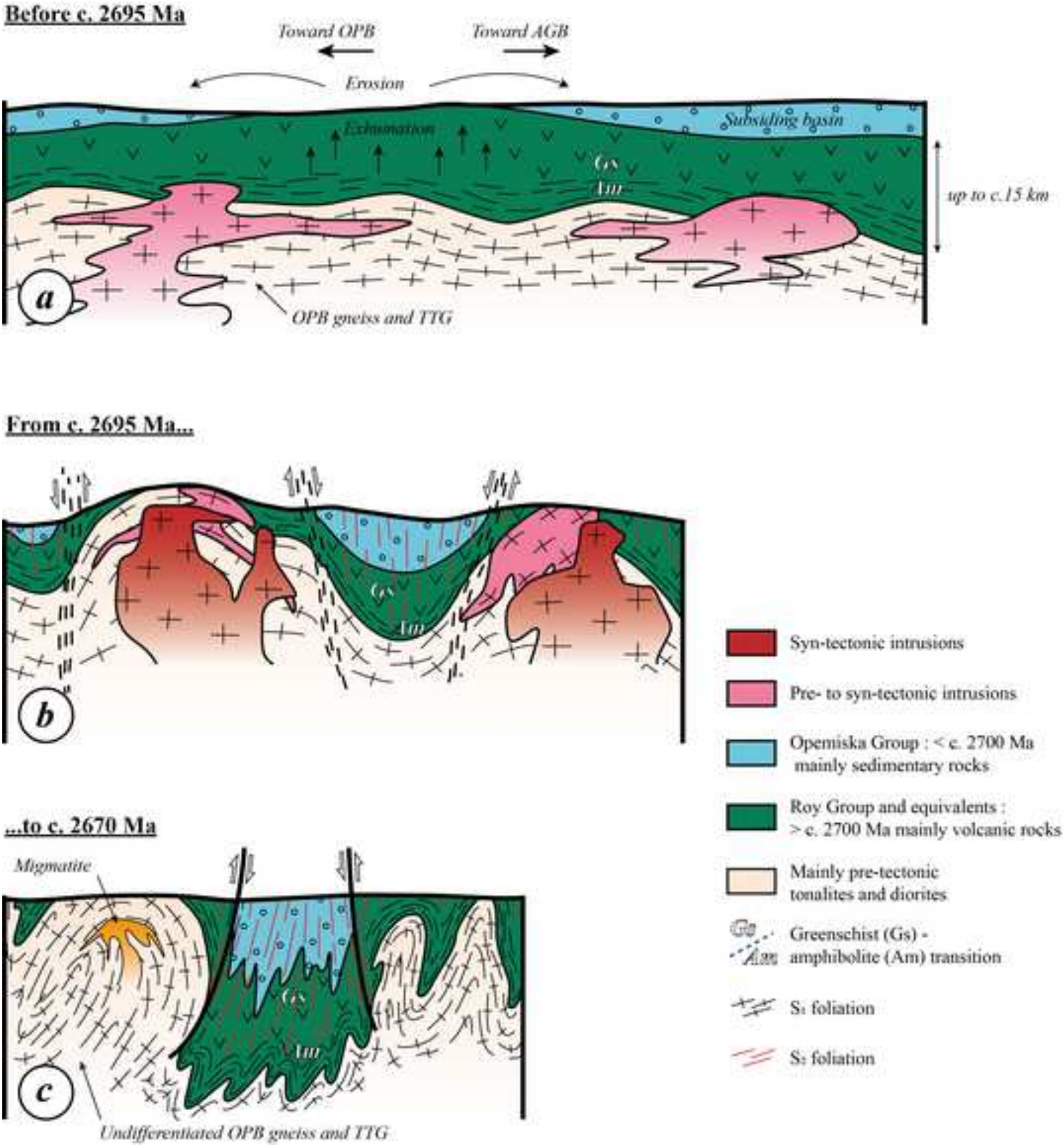

Figure 17 (color)

Click here to access/download;Figure;Figure 17.jpg

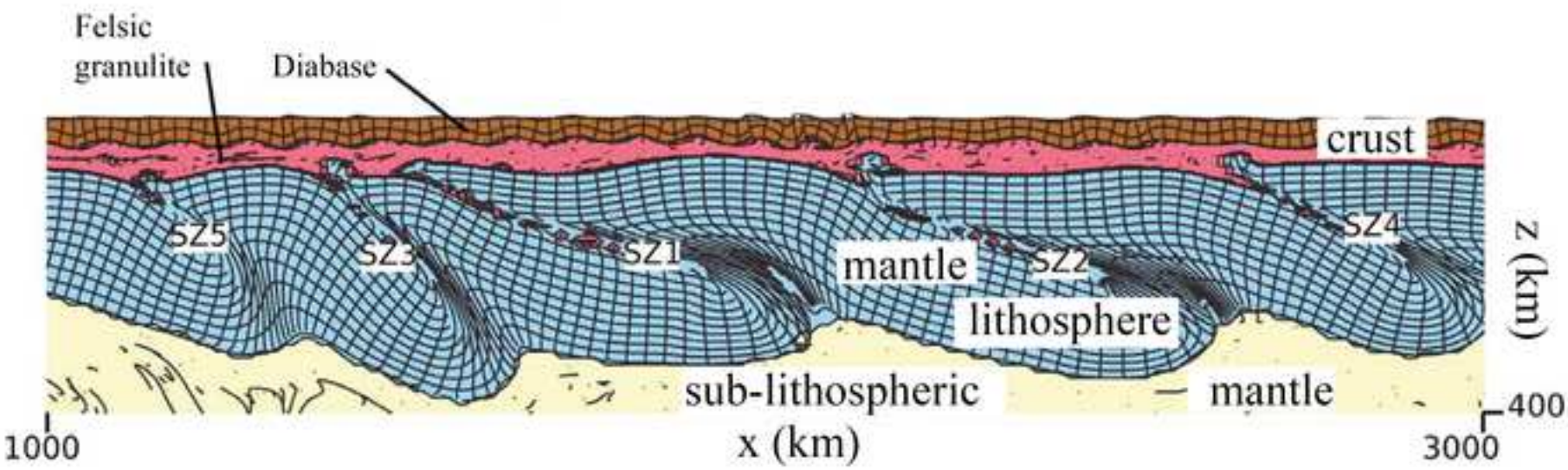

Figure 18 (color)

Click here to access/download;Figure;Figure 18.jpg

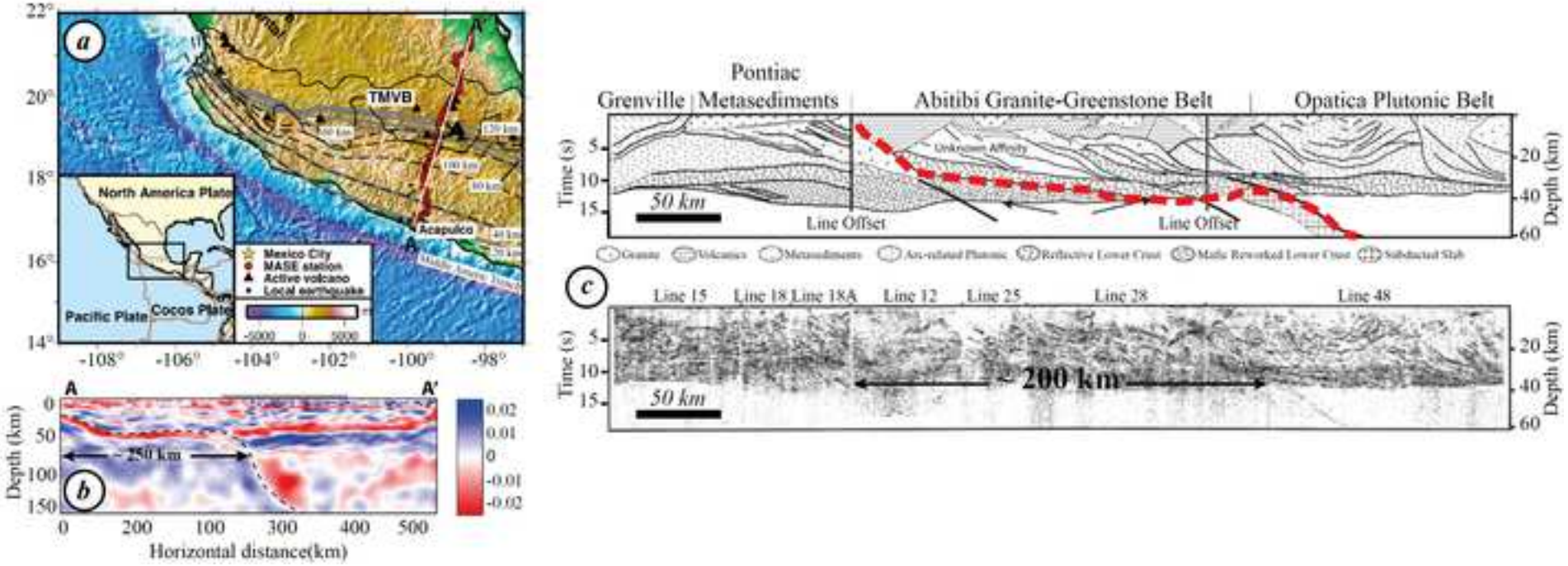

Figure 4 (color)

Click here to access/download;Figure;Figure 4.jpg

Declaration of interests

☐The authors declare that they have no known competing financial interests or personal relationships that could have appeared to influence the work reported in this paper.

☒The authors declare the following financial interests/personal relationships which may be considered as potential competing interests:

Yannick Daoudene reports financial support was provided by Ministère de l'Énergie et des Ressources naturelles du Québec. Yannick Daoudene reports financial support was provided by Mitacs Canada.

The paper presents the result of a postdoctoral study performed by the first author. YD made field observations, the structural and metamorphic analyses, and the lithological sampling. He wrote the paper and drawn most of the figures. As research director, AT supervised YD, and participated in several field trips, discussions in many ways and the writing of the paper. GR performed the Ar-Ar analyses, wrote the section 40Ar/39Ar Geochronology and participated in the elaboration of the discussion. FL accompanied the first author on the field and participated in discussions about regional geology.

All authors read and approved the final manuscript.